AFRL-SN-RS-TR-1999-173
Final Technical Report
August 1999

# OPTICAL NETWORKING

**Sanders - A Lockheed Martin Company**

**Defense Advanced Research Projects Agency**
**DARPA Order No. B667**

*APPROVED FOR PUBLIC RELEASE; DISTRIBUTION UNLIMITED.*

**The views and conclusions contained in this document are those of the authors and should not be interpreted as necessarily representing the official policies, either expressed or implied, of the Defense Advanced Research Projects Agency or the U.S. Government.**

## AIR FORCE RESEARCH LABORATORY
## SENSORS DIRECTORATE
## ROME RESEARCH SITE
## ROME, NEW YORK

19991015 034

This report has been reviewed by the Air Force Research Laboratory, Information Directorate, Public Affairs Office (IFOIPA) and is releasable to the National Technical Information Service (NTIS). At NTIS it will be releasable to the general public, including foreign nations.

AFRL-SN-RS-TR-1999-173 has been reviewed and is approved for publication.

APPROVED:    *(signature)*
JOHN MALOWICKI
Project Engineer
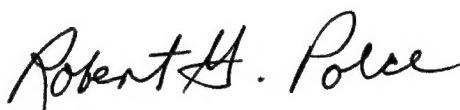
FOR THE DIRECTOR:    *(signature)*
ROBERT G. POLCE, Acting Chief
Rome Operations Office
Sensors Directorate

# OPTICAL NETWORKING

## Timothy P. Boggess
## Jeffry Powell

# REPORT DOCUMENTATION PAGE

*Form Approved*
*OMB No. 0704-0188*

| 1. AGENCY USE ONLY *(Leave blank)* | 2. REPORT DATE | 3. REPORT TYPE AND DATES COVERED |
|---|---|---|
| | August 1999 | Final  Sep 97 - Feb 99 |

**4. TITLE AND SUBTITLE**

OPTICAL NETWORKING

**5. FUNDING NUMBERS**
C  -  F30602-97-C-0325
PE  -  63761E
PR  -  B667
TA  -  00
WU  -  08

**6. AUTHOR(S)**

Timothy P. Boggess and Jeffry Powell

**7. PERFORMING ORGANIZATION NAME(S) AND ADDRESS(ES)**

Sanders - A Lockheed Martin Company
65 Spit Brook Road
Nashua NH 03061-0868

**8. PERFORMING ORGANIZATION REPORT NUMBER**

N/A

**9. SPONSORING/MONITORING AGENCY NAME(S) AND ADDRESS(ES)**

Defense Advanced Research Projects Agency   Air Force Research Laboratory/SNDP
3701 North Fairfax Drive                    25 Electronic Parkway
Arlington VA 22203-1714                      Rome NY 13441-4515

**10. SPONSORING/MONITORING AGENCY REPORT NUMBER**

AFRL-SN-RS-TR-1999-173

**11. SUPPLEMENTARY NOTES**

Air Force Research Laboratory Project Engineer:  John Malowicki/SNDP/(315) 330-4682

**12a. DISTRIBUTION AVAILABILITY STATEMENT**

Approved for public release; distribution unlimited.

**12b. DISTRIBUTION CODE**

**13. ABSTRACT** *(Maximum 200 words)*

This report explored the manufacturability of an integrated opto-electric device which functions as an optical AND gate and which could be used for computer communications, i.e., an Integrated Teraherz Optical Asymmetric Demultiplexer (I-TOAD). The motivation for such a device is that it might enable high-speed communication where the aggregate bandwidth of the shared media is hundreds of gigabits per second, while the interface to the computer is relatively inexpensive (e.g. 1 GHz CMOS). Our efforts focused on two distinct but related queries: (1) Can a manufacturable I-TOAD be built, and (2) If you could build a perfect I-TOAD, how would you build a computer network using such a device.

**14. SUBJECT TERMS**

Mach Zehnder, Time Division Multiplexed (TDM), Integrated TOAD, Optical AND, Optical LAN

**15. NUMBER OF PAGES**

152

**16. PRICE CODE**

| 17. SECURITY CLASSIFICATION OF REPORT | 18. SECURITY CLASSIFICATION OF THIS PAGE | 19. SECURITY CLASSIFICATION OF ABSTRACT | 20. LIMITATION OF ABSTRACT |
|---|---|---|---|
| UNCLASSIFIED | UNCLASSIFIED | UNCLASSIFIED | UL |

Standard Form 298 (Rev. 2-89) (EG)
Prescribed by ANSI Std. 239.18
Designed using Perform Pro, WHS/DIOR, Oct 94

# Table of Contents

# List of Figures

## LIST OF TABLES

# 1. Executive Summary

The Optical Networking contract explored the manufacturability of an integrated opto-electric device which functions as an optical AND gate and which could be used for computer communication, i.e., an Integrated Teraherz Optical Asymmetric Demultiplexer (I-TOAD). The motivation for such a device is that it might enables high-speed serial communication where the aggregate bandwidth of the shared media is hundreds of gigabits per second, while the interface to the computer is relatively inexpensive (e.g., 1 GHz CMOS).

Our efforts focused on two distinct but related queries: 1) Can a manufacturable I-TOAD be built, and 2) If you could build a perfect I-TOAD, how would you build a computer network using such a device.

As will be explained in the following sections, (given the limited time and accessibility of a high-speed laser) an integrated Mach-Zehnder cannot be operated at high repetition rate under single wavelength operation. Under single wavelength operation, the wavelength used must be near the bandedge. Unfortunately, operating too close to the bandedge results in not enough transmission and too far from the bandedge results in not enough absorption to generate carriers and thus change the refractive index. Because the device must be operated near the bandedge, absorption and temperature effects dominate the performance of the device. As a result, a more complicated and less manufacturable approach must be taken. Based on published research, even these more complex approaches have performance problems.

Perhaps more importantly, from a system point of view, our study found a limited use for the technology as a local or system area network (LAN or SAN). This limitation is driven by three factors: 1) the technology does not appear to be readily scalable beyond 500 GHz, 2) the protocol is only efficient with nodes that are close together (e.g., very large servers), and 3) because of these limitations, there does not appear to be a large enough market to ever drive the costs down so as to make the technology affordable. Taken together, these factors seem to doom the technology to be too expensive and too non-scalable for computer communication.

If a reliable and _lossless_ optical AND gate could be developed, then there would be many other applications which might benefit, but a LAN with a time division multiplexed (TDM) arbitration scheme will always be sub-optimal.

The remainder of this report will discuss the details that support these findings.

## 2. System Analysis

### 2.1 Overview of proposed system

In general, an Optical Time Division Multiplexed (OTDM) system defines a frame (i.e., a period of time) within which there are many channels, (i.e., smaller periods of time). A channel is defined to be the periodic pulse within a frame. For example, suppose that each frame was a 1-nanosecond period and that within each frame, there were 100 pulses. The Nth channel would be the Nth bit in every frame. (See Figure SA-1.)
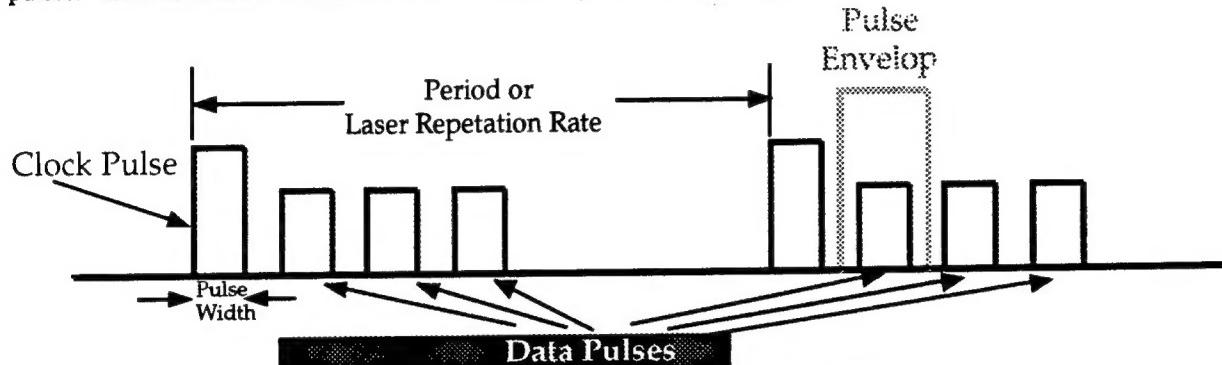


Figure SA-1: OTDM pulse train and definitions

The limit for how much bandwidth a system can have is therefore inversely proportional to the width of the individual pulses. Continuing our example, if there are 100 pulses in a 1 ns frame period, then the bandwidth would be $100/1e^{-9}$, or 100 Gbits/second. If the pulse width were decreased by a factor of 2, then the bandwidth could increase by a factor of 2 to 200 Gbits/s.

One way to accomplish an OTDM is to split a single light source into N fibers that are fed to attached processing nodes (where N is the number of nodes attached). For this discussion, lets assume there are 100 nodes attached (i.e., N=100). The light source acts as both energy source and system clock for the System Area Network (SAN), in that it transmits a very narrow pulse once per frame. For example, the light source might send out a 1-picosecond pulse every 1-nanosecond. (See Figure SA-2.) In this context, a SAN is defined as a network of computers that might be a cluster of workstations or a chassis backbone for an embedded system.
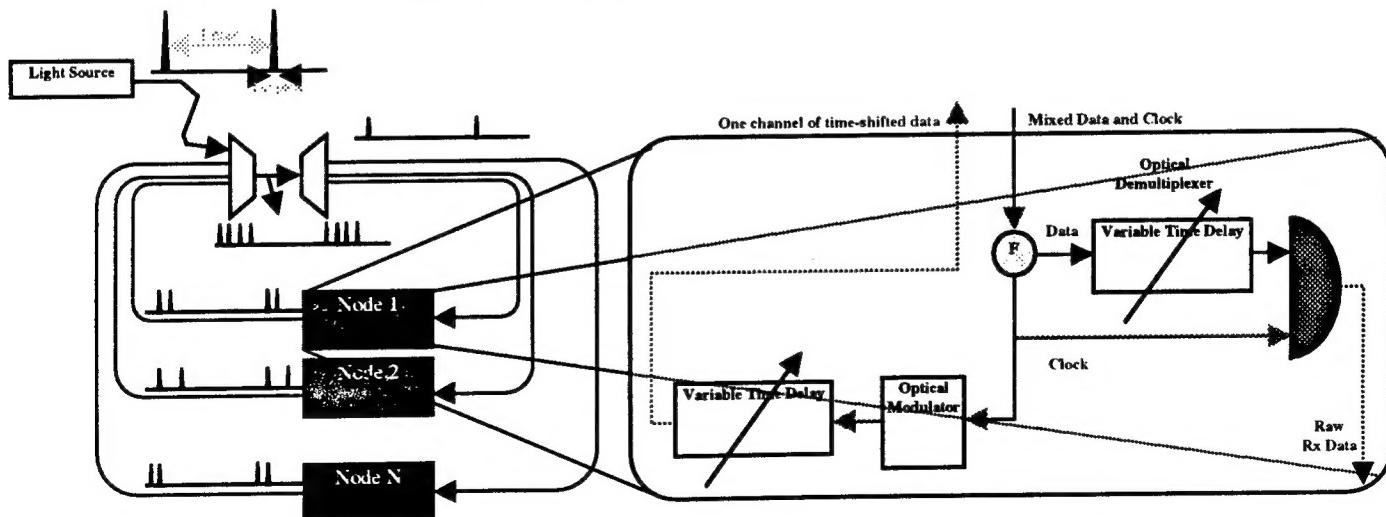


Figure SA-2: Possible OTDM Network        Figure SA-3: Network Interface Controller

2

Each framing pulse is either modulated or absorbed by each node, depending on whether the node has data to send or not. When a node transmits, the framing pulse will be delayed slightly and modulated. In our previous example, Node 1, (which is assigned to transmit on channel 1), would delay the framing pulse by 10-nsec and then modulate it. Each node will write to its designated channel (i.e., its time slice in the frame) and then pass the data on to a combiner that merges the N signals together. For our example, if all nodes are transmitting, there are 100 Gbps of data on the ring after the data is merged through the combiner.

As the light pulses travel around the fiber, every node has the opportunity to see each data pulse. However, the data must be demultiplexed at the receiving node so that only the correct channel is observed. (The negotiation of the correct channel will be explained a little later.) Once the correct channel is selected via a variable time delay, the signal is demultiplexed and passed on to an optical detector. One such demultiplexer is a novel device invented by Dr. Paul Prucnal of Princeton.

The proposed system has a single light source that is split to N nodes. The N nodes then have the opportunity to modulate the signal and send it back to a central hub, which then combines the signals and broadcasts the aggregate signal back to the nodes. In this system, the pulsewidth is ultimately the limiting characteristic to the scalability of the network. That is, the maximum achievable bandwidth is 1/pulsewidth. Of course, that upper bound is unachievable since it assumes you can pack the bits side-by-side, but nonetheless, it's a good bound

## 2.2 Protocol
### 2.2.1 Protocol Overview
If we concentrate on a single node interface (see Figure SA-3), the pulse train enters on one fiber and is split into data and clock channels. The data and the clock are passed to the TOAD which demultiplexes the appropriate channel and discards the rest of the data. The other nodes on the network are simultaneously processing their own channels of data, so the discarded bits are not lost to the system, but merely dropped from that fiber. The clock is simultaneously passed on to the transmitter which uses it as a carrier for its data. If the node has data to transmit, it modulates the carrier pulse, (i.e., framing clock pulse) and inserts it onto its designated channel.

The data emerging from the combiner can be best thought of as a 3-dimensional block. (See Figure SA-4.) The first dimension is the frame period. In figure SA-4, it shows a frame period of 1-nanosecond that is comprised of 32 channels. The second dimension is the interleaved data that each node sees between arbitration bits. In Figure SA-1, there are 15 data bits for every arbitration bit. Every arbitration bit requires buffering around it to ensure no loss of data due to slow switching. Correspondingly, there are 13 data bits for every 1 arbitration and 2 buffer bits. The third dimension is required for interleaved arbitration. The red rows shown are the scattered arbitration bits that come in over time. In Figure SA-4, it shows 12 arbitration bits for a complete cycle. The gray rows are buffer bits, which are wasted.
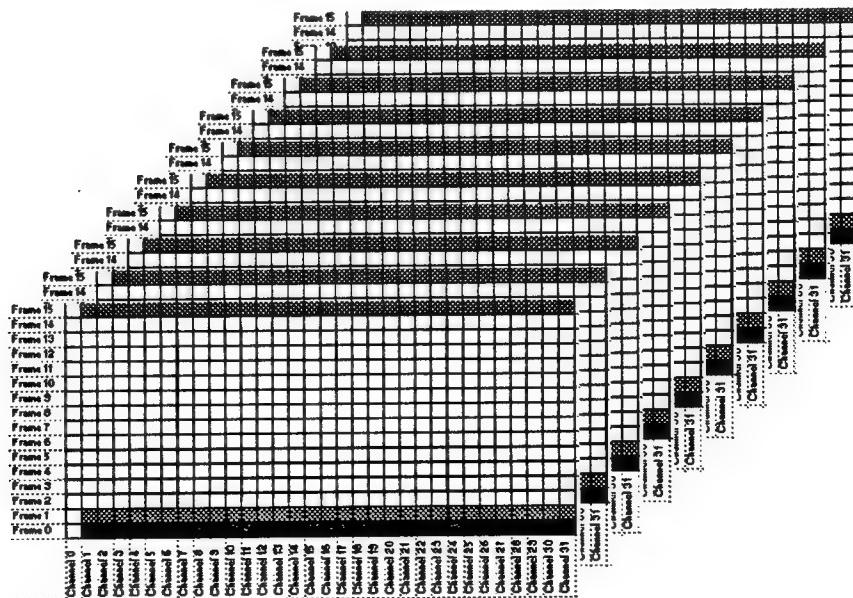


Figure SA-4: Multi-dimensional Data structure

3

The negotiation of correct channels is done using in-band signaling. That is, a small fraction of total bandwidth is used to arbitrate communication. This mechanism permits the nodes to request a channel using look-ahead arbitration. Since we anticipate no more than 1024 nodes for the first instantiation of the OTDM system, only 10 bits are necessary for arbitration. This is most easily explained using a concrete example.

Suppose that Node 1 wants to send data to node 7. Node 1 will send out its node ID to Node 7 on its arbitration channel. (That is, Node 7 will receive a message from node 1 on its own channel—channel 7—at the specified frame time.) Node 7 will then realize that it needs to look at channel 1 to receive a message. Since a node doesn't need to send data to itself, it will not be transmitting data during the arbitration bit. As a result, it is safe for other nodes to use that channel to inform a node that another node wants to send data to it. Going back to the example, suppose Node 7 is receiving 1000 bits of data on its way from Node 3 with just 2 bits until the arbitration bit. Node 7 will continue to accept data for 2 more framing cycles and then stop for one bit. During that 1 bit cycle, Node 7 adjusts its channel to its own transmit channel, i.e., channel 7. After the arbitration bit is received, it is stored and the reception of Node 3's message is continued. After 10 arbitration bits are collected ($2^{10} = 1024$), Node 7 decodes the arbitration message which is Node 1's ID number. Therefore Node 7 knows that Node 1 is trying to send a message and that Channel 1 is the correct channel to monitor.

One final concern with the system is the synchronization of the pulses. There are 2 separate but related synchronization problems: (1) getting the nodes synchronized to the framing pulse at system initialization and (2) adjusting the system dynamically to compensate for any drift due to thermal conditions. With the aid of the TOAD, the synchronization is straightforward.

The initialization problem is handled by lengthening the path the pulses travel by the framing distance. For example, a 1-Gigabit per second frame time with 100 nodes attached using a 1-picosecond pulse width would have a channel width of 10 picoseconds. This translates into a physical distance of 300 mm (1 nanosecond *c meters/s = 300 mm, where c is the speed of light.) The TOAD will not return any output until the correct length is arrived at, so synchronization is simple. For this particular example, a conservative search would require no more than 4000 samples to find the pulse center to within 1/4 pulse width.

Once synchronization is achieved, the same feedback system must be used to ensure synchronization is maintained. But since changing thermal conditions will vary slowly relative to the network traffic, the synchronization only needs to be checked infrequently and can be done as a background task.

In order to implement the synchronization, the fiber need not actually be stretched 300 mm. The variable time delays are used for the vast majority of the distance. For the example discussed above, the fiber length need only be stretched 3 mm. This stretching can be done in at least four different ways. Ideally, the variable time delays will have an extra 3 or 4 bits of resolution that can be used for synchronization. This would enable initial synchronization to occur in less than 4 usec. Although not quite as elegant as the digital solution, synchronization could also be done with piezo fiber stretcher, piezo free space length modulator, and electromagnetic free space modulator.

The limiting factor for OTDM systems is the pulse width of light source. Some experimental lasers have been tested with pulse widths as short as 10 femtoseconds (fs) which would give ample room for growth. However, current technology limits pulse widths to about 1 picosecond. As a result, the maximum baud rate available is 1/1 ps = 1 Terabit/s. (This assumes that the pulse envelope is equal to the pulse width, but provides an upper limit.) For a 10 fs light source, the upper limit would be 100 Terabit/s.

### 2.2.2 Initialization

At start up, initialization can be relatively easy. The laser starts pulsing and each node does a search over the available channels until it locates the clock. That frame is then assigned the channel zero for that node. Each node must know his own identification number which will uniquely define his channel number. The lowest channel number then sends a pulse to determine his distance from the hub. Upon reception of the pulse, the node knows how many clock ticks are required to reach the combiner. In turn, he knows how far ahead he must send a pulse to arbitrate for a particular cycle.

4

This synchronization period is bounded since the number of channels is finite, so node 2 knows when node must be completed and begins his timing analysis in his turn. This synchronization continues until all nodes have been registered.

A much harder problem is what to do about a node that comes up while the system is already operating, i.e., live insertion. In order for on the fly synchronization/initialization to occur, a node must be able to identify the framing pulse unambiguously. The most efficient way to do this is the encoding of the clock pulse in some way, e.g., polarization. If the clock pulse can be identified unambiguously, the node sends itself a message to establish timing and to ensure that another node was not sending a message to it inadvertently.

In the simulation, initialization was ignored.

### 2.2.3    Arbitration

As the project evolved, it became clear that there was no perfect solution and that trade-offs would have to be made. There are two significant obstacles to overcome when designing such a system. The *first* obstacle is that the data coming in is significantly more than the electronics at any one node can handle. As a result, alignment is critical— even for a discrete event model with perfect signals and timing. The *second* hurdle is doing arbitration on a system without electronic buffering (as in the IEEE Scalable Coherent Interface (SCI), IEEE-1596) and without means of detecting collisions.

In conventional electronics systems, for example SCI, a high-speed buffer pulls data off a shared medium and passes the data on to slower speed electronics. This approach becomes very expensive when dealing with data rates as high as 100 Gbits/s, which is unacceptable when the intent of the system is to provide low cost electronics for extremely high bandwidths. Even if cut-through routing is used, conventional electronics cannot handle the traffic. The only cost effective solution to these incredible bandwidths is to be able to take only a fraction of the data, one bit at a time at a rate that is cheap to produce. That is, the only way to make it work cost effectively is to time division multiplex the data and find a way to manage the temporal alignment.

5

Figure SA-5: Data can be thought of as two-dimensional

The second problem, arbitrating the network, is really a set of lots of smaller problems. The best way to think about the data stream is a two-dimensional array, see Figure SA-5. Each frame represents the data that flows through the fiber in one time cycle. Continuing our example above, one frame is equal to 1-nanosecond. Within that nanosecond, every node will have all of the data available in that frame, however, the electronics controlling the node can only handle 1 bit in 1 nanosecond. The goal is to pick the right bit out of all the bits in the frame.

The second dimension represents time. That is, every frame is a nanosecond. So if a node were locked into channel 3, following channel 3 through its set of frames would tell what data that node received. Figure SA-5 shows a 32x32 grid, which would represent a 32-node system and 32 bits of data.

Connecting the transmitter and receiver is somewhat of a challenge. Because the data will overwhelm a node, it must know ahead of time what channel to watch. The problem is that you can't tell it what channel without having some communication path already open. To further complicate the problem, bits will OR when overlaid on the same channel.

In order to manage this complexity, a node must have a designated slot to look at a certain time to establish communication with another node. As a result, it makes sense to designate a time for all nodes to arbitrate. For example, if node 2 want to send a message to node 7, node 2 would send a message to node 7 on its own channel, i.e., channel 7, telling node 7 to listen to channel 2 at time $t_0$. This works as long as no other node wants to send at the same time. If node 5 (101) and node 2 (010) try to arbitrate at the same time, the receiver will see (111), i.e., node 7!

6

If bits arrive 1 bit at a time, so that transmitters can see what was sent, then the transmitters can turn off when they detect an error. CSMA/CD can be used as with Ethernet, but as with Ethernet, the efficiency would suffer. As the network approached saturation, the network would be paralyzed with its own attempts to retry arbitration. An alternate approach permits the transmitter with the highest ID number to continue transmission, while the other nodes shut down. However, this paradigm requires that all nodes see each protocol bit before they send the next. As a result, the distance from the hub to the furthest node greatly impacts the speed at which the system can arbitrate.

This strategy of biggest ID number wins arbitration permits efficient transmission, however, the network is now unfair. The node with the largest ID would dominate the network, so that in a congested network, the lower ID numbers would never be permitted bandwidth. Clearly, this is unacceptable network behavior. However, if every node had the largest ID number for an equal amount of time, then the network would be efficient, fair, and operable.

In order for the fairness to work properly, the Ids must be switched synchronously so that no two nodes have the same ID at any given moment. This can be done by having a single list of numbers that all the nodes use in a cyclical manner, each starting with a unique offset.

If arbitration occurs before transmission then the resulting network is very inefficient – particularly if the distance from hub to node is long. To improve efficiency, the network needs to arbitrate and send data simultaneously, i.e., interleave the protocol bits with data. Unfortunately, interleaving creates its own set of problems.
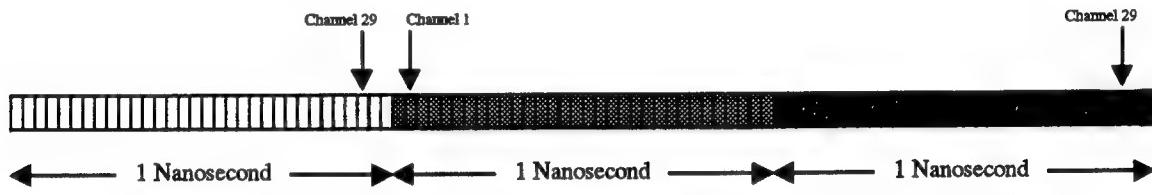


Figure SA-6: Channel switch can exceed the capabilities of the electronics if too close

Recall that the goal of the OTDM is to provide extremely high data rates inexpensively. In order to do so, all the components need to be relatively inexpensive, and that includes the variable time delays that temporally align the channels. With an interleaved arbitration, the switch at the input might have to switch between channels at the data bit rate rather than the frame rate unless something is done to protect against this.

Figure SA-6 shows three frames seen by node 1, where the blue frame is an arbitration frame. If in frame 1 (yellow), channel 1 is receiving data from channel 29, then to check its protocol bit on channel 1 in frame 2 (blue), it must switch in just 125 picoseconds. Since increasing the clock to multi-gigahertz is impractical, some other work around is required. The simplest solution is just to waste the frames around the arbitration bits in order to ensure proper switching. Recall Figures SA-5 and SA-4. As shown, the yellow column represents the system clock that must always be present. The red rows represent the arbitration bits, and the gray rows represent the wasted "arbitration buffer" bits. The exact size of the packets, the number of bits in-between arbitration bits, and the number of nodes on the system all affect the efficiency of the system. As shown (which is smaller and more inefficient than expected in real systems), the system in Figure SA-5 has a bandwidth efficiency of about 80%. At 1 GHz clock rate and 32 channels, that would be 25 Gbits/second of useful data on a shared medium with all electronic circuits running 500 MHz CMOS.

A final implication of the interleaved arbitration is the packet length dependency on the distance from hub to the furthest node. As discussed above, we want interleaved arbitration and data bits and we want to receive the last protocol bit from everyone before we send our next. As a result, the number of data bits between arbitration bits is equal to or greater than the time it takes for the round trip delay of the furthest node. If the furthest node is 3 meters, then the round trip delay is roughly 17 nanoseconds plus logic time. If the logic takes 8 clock cycles, then there should be about 25 data bits in-between each protocol bit. Assuming a packet payload size of 64 bytes (as is the IEEE SCI payload), there would be 20 bits available for arbitration, or over 1 million nodes!

7

### 2.2.4  Synchronization of packets

Interleaved Arbitration (ILA) requires that all the nodes be synchronized so that when they send arbitration bits, these bits arrive simultaneously at the combiner, and ILA requires that each arbitration bit (A-bit) is sent only after the OR'd result of the previous A-bit is received.

These two features require that the Optical Network Interface Controller (ONIC) provide synchronization both in terms of transceiver and receiver function. Once all the nodes are synched they will have pointers to the send and receive packet cycle and then proper transceiver and receiver function can be implemented. The key is how to implement the initial synchronization and establishing the format of the packet cycle or simply the packet.

One way to set up the timing is to assign one of the nodes the role of controller – perhaps the node with the lowest id number. The controller then sends out a sync pattern with which the other nodes can align themselves. Recall that there are two levels of timing required for the system to work. The first level of timing is that every node must know where a frame begins so that it can align channels for receipt and transmission. The incoming node bandwidth will be 100-1000 times faster than any one node can absorb, so picking the channel out of the frame is essential.

The second level of timing is the packet level timing. The only critical point for this level of timing is that the arbitration bits line up, i.e., every node must have the first bit of the arbitration sequence arrive at the combiner at the same instant. This can be done must simply by requiring that every node start its packet transmission at the same time and that every packet is the same length. Although simple, this scheme is somewhat inefficient.

The offset for each node between the beginning of its packet transmission cycle and the delimiting frame pulse would be inversely related to the node's fiber length. This would ensure that nth packet bit sent by each node would be received at the combiner at the same time. The calculation of this offset (S) for a given node, again based on the maximum node fiber length, follows:

$$S = \text{round}(T_{round\_trip\_MN} - T_{round\_trip}),$$

where

$$T_{round\_trip(n)} = 2.0 \times T_{one\_way(n)} + T_{synch\_delay(n)},$$

and MN and n reference the maximum node distance and the selected node respectively. Further,

$$T_{synch\_delay} = \text{trunc}(2.0 \times T_{one\_way}) + 1 - (2.0 \times T_{one\_way}),$$

and

$$T_{one\_way} = \text{fiber\_length} / \text{fiber\_transmission\_speed},$$

and

$$\text{fiber\_transmission\_speed} \approx 1.8 \times 10^8 \, \text{m/s}.$$

S will yield the first count on a revolving transceiver packet cycle wherein time is allowed for data bits, arbitration bits and a couple of channel switching delays.

| Maximum Round-Trip Fiber Length (m) | Minimum Segment Cycles | Minimim Segment Size — Switching Bits / Switching Time | | | | | | Segment Data Bits — Switching Bits / Switching Time | | | | | |
|---|---|---|---|---|---|---|---|---|---|---|---|---|---|
| | | 0 ns 0 | 0 ns 2 | 1 ns 3 | 2 ns 4 | 5 ns 7 | 10 ns 12 | 0 ns 0 | 0 ns 2 | 1 ns 3 | 2 ns 4 | 5 ns 7 | 10 ns 12 |
| 0.1 | 0 | 2 | 4 | 5 | 6 | 9 | 14 | 1 | 1 | 1 | 1 | 1 | 1 |
| 0.2 | 1 | 2 | 4 | 5 | 6 | 9 | 14 | 1 | 1 | 1 | 1 | 1 | 1 |
| 0.5 | 2 | 2 | 4 | 5 | 6 | 9 | 14 | 1 | 1 | 1 | 1 | 1 | 1 |
| 1 | 5 | 5 | 7 | 8 | 9 | 12 | 17 | 4 | 1 | 1 | 1 | 1 | 1 |
| 5 | 27 | 27 | 29 | 30 | 31 | 34 | 39 | 26 | 24 | 23 | 22 | 19 | 14 |
| 10 | 55 | 55 | 57 | 58 | 59 | 62 | 67 | 54 | 52 | 51 | 50 | 47 | 42 |
| 20 | 111 | 111 | 113 | 114 | 115 | 118 | 123 | 110 | 108 | 107 | 106 | 103 | 98 |
| 30 | 166 | 166 | 168 | 169 | 170 | 173 | 178 | 165 | 163 | 162 | 161 | 158 | 153 |
| 50 | 277 | 277 | 279 | 280 | 281 | 284 | 289 | 276 | 274 | 273 | 272 | 269 | 264 |
| 100 | 555 | 555 | 557 | 558 | 559 | 562 | 567 | 554 | 552 | 551 | 550 | 547 | 542 |

| Length (m) | Cycles | Packet Size: 1024 Nodes (10 A-Bits or Segments) — Switching Bits / Switching Time | | | | | | Efficiency: Data Bits Vs. Total Bits — Switching Bits / Switching Time | | | | | |
|---|---|---|---|---|---|---|---|---|---|---|---|---|---|
| | | 0 ns 0 | 0 ns 2 | 1 ns 3 | 2 ns 4 | 5 ns 7 | 10 ns 12 | 0 ns 0 | 0 ns 2 | 1 ns 3 | 2 ns 4 | 5 ns 7 | 10 ns 12 |
| 0.1 | 0 | 20 | 40 | 50 | 60 | 90 | 140 | 50.0 | 25.0 | 20.0 | 16.7 | 11.1 | 7.1 |
| 0.2 | 1 | 20 | 40 | 50 | 60 | 90 | 140 | 50.0 | 25.0 | 20.0 | 16.7 | 11.1 | 7.1 |
| 0.5 | 2 | 20 | 40 | 50 | 60 | 90 | 140 | 50.0 | 25.0 | 20.0 | 16.7 | 11.1 | 7.1 |
| 1 | 5 | 50 | 70 | 80 | 90 | 120 | 170 | 80.0 | 14.3 | 12.5 | 11.1 | 8.3 | 5.9 |
| 5 | 27 | 270 | 290 | 300 | 310 | 340 | 390 | 96.3 | 82.8 | 76.7 | 71.0 | 55.9 | 35.9 |
| 10 | 55 | 550 | 570 | 580 | 590 | 620 | 670 | 98.2 | 91.2 | 87.9 | 84.7 | 75.8 | 62.7 |
| 20 | 111 | 1110 | 1130 | 1140 | 1150 | 1180 | 1230 | 99.1 | 95.6 | 93.9 | 92.2 | 87.3 | 79.7 |
| 30 | 166 | 1660 | 1680 | 1690 | 1700 | 1730 | 1780 | 99.4 | 97.0 | 95.9 | 94.7 | 91.3 | 86.0 |
| 50 | 277 | 2770 | 2790 | 2800 | 2810 | 2840 | 2890 | 99.6 | 98.2 | 97.5 | 96.8 | 94.7 | 91.3 |
| 100 | 555 | 5550 | 5570 | 5580 | 5590 | 5620 | 5670 | 99.8 | 99.1 | 98.7 | 98.4 | 97.3 | 95.6 |

Note 1: First column data represent scenario employing separate arbitration xcvr and rcvr.

Note 2: Segment Format: A,S,S,...,D,...,S,S,...

### 2.2.5 Fairness

Recall that as the bit streams are combined from the nodes, it has the effect or "OR"ing the data. As a result, the protocol is complicated because it is not easy to detect a collision in a standard way. One way that does work is to arbitrate in a process of elimination mode, where the highest arbitration ID always wins.

For example, if nodes 1 (001), 4 (100), and 7 (111) are simultaneously trying to send to node 3 (011), their ID bits will arrive at the same time and be "OR'd" together. In this case it would be ( 0 OR 1 OR 1) = 1 (using MSB first).

Each of the three nodes waits to send its next arbitration bit until it gets the results of the first bit back. Node 1 can tell that other nodes are arbitrating and that their ID(s) are higher, so it drops out of the vie. Nodes 4 and 7 are still unaware of other contenders and continue. The next bit is (0 OR 1) = 1, which is observed by the two nodes and node 4 bows out. That leaves only Node 7 who sends out his last bit (1) and wins the arbitration cycle. The final bit is necessary since node 6 (110) may have also been vying. Since a node can't detect collisions, arbitration must be done as a process of elimination.

The problem with this scheme is that it is inherently unfair. That is, the higher the ID number, the more bandwidth each node would have available to it. Clearly, the arbitration IDs must rotate in order to assure fairness. There are at least three ways to overcome this problem:
(1) Generate a random sequence and have nodes pick up their number on each cycle,
(2) Have each node generate a random list that is exactly the same at all nodes so that every node has a random, but unique number each time, or
(3) Have each node generate a random number independent of each other, but assure uniqueness.

The first method has the obvious fault that distributing the numbers will be difficult and time consuming. The second method minimizes the bits required for arbitration, but has a potential synchronization problem. Since the network will operate plesiochronously, the slight drift in the local clocks will require that some sort of dead-reckoning be used to resynchronize the random numbers periodically. Although this could probably be solved, it would be a challenge.

The third method simplifies the arbitration synchronization considerably at the cost of adding extra bits. (Recall that the number of arbitration bits directly affects the minimum packet length and the arbitration latency.)

Our approach, the third method mentioned above, is to implement an ID randomizing scheme that entail alternately reversing the order of the ID's and the prepending 5 uniform randomly selected fairness and priority bits. This will allow us to assess the ramifications of such an approach given different configurations and physical parameters (e.g., number of nodes and fiber length).

### Approach
This analysis was an attempt to assess the relative fairness of using 'numbers' produced by prepending various numbers of randomly selected bits to static ID's or alternately reverse ordered ID's given the maximum channel contention scenario in which all nodes vie.

### Method
A Quick BASIC program was written to produce data for the two types of cases described above:

1. Prepending of X random bits to ID's, and
2. Prepending of X random bits to alternately reverse-ordered ID's,

where X was incremented from 0 or 1 to 6 for each successive case.

Simplifying the study, we used 4-bit ID's or 16 nodes which means that we were looking at 'numbers' in the range of 4 to 10 bits in length. We ran 20,000 trials for each case. The program calculated for each node a 'number' by essentially converting the binary sequence to a base 10 number value. The node drawing the largest number was identified as the winner of the trial. The total number of wins for each node was tabulated. Some other statistics were tabulated.

### Results
For a similar degree of fairness, the second type of cases, i.e., cases in which node ID's are alternately reverse-ordered, few prepended bits are required. Even with the improvement provided by reverse-ordering the ID's, the best second case scenario required more prepended bits than ID bits to yield "fairness" describes as less than a 5 per cent difference in the number of wins between the most winning and least winning nodes.

### Final Observations on Fairness
The idea of prepending "fairness and priority" bits is elegant in that this scheme allows nodes to independently generate unique 'numbers' for each packet cycle channel contest. The problem with this idea is that the number of

bits required to produce an acceptable degree of fairness may be greater than the number of node ID bits. Very quickly, you can envision very large contest 'numbers' and, so, very large packets as

1. Increasing the number of nodes on the network requires an increase in the number of bits needed to convey ID's (e.g., 16 nodes: 4 bits; 32 nodes: 5 bits and etc.),
2. Increasing the number of nodes and the corresponding number of ID bits requires an increase in the number of prepended bits for "fairness" (i.e., an increase in the length of the contest 'number'),
3. Each bit in a contest 'number' is conveyed as the arbitration bit for a single packet segment, and
4. Irrespective of "fairness" and the number of segments, each packet segment must be large to offset the overhead of carrying arbitration and switching bits.

### 2.3 Future Studies

Based on this project, the protocol does seem to behave properly, but a lot of work is needed before a full system is built. Specifically, what is the optimal packet length? What are the advantages of parallel ports? Is the power budget sufficient for a real system? How can a controller track the clock pulse? Can an optical detector determine the slope of a pulse? How are the nodes resynchronized if synchronization is lost? How do you turn off a chattering node? How many arbitration bits do you need? How do you overlay a more conventional protocol on top of the OTDM? How do you separate the data from the clock unambiguously? The answers to these questions are beyond the scope of the current contract.

### 2.4 Simulation

This project used the discrete event-modeling tool called BONeS Designer®, which is a powerful and flexible software solution for design and analysis of system architectures, networks, and protocols. BONeS models the protocol/messaging layers of a system. It can be used to define the system architecture--an abstract model that treats the system as a collection of shared resources (CPUs, buses, memory, database servers, etc.), queues and delays.
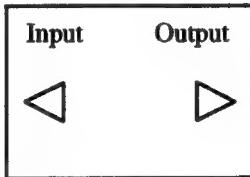


Figure SA-7: BONeS modules are all "Black Boxes"

BONeS permits top down or bottom up design, however, bottom up or a combination of bottom up/top down is probably most common approaches. Every functional block is represented as a "Black Box" in which there are inputs, outputs and some transfer function in-between. The transfer function is composed of either library functions or c code that executes one particular function. Simulations are typically hierarchical, so a top-level box might contain many layers underneath it. As events happen, tokens are generated which are then passed through the output ports to the input ports of the receiving node. In some cases, the event might be the passage of data itself.

One of the nice features of BONeS is that the tool is very abstractable, permitting a wide range of simulations to be created. In this project, BONeS was used to model an optical time division multiplexed (OTDM) computer network. Each OTDM component was modeled from the BONeS primitives provided in the tool, and then these components were snapped together to form a four node system. For more information on BONeS, see http://www.cadence.com/alta/products/newdatasheets/designer.html.

Since the primary goal of this exercise was to validate the protocol design, the four-node system was considered adequate. To show scalability, the model would need to be exercised with 100 – 1000 nodes. As might be expected, such a large system would have significant simulation time requirements.

See Appendix C for full set of simulation models and results. (Available only in the paper copies.)

## 2.5 System Level Advantages and Disadvantages

| Advantages | Disadvantages | Workaround for Disadvantage |
|---|---|---|
| No switch fabric contention. | Severe power losses throughout network | Low noise optical amplifiers either right before splitter or right after. |
| Allows electronics to run at convenient speeds, e.g., CMOS at 1 GHz. | Cost and labor associated with single mode fiber. | Automated pigtailing equipment, but might still leave field servicing difficult |
| Protocol Independent. Can lay many different protocols on the top of OTDM. (Can even run them concurrently if required.) | Non-hierarchical switch fabric would make extending the network difficult and expensive | Encode data packages with header addresses |
| Potentially Terabits/s aggregate bandwidth available (100 Gbits/s today) | Limited bandwidth scalability to 1/pulsewidth. Scalability beyond 500 Gbps doubtful in the near future. | No TDM workaround possible until technology matures |
| Permits asynchronous bandwidth distribution. | Protocol is clumsy may result in long arbitration delays. | Keep fiber length to a minimum, preferably all the same length. |
| Supports *both* message passing and shared memory models. | Protocol will need relatively long packets to remain efficient. Also, need high-speed NIC to keep up with data rates. | No work around due to "OR"ing at combiner |
| Constant Switch Latency of 2-5 nsec. | Arbitration may be substantial which may make overall latency long | Keep packets long, do look-ahead arbitration, and keep fiber lengths short |
| Physical limitation of node-to-hub distance of up to 100m | Protocol should logically work for nodes far away, but performance will suffer | No work-around because of "OR"ing at combiner. Fiber length translates into arbitration delay. |
| Permits future speed up of electronics. Either as complete system replacement or as an incremental upgrade. | Heterogeneous incremental upgrade only possible as factors of 2. Slower nodes would reduce network efficiency | No work-around. Slower elements can operate at half frequencies, but results in lost bandwidth. |
| Has potential to provide *revolutionary* new networking capability for commercial systems (and military). | High bandwidth combined with very local proximity requirements narrows the applicability of technology to a very narrow market. As a result, the price is likely to remain noncompetitive. | A market is needed to drive the cost of the components. No easy work-around known. |
| Concurrent transmit and receive at full data rate. | Broadcast is difficult. | Need extra arbitration bits that in turn will drive up the packet size and arbitration delay. |
| Allows optics to do what they are good at and electronics to do what they are good at. | Connectors, switches, and inherent device losses mean that this is a suboptimal application for photonics. | These problems will lessen with maturity but may never fully abate. |
| Decreased System Weight, Power, Size, life cycle costs. | Individual Components are relatively large at this time. LCC cost improvement requires that component prices come down. | Miniaturization is probably possible, but requires investment. Component cost reduction requires volume. |

# 3. Optical Device Analysis and Report

## 3.1 Background

### 3.1.1 Overview of all-optical switching technologies

All-optical switching technologies are one of the keys necessary to realize a high-speed time division multiplexing-demultiplexing system. While fiber-based nonlinear optical loop mirrors (NOLM) have been demonstrated using Sagnac interferometers, the optical nonlinearity of the fiber is so small that the NOLM typically requires up to kilometer long fiber lengths. Shorter fiber lengths have been obtained by replacing the long fiber length with a nonlinear element (a semiconductor amplifier), thus creating the first terahertz optical amplifying demultiplexer (TOAD) switch. The principle of the NOLM is maintained, however and the size, operation, and practicality of the device are crucially dependent upon the length of the fiber and the cost of the amplifier. These factors make small, low cost, environmentally robust, time-division-multiplexing systems difficult to develop. In contrast, we proposed to construct an integrated TOAD switch that allows high speed all-optical switching and permits electronic input for feedback from both temperature sensors and from other timing systems to allow small scale adjustment of the system for drift in repetition rates. Such timing adjustments can be very important in high-speed time division multiplexing systems. The goals of our development program were: 1) to demonstrate the required switching functionality, 2) to formulate a development path to future enhanced devices, 3) to create devices which are consistent with high yield and at low cost (i.e. manufacturable in large numbers).

### 3.1.2 Introduction to the Mach-Zehnder geometry

The Mach-Zehnder interferometer geometry is one which permits optical intensity through changes in a material's refractive index. A schematic of a generic integrated optical Mach-Zehnder interferometer is shown in Figure BG-1. In such a system, light is input into a waveguide and is split into two branches. The two light beams travel through independent control sections. These control sections consist of waveguide regions that can be modulated in such a way that the refractive index of the section can be changed. This can be done electronically or optically as described below. The final incarnation of the integrated TOAD device was intended to rely on both of these control mechanisms. By controlling the refractive index of a material, the optical phase of a traveling optical wave can be adjusted. This is because the effective optical path length of the control region is a function of the refractive index. This makes sense because the wavelength of light in a material, $\lambda m$ is a function of the wavelength in free space $\lambda o$ and the refractive index in the material, n ($\lambda m = \lambda o / n$).
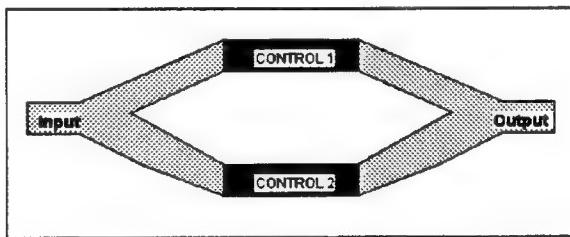


Figure BG-1 Schematic of a generic Mach-Zehnder interferometer

If the relative phase between the two optical signals is zero, the two beams will meet at the output and constructively interfere. Thus the two light beams will add together and give a large optical output. If, however, the relative phase between the two branches is changed to $\pi$, then the two output beams will destructively interfere (they will be completely out of phase). In such a case, when the beams combine at the output, the two out of phase beams cancel one another and the output displays zero amplitude. Thus in a system, the interferometer could be constructed to normally have the two light beams destructively interfere—and thus give zero output--unless a control pulse was used to alter one or both of the two branches to create constructive interference and allow signals to pass through.

### 3.1.3 Operation of quantum wells

**What are excitons?**

In semiconductor materials, the lowest order absorptive edge is at a wavelength that is slightly below the bandgap of the material. In fact, it occurs below the bandgap at an energy that roughly corresponds to the binding energy between a single electron and a single hole. This absorption 'resonance' is quite strong and is attributed to an excited electrical state called an exciton. An exciton is, essentially, semi-extended polarization of a semiconductor crystal over length scales of about 100 angstroms. The total dipole moment of this semi-extended state is mathematically equivalent to the dipole moment of a single electron and a single hole bound together by Coulomb attraction. Such an absorptive resonance would be little more than an interesting effect were it not for the fact that the properties of these absorptive resonances can be controlled either electronically or optically. It is this control which allows our integrated TOAD devices to operate. Excitons exist in both bulk and quantum well structures, although the additional electronic potential profile afforded by quantum wells strengthens this resonance.

**Modulation of semiconductor absorptive properties**

<u>Franz-Keldysh Effect (bulk materials) / Quantum confined Stark Effect (quantum wells)</u>

In both bulk and quantum well structures, applied electric fields can modulate the absorptive properties of the semiconductor material. In bulk materials, a material's absorptive edge is modified through the Franz-Keldysh effect. This is shown in Figure BG-2. With zero applied bias, the semiconductor has an absorptive energy ($E_0$) approximately equal to the bandgap (minus the exciton binding energy that is small in bulk materials). With applied electric field, the semiconductor bands tilt. This allows photons with energies less than the bandgap, ($E_1$), to be absorbed. The electrons that are promoted by energy E1 are influenced by the applied electric field and can quantum mechanically tunnel into the conduction band of the semiconductor. E1 is lower in energy than E0, so the absorptive edge of the material is shifted to lower energy (longer wavelength) with applied electric field. This is shown in Figure BG-3
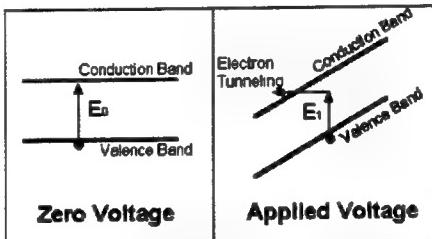


**Figure BG-2: Franz-Keldysh modulation.**
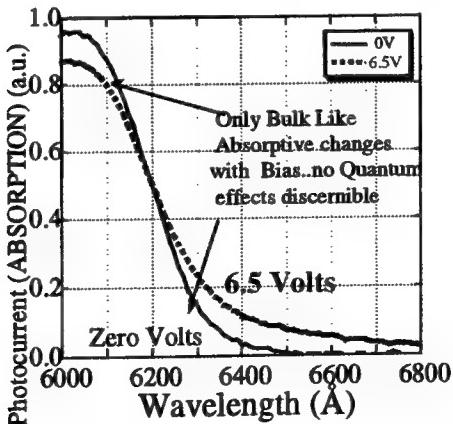


**Figure BG-3: Franz-Keldysh absorptive plot.**

A quantum well is essentially a 2 dimensional 'bulk' material. The properties of electrons and holes in 2 dimensions are fundamentally different from their properties in 3 dimensions. Electrons and holes take on highly quantized energy levels, analogous to the quantized levels in sparse atomic systems. Figure BG-4 shows the

14

absorptive properties of quantum wells. With zero applied bias, the absorptive transition is between two predominant quantized states—one in the conduction band and one inside the valence band. This transition occurs at some well-defined energy ($E_0$) that corresponds to the energy difference between these two states minus the exciton binding energy which can be on the order of 10 meV. The energy resonance of this state leads to a characteristic highly resonant exciton absorptive resonance in quantum wells. With bias, the energy bands of the semiconductor shift. This causes three things to occur.

1) The energy levels in the quantum wells move; the absorptive resonance shifts to energy level $E_1$, which is less than $E_0$.

2) The overlap between electron and hole probability amplitudes decreases. This causes a decrease in the absorptive resonance level.

3) The electron and hole wavefunctions sample the quantum well barrier more. The roughness at the interface at the atomic level causes exciton broadening.

The resultant behavior is shown in Figure BG-5. With applied electric field, large changes in absorption can occur over wide wavelength ranges.

## Zero Applied Bias    With Applied Bias
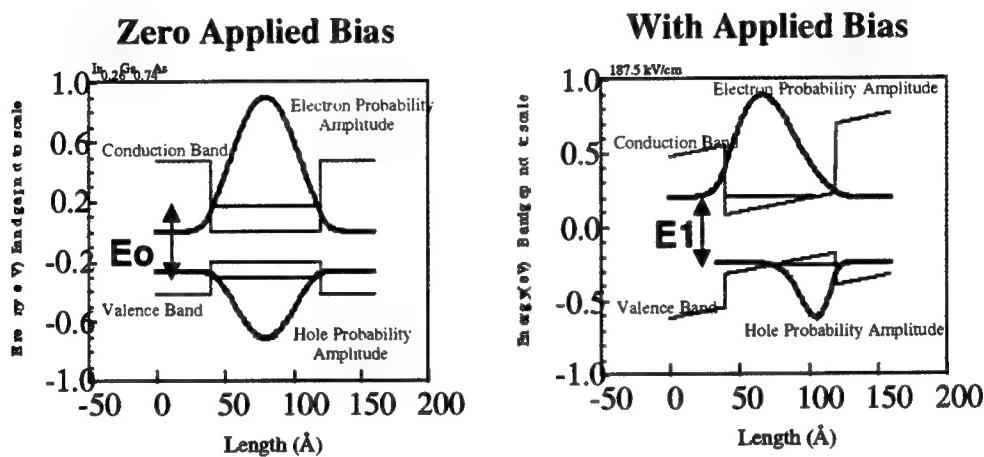


Figure BG-4: Quantum confined stark effect operation
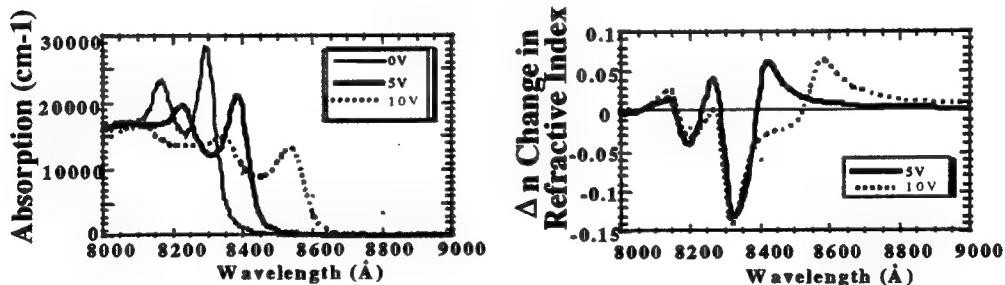


Figure BG-5: Quantum confined Stark effect: (left) absorption and (right) dispersive changes with applied voltage

These types of switches, operationally equivalent to GaAs spatial light modulator pixels, are usually fabricated by placing the active region in the intrinsic region of a p-i-n diode which is reverse biased to apply electric field. Switching speed is limited by the RC time constant associated with charging up the device and, in traveling wave modulators, by the difficulty in keeping propagation times between electrical and optical signals in phase. Speeds of nearly 50 GHz have been demonstrated with speeds of 100 GHz proposed.

### Optical control of semiconductor properties

The above techniques depicted the effect of electric field on the properties of semiconductor materials. Optical pulses can be used to control the behavior of these semiconductor materials. Such switching has the potential to increase the switching speed considerably. Switching in these types of devices rely on traveling wave

15

switch configurations—where the control pulse and the signal pulse travel down the same waveguide structure. Thus the switching time can be fast, but the interaction length between control and signal can be long. This is analogous to pipelining architectures in computer architecture where processing can be performed quickly instantaneously although any particular operation could take many clock cycles to complete. The main physical mechanisms for switching are the AC Stark Effect and Phase Space Filling.

## AC Stark Effect

The AC Stark effect is based upon the principle that light injected slightly below the bandgap of a material can control the absorptive properties of the material at the bandgap edge. This is schematically shown in Figure BG-6. If the normal absorptive edge is at $E_0$, then with input light just slightly below $E_0$, the absorptive edge is shifted to $E_1$. Because of the high input optical powers required, and the relative immaturity of devices based upon this technique, the baseline approach for this program did not rely on this effect.
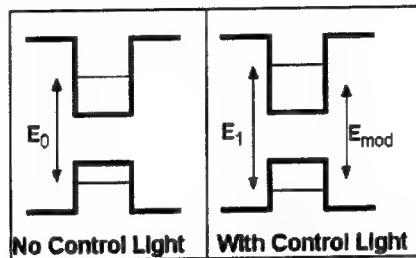


**Figure BG-6: AC Stark Effect**

## Phase Space Filling

In our desired approach, the input control light can occur above the bandgap. In such a situation, the control pulse is absorbed by the input control signal. This absorptive process generates a lot of photocarriers in the semiconductor which fill up the available absorptive states in the semiconductor. This 'phase space filling' eliminates the available energy states into which electrons can be promoted after absorbing a photon. As low energy states fill up, the percentage of free low energy states is reduced while many higher energy states are available. Thus the absorption at the original bandgap is reduced and the high absorption band edge of the material is effectively shifted to higher energy. Because of carrier recombination and sweep out, there will always be some low energy states available, but their numbers will be considerably reduced—the absorptive properties of the material are thus significantly affected. Control power levels of a few picojoules with short pulses (less than 1ns) are consistent with operation on reasonably long waveguides (400µm to a couple of millimeters). Figure BG-7 depicts schematically this process in both bulk and quantum well materials while Figure BG-8 demonstrates schematically the behavior of the absorptive process with application of the pump beam.
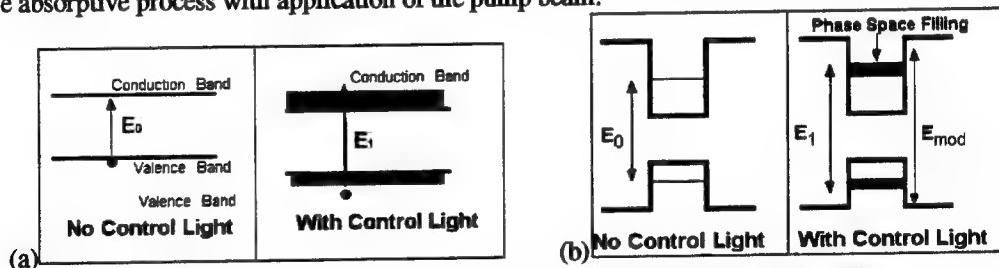


**Figure BG-7: Phase Space Filling with (a) bulk and (b) quantum well material**
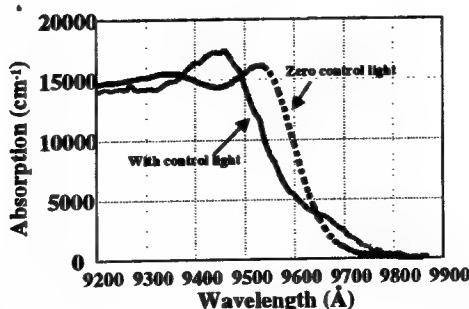


**Figure BG-8: Schematic of phase space filling effect**

16

Quantum well and bulk semiconductor absorptive properties can be modulated via both electrical and optical control signals. The electronic control signals are limited in speed by the RC time constant of the electrical device. Optical control signals can be operated very quickly. In fact, using phase space filling techniques, switching with an on-off interval of less than 6ps has been demonstrated. This exceeds our current system needs.

Kramers-Kronig Relationship

The optical switching devices proposed are based upon changes in refractive index. The bulk and quantum well modulation properties were described above as changes in absorption near the band edge. Absorption and refractive index are intimately related physically; both are two parts of the same microscopic dipole effects. Mathematically, the real and imaginary parts of a material's complex susceptibility related by the Kramers-Kronig relationship. In semiconductors, in our wavelength region of interest, the Kramers-Kronig relationship can mathematically closely relate the changes in absorption and changes in refractive index via the following:

$$\Delta n(\lambda_0) = \frac{C}{\pi} \, P \int d\lambda \, \frac{\Delta \alpha}{1 - (\lambda/\lambda_0)^2}$$

Where n is the refractive index, C is the speed of light, $\lambda$ is the wavelength, $\lambda_0$ is the particular wavelength of interest, and P indicates the principle value of the integral should be taken. The Kramers-Kronig formula is the mathematical expression that indicates that the changes in absorption being induced at the bandgap also cause refractive index changes below the bandgap of the material—in the region where absorption is small. Thus, the signal pulses can propagate with little absorption and have their phase changed appreciably. For example, in Figure BG-5, at a wavelength of 8800 angstroms, the absorption with bias is low for all bias points, but refractive index is changed with bias.

### 3.1.4    Device Operation and Issues

**Operating Principle**

The device operation for the integrated TOAD is based upon combining the technology and physical mechanisms described above. All of the mechanisms above have been experimentally demonstrated independently by several groups and have produced viable devices. In particular, waveguide optical switches have been experimentally demonstrated and have switched 6ps pulses. Electro-optical modulators using the Franz-Keldysh and/or quantum confined Stark effects have been demonstrated with speeds up to 50 GHz. Mach-Zehnder interferometers have been built in a variety of materials from Lithium Niobate to GaAs. By refining the all-optical switching techniques for manufacturability and by integrating electrical control with optical control in these devices, we obtain a robust field deployable system. Such a device would use optical switching to produce high speed data selection of bits from each data frame while the electrical control would allow for small scale timing jitter and temperature correction—as well as for the integrated device to be electrically compensated for standard manufacturing variation. Thus, we obtain an extremely high yield product that will drive down device and thus system costs considerably. Larger timing and temperature variations can be compensated with the delay line structure incorporated as part of the LAN system.

**Operating Issues**

One concern with all TOAD systems—fiber based and integrated device based—is the recovery time of the switching event. In the integrated device case, when the control optical pulse travels down the waveguide device, it generates carriers that cause phase-state filling which changes the refractive index of the device locally; this affects the signal pulse. However, in order for the device to 'recover', the carriers must be removed from the device. Usually this occurs through simple recombination mechanisms. In contrast, our devices were designed to use a combination of simple recombination and carrier sweep out through the electrical contacts on our device. The use of electrical contacts significantly enhances the speed at which these devices can operate. Switching turn-on behavior is very fast, but turn-off time is ultimately limited by the carrier removal time.

However, turn off times *can* be made independent of carrier removal times by using two control inputs. This further enhances our high speed switching capability as follows. A single control pulse down one of the branches changes the refractive index in that branch and turns the device 'on'. Then, instead of waiting for carrier removal to turn the device off again, a second control pulse is quickly inserted into the second input line. This changes the refractive index in the second line in the same way as the first line. Thus the two lines are excited with

17

carriers, but are nearly equal in response. Thus the device turns 'off'. Both lines' carriers decay in the same fashion and the device recovers for the next switching event. Thus there is still a recovery time associated with the device, although the framing method for our TDM system gives ample time for this recovery to occur.

## 3.2 Technical Summary

Optical switching can be achieved through small changes in refractive index. By combining changes in refractive index with long path lengths, changes in an input optical signal's phase and/or wavelength can be achieved. Changes in refractive index can be induced in many ways. We have discussed four of these modulation techniques the Franz-Keldysh effect (bulk semiconductors), the quantum confined Stark effect (quantum well material), the AC Stark effect, and phase space filling. Where the former two use electrical control and the latter use optical control to achieve changes in the absorptive properties near a semiconductor's bandgap and, consequently, change in refractive index below bandgap. These changes are well known and have been experimentally demonstrated. If a waveguide is created of semiconductor material and optical signals are launched down this waveguide, the phase of the traveling optical signal is changed by these changes in refractive index. Phase changes are dependent upon: input wavelength, optical control pulse intensity, electrical control voltage, the dimensions of the waveguide, and the coupling mechanism of the optical control pulse.

While this represents an enormous design parameter space that could not be completely covered, detailed simulations, extensive prior experience in the field, and a conservative and iterative design approach all allowed us to converge on an acceptable design solution. Our design focused on using either the Franz-Keldysh or quantum confined Stark effect for electrical control and on phase space filling for optical control.

Changes in phase can be easily used to perform the demultiplexing operation we desire. When two optical beams combine in-phase, they combine to allow the input signals to pass through. When two optical beams combine out of phase, they cancel each other out and prevent data from being transmitted. By creating two parallel waveguides, control signals can determine whether the phase change is equal or disparate between the two waveguides. By creating a system in which the normal mode of operation is for the beams to cancel, then control pulses in a single waveguide can cause in-phase operation. This turns the switch 'on'. The switch can then be turned off by either sweeping out generated photocarriers and/or by using a control pulse in the second waveguide to balance the system.

A Mach-Zehnder interferometer is a construction which allows inputs of control and signal pulses into two waveguides and combines the output of the waveguides in a specific manner. While two straight waveguides would be sufficient for operation and demonstration of our device operation, (by using external optics to create a Mach-Zehnder interferometer) the formation of a monolithic Mach-Zehnder simplifies packaging and will ultimately reduce costs.

The ultimate goal of the device development was to create an Integrated Terahertz Optical Asymmetric Demultiplexer which had the potential to be commercially produced. As such, we tried to minimize labor intensive or environmentally sensitive features such as pigtailing and Semiconductor Optical Amplifiers and maximize tolerance to fabrication and packaging errors.

The overall approach we have decided to take with our devices is illustrated in Figure TO-1. As shown in the figure, the signal light will travel through the waveguide, while the control light will impinge upon one of the branches of the switch from the top. We have designed devices to allow for operation when the control and signal wavelengths are different as well as when they are the same. This second method may be more difficult as there is a tradeoff-- the signal light should not be absorbed and yet the control light (at the same wavelength) must be absorbed to change the refractive index).

Control In (514, 860, 905 nm)

lens3

Signal In (905 nm)

lens1

$V_{bias}$

spot size:
5 x 500 micron

5 micron

10 micron

500 micron

lens2

Signal Out (905 nm)

| Control/Signal Beam Matrix | |
| --- | --- |
| Control | Signal |
| 860nm | 905nm |
| 514nm | 905nm |
| 905nm | 905nm |

5micron

0.5-5.0 micron

Note:
lens1: focusing lens (0.5 x 5 micron)
lens2: collimating lens (device ouput: 0.5 x 5 micron)
lens3: focusing lens (5 x 500 micron)
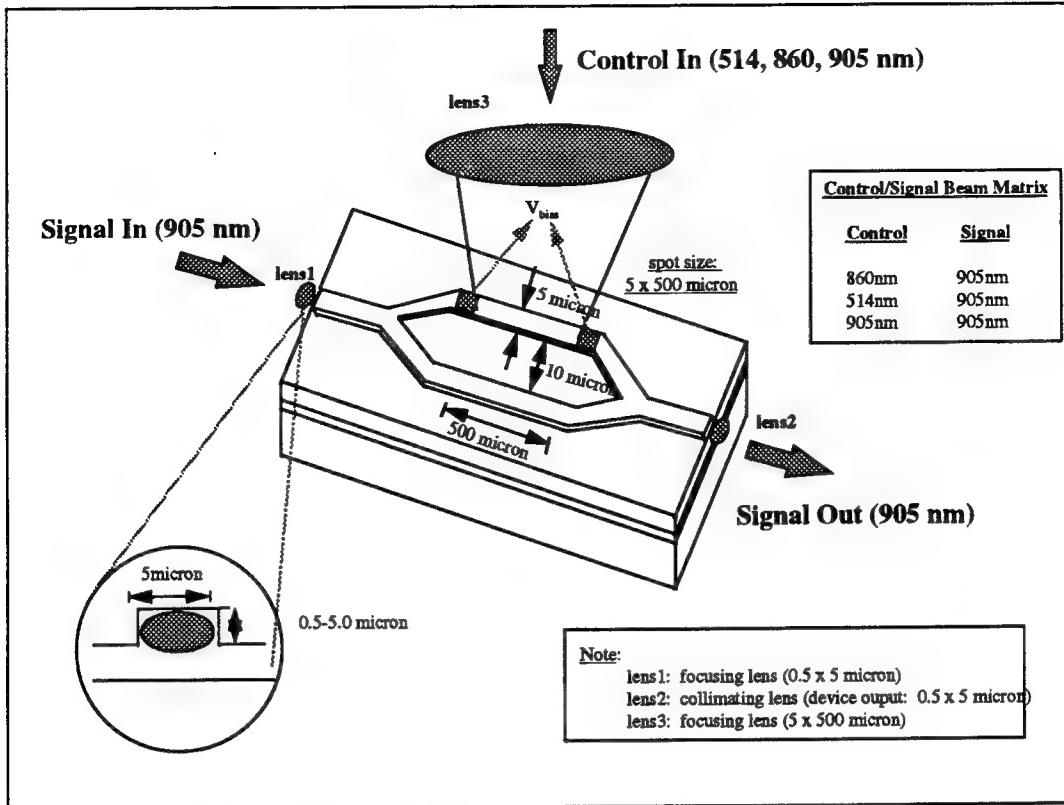
Figure TO-1: Mach-Zehnder demultiplexer development

## 3.3 Device Process Flow Description

After the growth of a wafer, it is cleaved into quarters. This allows for efficient use of material and feedback adjustments to the process.

Mesa isolation involves photoresist patterning and dry etching. The exposure is adjusted to vary the width of the waveguide (by 0.5 μm to 1.0 μm) so that a new mask need not be made. The width is a key factor in controlling the number of modes of the light propagating down the waveguide. Next the mesas are dry etched (in SiCl4). The etch depth (a small amount into the undoped region) affects the effective refractive index change, which is designed to obtain single mode transmission. Then a brief wet etch (~0.1 μm) is used to undercut the photoresist to make liftoff of the subsequent dielectric deposition easier. The dielectric, zinc sulfide (ZnS), was used after a low temperature nitride failed to withstand the ohmic metal anneal. The function of the dielectric is to isolate the metal runs (which contact the top of the mesa) from the undoped and doped lower layers. The ZnS is lifted off after deposition. This self-aligned process leaves the top of the waveguides without dielectric so contact can easily be made and metal lines run to large bond pads.

Next, the photoresist is patterned to lift off the ohmic metal. The metal contacts the top of the mesa (n-type) at two points and runs over the side and out to the bond pads. After the ohmic metal is evaporated, more gold is sputtered to give good step coverage up the sides of the mesa. Rapid thermal annealing is done after the metal liftoff process is completed. The resulting contacts are probed to confirm that they are ohmic. Note, the anneal does not drive the metal through the dielectric.

After photolithography the pattern for the bottom (p-type) metal is first used to etch the ZnS. For the shallower mesas it was then used to either wet or dry etch down to the bottom cladding (p⁺), before the substrate (bottom) contact was made. After liftoff the contacts were probed to confirm that they were linear and low resistance.

The branches of the waveguides are electrically isolated by opening windows in a thick photoresist pattern and doing several implants (with protons and oxygen down through the top doped cladding region). After cleaning

19

the wafer, electrical probing is done to confirm that isolation exists and that the resulting diode I-V curves were strong and diode-like (minimal leakage).

Finally, sections of material are cleaved out and mounted onto ceramic in a package with easily connectable leads. After wire bonding (from material to package), the package is mounted onto a convenient fixture for optical testing.

We altered our process slightly to correct a yield problem we were having with the ion implant (the photoresist was reflowing and bubbling on some spots on the wafer). The adjustment we made essentially used thinner photoresist and hardened it somewhat before the implant and was successfully implemented. We also employed a pattern generator to make local changes on individual devices (such as placing gold in between the arms of the interferometer or masking that area for an implant to prevent carrier diffusion between the two arms). This machine is used as an alternative to ordering another mask set (and is thus less expensive). This process was successfully tested and implemented on our second-generation wafers for the purpose of placing gold between the arms of the interferometer.

## 3.4 Simulation

We initially used a 2-dimensional beam propagation program written in FORTRAN to simulate various Y-branches and Mach-Zehnder devices before the structures were fabricated. The algorithm used has been described in the literature by Yevick et. al. After several simulations, coupled with what can actually be defined by a mask layout program, we settled on the structure shown in Figure SS-1. This figure is exaggerated in the vertical direction for visibility. The angles involved, as shown in the figure, are quite small, on the order of 2-4 degrees. These angles were reduced to smaller values in the second generation (0.8-1.5 degrees). The critical portion of this structure is the Y-branch, which must produce near to a 50-50 split of the input light. Both the 2-D simulation and the later 3-D simulation indicated an equal splitting ratio between the two branches and approximately 10% loss. Simulations of the full Mach-Zehnder device were also performed with this 2-D program, but their accuracy depended somewhat on the material properties of the devices we grow, in particular the amount of refractive index change with input power $n_2$. Our literature search indicated a range of values for this number. By varying our control light intensity and spot-size, as well as the wavelength of the light, we planned to be able to optimize the switching ratio at the output of the device. The 2-D simulation proved to be inadequate and the 3-D version was poorly written in terms of memory use and ease of input construction so we decided to use a commercial waveguide design tool (BEAMPROP from RSoft Corporation, Ossining, New York).
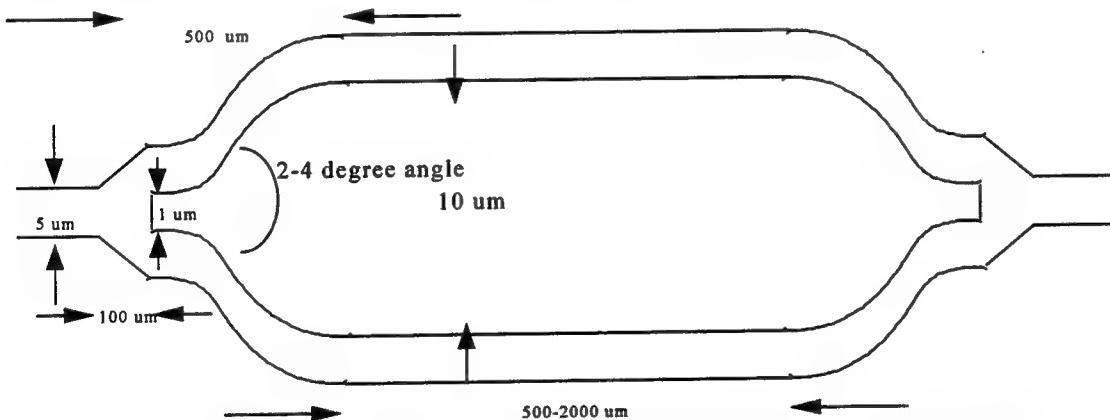


**Figure SS-1: Structure of Mach-Zehnder device: dimensions vary to some extent**

To overcome the limitations of 2-D approximations of 3-D structures in our simulations, we used beam propagation software written by RSoft Corporation to refine our devices for the second generation. This software allowed us to model much more exactly how our devices should work and enabled us to find some of the problems with our first generation devices. Included with this report is a CD containing 4 AVI files. The first of these files includes a brief description of the software and its capabilities. The second file shows a sample real-time simulation of the 'ON' state of one of our Mach-Zehnder devices at a lower resolution (to speed up the simulation). The third file is the 'OFF' state simulation for the same device. The last file shows a few more capabilities of the software as well as the output of the 'OFF' state displayed in another format.

In terms of the actual parameters used for the simulation, we provide the following information: 1. the epitaxial structure of our devices which includes the layer thicknesses for the simulation, 2. the top view dimensions of the device (shown in Figure SS-1), 3. indices of refraction for the epitaxial layers (from the literature), and 4. other important distances and parameters. Figure SS-2 shows the epitaxial structure of our waveguide (after etching) along with the calculated single mode profile. The aluminum compositions and indices of refraction (at 905 nm, the wavelength of our signal laser) are shown in Table SS-1. Other values of index of refraction were also used to explore operation at wavelengths other than 905 nm. The device was designed to work over a range of wavelengths (from 860-910 nm).

|  | Al composition | Index of refraction |
|---|---|---|
| **Bulk core** | | |
| n-cladding | 0.13 | 3.494 |
| p-cladding | 0.13 | 3.494 |
| core | 0.0 | 3.589 |
| inner core | 0.01 | 3.580 |
| | | |
| **Quantum well core** | | |
| n-cladding | 0.185 | 3.46 |
| p-cladding | 0.185 | 3.46 |
| core | 0.095 | 3.517 |
| inner core | 0.085 | 3.523 |

**Table SS-1: Aluminum compositions and indices of refraction (at 905 nm)**
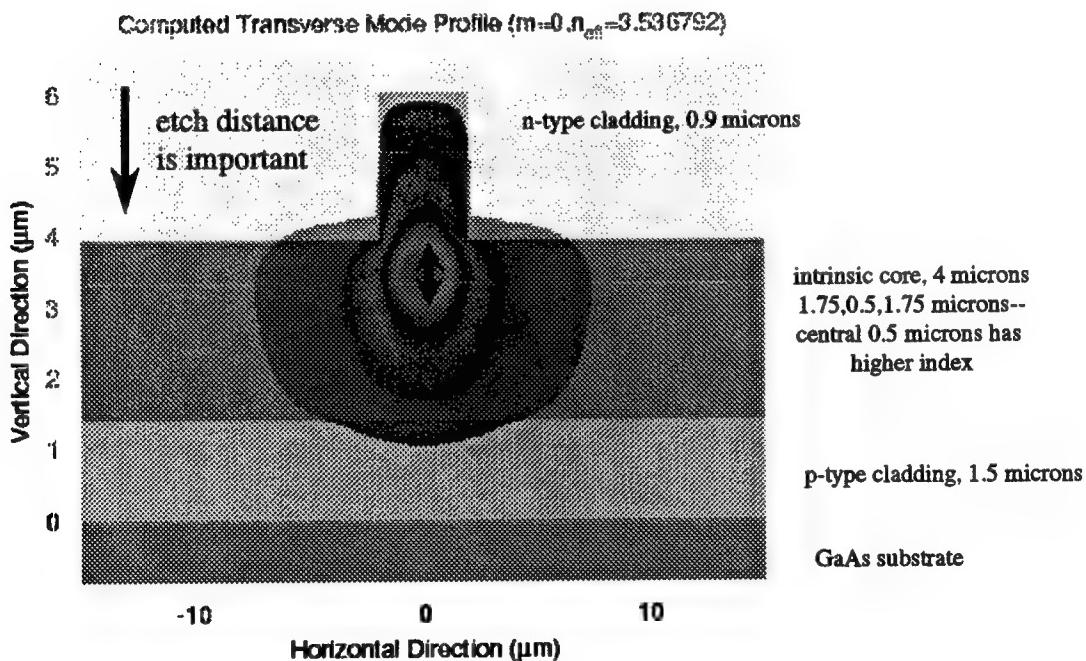


**Figure SS-2: Epitaxial structure and calculated mode profile of waveguide**

The top dimensions shown in figure SS-1 vary somewhat depending on the specific device tested. The important distances and their ranges are: 1. waveguide thickness (3.5-5.0 microns, controllable by photolithographic exposure, narrower is better), 2. branching angle (0.8-2.0 degrees, smaller is better), 3. maximum distance between guides (12-22 microns, larger distance means less coupling), 4. straight waveguide branch length (250-500 microns). The branching sections of the waveguide were cosinusoidal in shape and were defined at higher resolution on the masks.

Other important parameters include the etch depth, the resolution of the simulation, the wavelength, and the loss of the core material. The etch depth was chosen to make the guides single mode (too deep allows multiple modes, too shallow does not guide the light. The simulations were performed at a variety of resolutions, typically 0.01 microns in the best cases, resulting in simulations that ran in 30-45 minutes. Wavelengths between 860 and 910 nm were simulated. The loss in the material was varied between 0 and 20 $cm^{-1}$. The difference between the 'on' and the 'off' states was obtained by either raising or lowering (thermal or high speed effects) the refractive index in one branch of the interferometer by an amount calculated to result in pi phase change over a distance corresponding to the control beam spot size. The amount of change was also dependent upon what we believed to be the value of $n_2$ in the material. A variety of fields were launched into the device (Gaussians, calculated modes, fiber modes, and fields at an angle) to determine the effects upon contrast. The device should have resulted in a contrast ratio of at least 3:1 in the worst case we could envision (large Gaussian mode, off center and at an angle). The accompanying CD AVI files should give you a feel for the simulations performed.

Figure SS-3 shows the simulated on (top) and off (bottom) states of a Mach Zehnder switch (the two lines in the right figures indicate the amount of power in each branch of the switch vs. distance). The light is input at the bottom of the graph and propagates to the top. This simulation indicates very high contrast and is somewhat idealized. We have been able to model some of the effects of nonidealities on our contrast ratios using this software, and continue to do so. These include misalignment at the input (resulting in non 50/50 splitting ratio and more noise), absorptive changes between the two arms (also limiting contrast ratio), and other effects. This software also outputs the structure in mask layout format, so that what we simulated can be put directly into the mask layout.
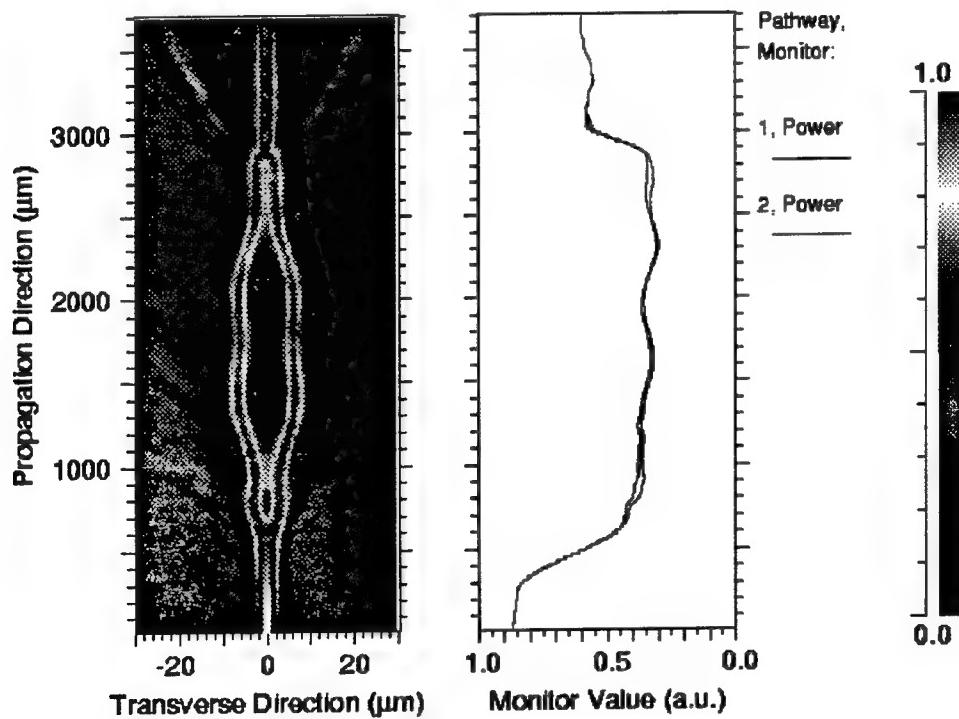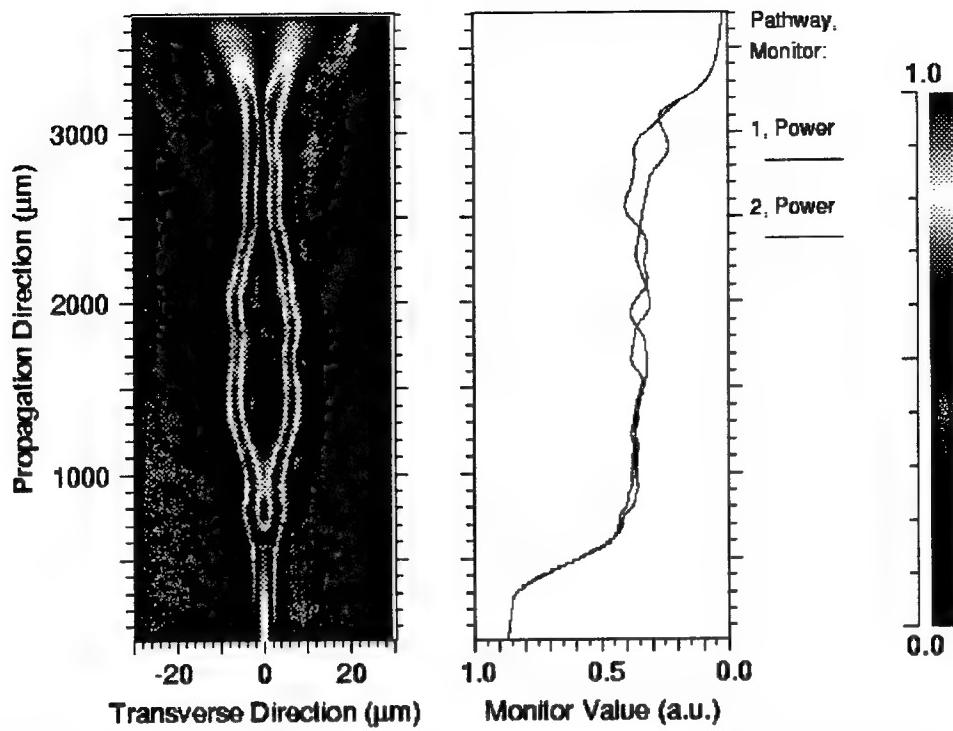
**Figure SS-3: Simulated output of second generation Mach-Zehnder device on (top) and off (bottom) states**

A significant design challenge exhibited in our first generation devices is the fact that in changing the refractive index of one arm of the switch, you must also change its absorption (as they are related by the Kramers-Kronig transformation). In order to overcome this, we must be able to apply bias to our structures (with no control light) to minimize the output as much as possible. Figure SS-4 shows the output of a Mach-Zehnder device in which the initial splitting ratio is 50/50. As control light is applied to one arm, the absorption increases and the refractive index changes. The output has been plotted vs. the amount of light remaining in one branch (50% on 1 side, 0-50 in the other) and the phase difference between the two arms. As you can see from the figure, you must start as near 50/50 and $\pi$ phase change as possible to obtain high contrast. This turns out to be somewhat difficult in reality, and we are working on this problem in the second-generation devices. Figure SS-5 shows a case where the initial splitting ratio is not 50/50 and where the minimum lies in that case (i.e. where you would like to preset the device using bias to obtain optimum contrast).

**Mach Zehnder Output, Initial Splitting Ratio 50/50**
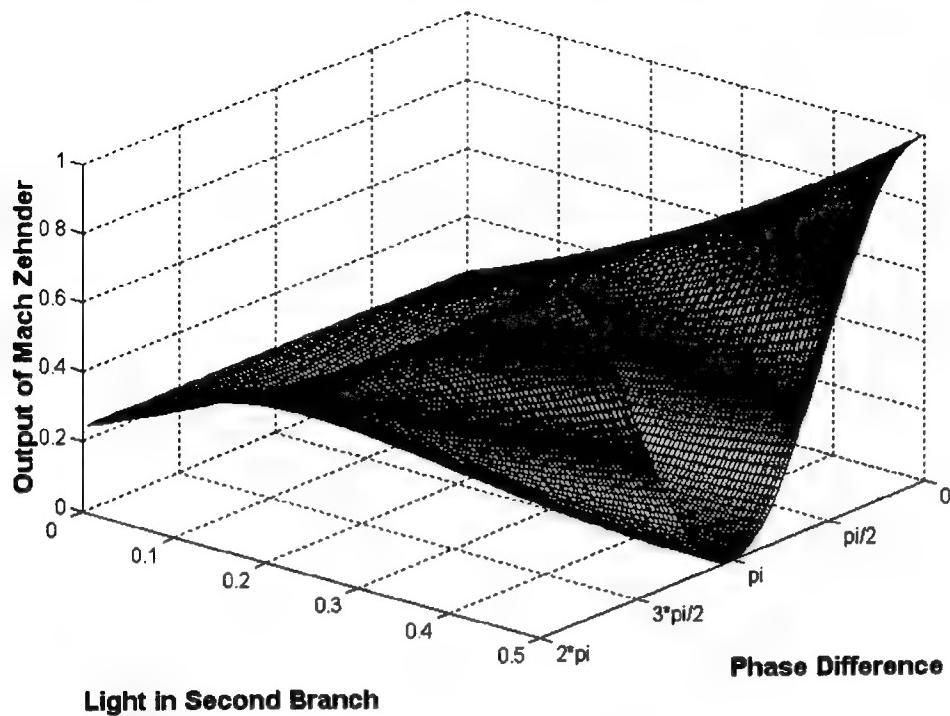


**Figure SS-4: Mach-Zehnder output vs. phase difference and intensity difference, initial split 50/50**

**Mach Zehnder Output, Initial Splitting Ratio 70/30**
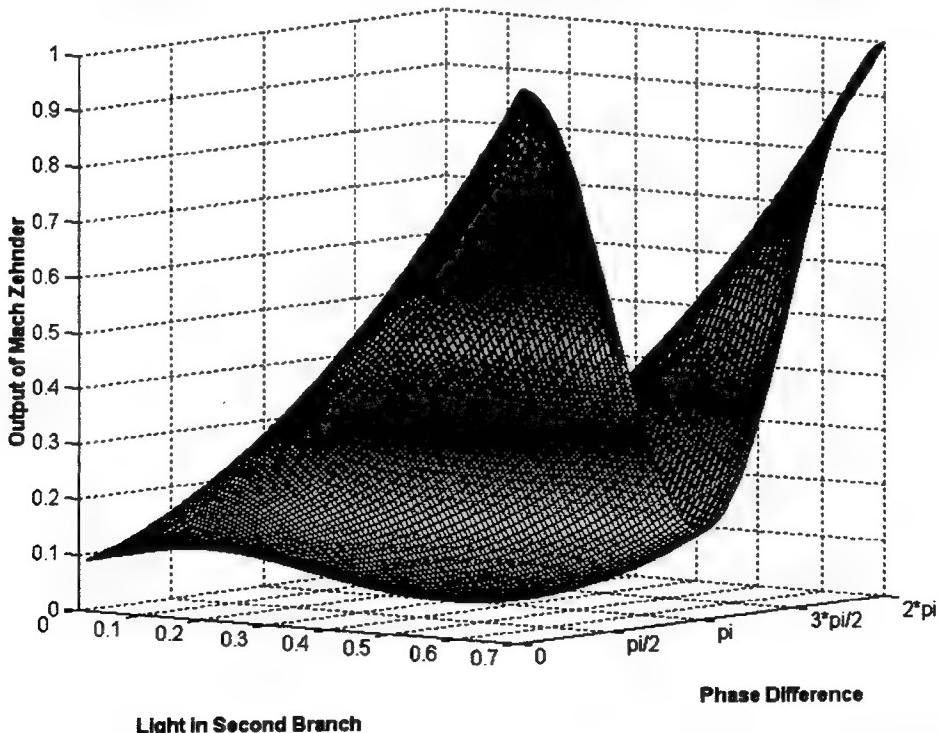


**Figure SS-5: Mach-Zehnder output vs. phase difference and intensity difference, initial split 70/30**

### 3.5  Test Plan

The waveguide devices were evaluated in two iterations of testing.  The test setup was constructed and optimized by using the existing Sanders' waveguide test structures. The test setup was further optimized during the device testing as necessary.  Both generations of Mach-Zehnder prototype device characterization included high speed testing at Boston University using their picosecond pulsed laser.  In this section of the report we will describe our test procedures and experimental setup—essentially a summary of our test plan.

### 3.5.1  Experimental Setup

The test setup shown in Figure TS-1 was constructed to evaluate all waveguide test structures and Mach-Zehnder prototype switching devices.  The most critical step in the test is to position a device-under-test (DUT) in the focal plane of the input focusing objective lens.  The longitudinal, lateral, and angular misalignment does degrade the device performance, especially the coupling loss and Y-branch splitting ratio.  Device alignment for both input and output signal couplings was achieved with input/output beam monitoring CCD cameras.  The lateral alignment of signal and control beams in the waveguide structure was observed from the top of the device with another CCD camera.  A pair of half-wave plate and polarizer was used to adjust the optical power without altering the polarization angle. A detector measured the signal and control optical power.  The half-wave plate placed in just before the input coupling lens alters the polarization angle of input signal.  The darker colored beam path was used to measure the transmission, switching contrast ratio, and switching speed.  A Mach-Zehnder interferometer beam path is designated with the lighter path in  Figure TS-1
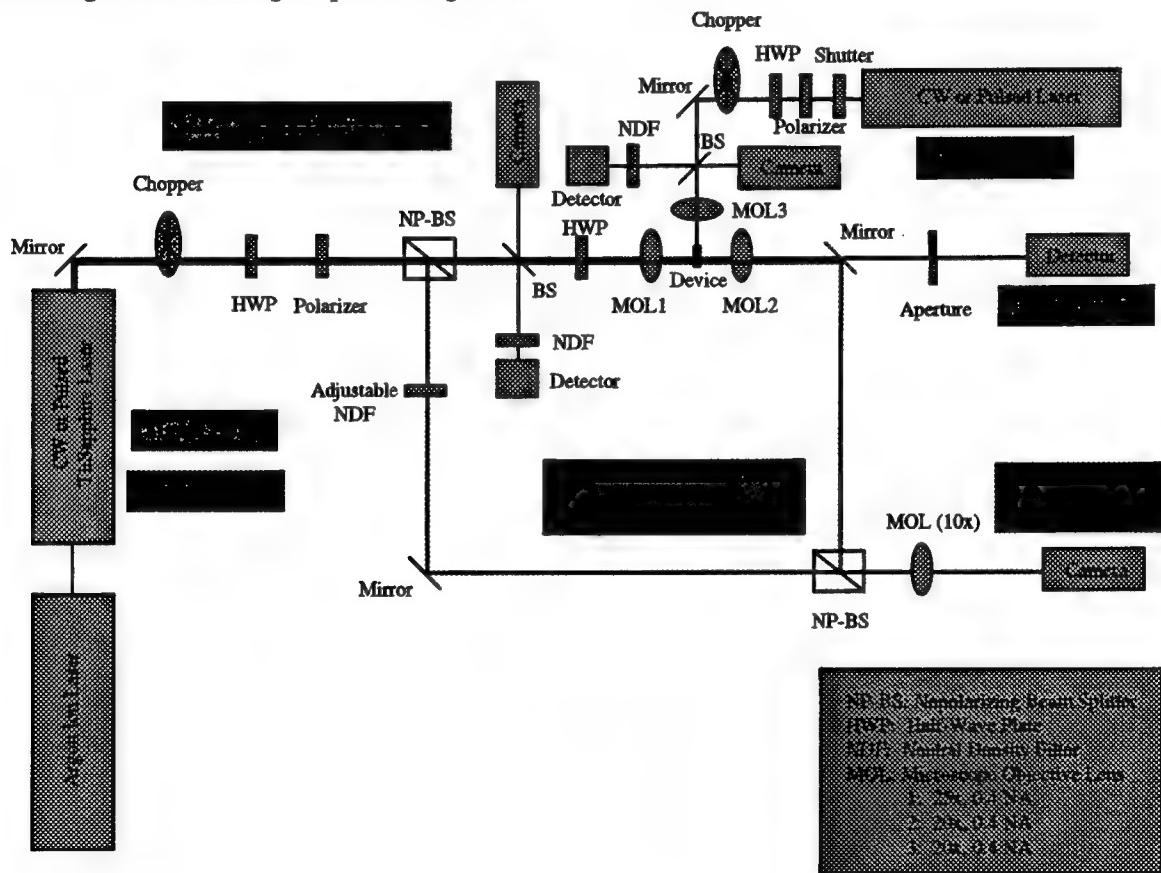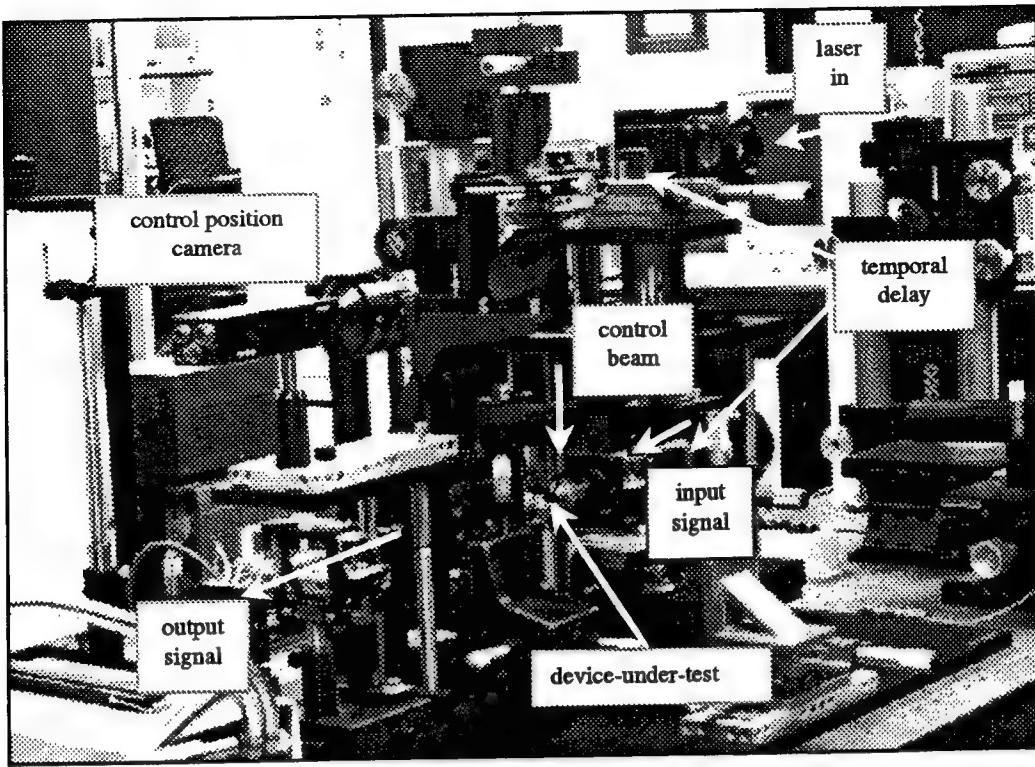
**Figure TS-1. Waveguide Test Setup, schematic and photograph**

The test setup was initially constructed and validated using waveguide structures created at Martin Marietta Laboratories in Baltimore. These structures included straight waveguides, Y-branches, and crossbars and are shown in Figure TS-2. Sample measurements made in our lab on these structures are in Figure TS-3. The main focus of this work was to verify that the waveguide characterization setup we have constructed and the measurement techniques we are using would work for the structures fabricated in this program. As can be seen in the figures, and because of the similarity in sizes between these devices and the ones we produced, we were easily able to begin taking measurements once our devices had been fabricated. After these measurements were made, some modifications were made to the setup to allow us to bring the control light in from above the wafer.
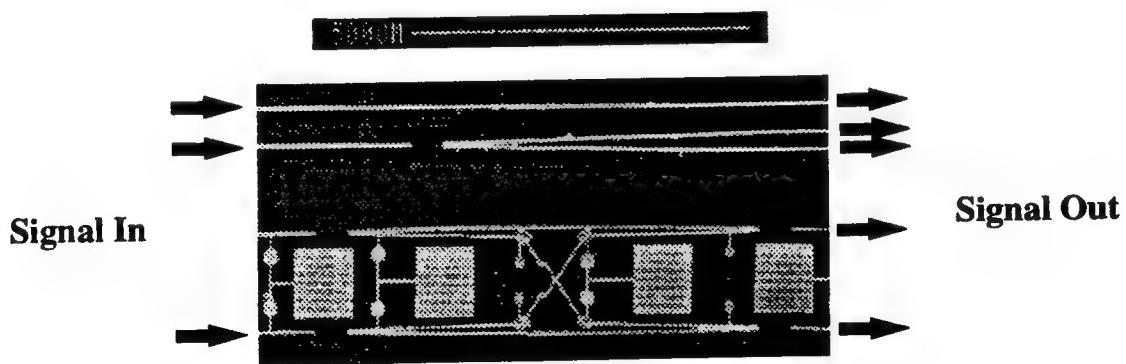


**Figure TS-2: Waveguide structures fabricated at Baltimore Labs: straight guide, Y-branch, and crossbar switch**

26
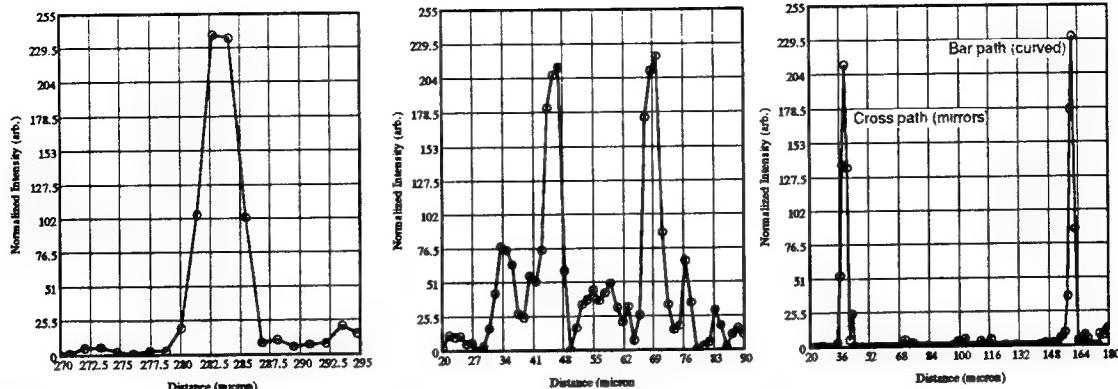
**Figure TS-3: Output intensity from the three guides in the above figure: straight guide, Y-branch, and crossbar switch**

We also used our setup to get some preliminary measurements of $n_2$, the nonlinear refractive index change with optical intensity. These results are shown in Figure TS-4, which shows a value of $n_2=2x10^{-7}$, which is in agreement with what we found in the literature. These measurements were made inputting the light into the guide, instead of from the top.
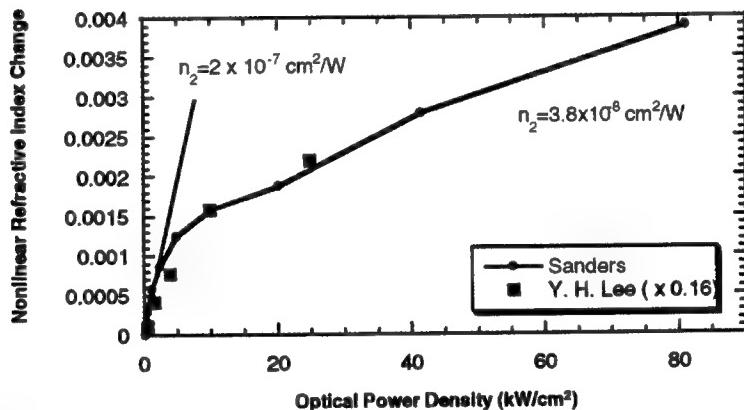


**Figure TS-4: Nonlinear refractive index change with optical input intensity.**

A range of signal and control wavelengths was used for the testing in order to determine the optimum operating conditions (see table TS-1). Both single and dual wavelength operation were investigated. The control signal was introduced from the top of the device.

| Laser Source | Signal Beam | Control Beam | |
|---|---|---|---|
| Single Wavelength | $905 \pm 10$ nm | $905 \pm 10$ nm | Dual |
| Wavelength | $905 \pm 10$ nm | 830 - 920 nm | |

**Table TS-1: Wavelengths investigated for signal and control beams**

The following table lists the test equipment used during this program:

27

| Description | Nomenclature | Model/Serial number |
|---|---|---|
| Argon Ion Laser | Coherent Inc. | Innova 90 / 13143 |
| Ti:Sapphire Laser | Coherent Inc. | 899 Ring Laser |
| 860 nm Diode Laser | Micro Laser Systems | L4860S-150TE / 144 |
| 905 nm Diode Laser | Power Technology Inc. | – |
| Pulsed Ti:Sapphire Laser | Spectra-Physics | Tsunami |
| CCD Cameras | Pulnix | TM7EX |
| Frame Grabber | Epix | 4MEGVideo |
| Amplified Silicon Photodetector | Thorlab Inc. | PDA150 |
| High Speed Detector | TBD | – |
| Mechnical Shutter | Uniblitz | T132 |
| Optical Power Probes/Meter | Coherent Inc. | LM10/MT65, LM2/NA26, Labmaster |
| Optical Power Probes/Meter | Newport Inc. | 818-IR/1835-C, 1171/1056 |
| Digital Oscilloscope | TBD | – |
| Optical Spectrum Analyzer | HP | HP70915A |
| Temperature Controller | Micro Laser Systems | CT15W |
| Ultra Low Noise Current Source | ILX | LDX-3620 |
| Chopper | EG&G | – |

## Table TS-2: List of test equipment

The tests performed are divided into 4 categories: transmission, phase shift and $n_2$, switching characteristics, and high speed testing.

### 3.5.2   Transmission Testing

Near field output intensity of straight  waveguides, Y-branch waveguides, and Mach-Zehnder all optical switch were observed using a CW laser.  30% coupling loss is expected at the entrance and exit planes due to no anti-reflection coating on devices.  The light coupling efficiency to the core material, Y-branch splitting and recombining ratio, and crosstalk are responsible for additional coupling losses.  The linear and nonlinear absorptions are the primary material limiting factor for the transmission.

The objective of this test was to investigate the sources of transmission loss and ultimately to set the transmission specifications of a Mach-Zehnder prototype device.  The transmission test also measures the impact of crosstalk on switching contrast ratio.

A CCD camera and an optical power probe measure the spot size of input signal and the surface reflectivity, respectively.  The output CCD camera captures the near field output intensity of the signal beam propagating through a device.  The output signal with respect to input signal optimized with the polarization is recorded to perform the transmission test.  The test was repeated at several wavelengths to obtain the transmission spectrum.  A Sanders' laboratory notebook was used to record the input/reflected/output signals with a silicon photodetector and the optical power of signal/control beams with an optical power probe.

28

### 3.5.3     Phase Shift and $n_2$

The phase changes of GaAs waveguides as a function of input optical power density and of electronic control on the device were observed. 180 degrees phase change for a given optical power density is required for the optimum switching. The nonlinear index refraction, $n_2$, of a waveguide material was calculated using the measured phase change and intensity values and compared with published data on similar quantum well materials for the test validation.

The optically induced phase change in a waveguide is the key switching parameter responsible for the change between constructive and destructive interference. The objective of this test was to measure the required control optical power density for the switching and to validate the test setup and methods. The validation of the test can be achieved by comparing the measured nonlinear index of refraction, $n_2$, with the published data on similar quantum well materials.

The straight waveguide test structures were used to measure the requirement of control optical power density for the 180 degrees phase change. The signal beam was divided into two parts with a non-polarizing beam splitter. One beam passes through a straight waveguide while the other input beam passes through free space. The recombined two output beams interfere. The fringe modulation depth is optimized by adjusting the neutral density filter in the free space path. The phase change in the output fringes with respect to the control signal were recorded using a CCD camera and a frame grabber. The captured frames were averaged, but the number of frames to be averaged strongly depends on the stability of the interferometer and was determined at the time of test. Once the phase change with respect to the control signal is measured, it is simple matter to calculate the nonlinear index of refraction with the proper formula. The test was repeated with an electrical signal as the control signal.

A CCD camera recorded the interference fringes for the measurement of relative phase shift and the nonlinear index of refraction. The wavelengths, optical power, polarization and spot sizes of signal/control beams are the key parameters to be recorded in the laboratory notebook.

### 3.5.4     Switching Characteristics

The switching contrast ratio of a Mach-Zehnder prototype device was measured. The high power optical control beam was exposed in only one arm of a Mach-Zehnder device. The phase of the signal beam in one arm of a Mach-Zehnder device experiences a change as it propagates through the waveguide. If the relative phase between the two arms is changed to 0 (from 180 degrees), the two output beams will constructively interfere and generate the output signal. The switching contrast ratio is the 'on' to 'off' signal intensity ratio.

Switching contrast ratio is the important device parameter for the optical networking application. The measurement of the waveguide response time demonstrates the high speed switching. The objective of this test was to demonstrate that a quantum well based Mach-Zehnder all optical switch is suitable for the high-speed optical networking application.

The output signal of a Mach-Zehnder device was tuned with the control bias voltages to create destructive interference. The output signal is recorded with and without the optical control signal. The mechanical shutter was used to block the control signal and to measure the device response time. The control signal intensity was adjusted to increase the switching contrast ratio. The control signal intensity for a given waveguide interaction length that leads to the maximum switching contrast ratio was compared to the one obtained with the nonlinear index of refraction measurement. In order to measure the waveguide response time, a pump-probe adjustable delay setup was used (see high speed testing section).

### 3.5.5     High Speed Testing

High-speed demonstration of an integrated Mach-Zehnder all-optical switch is the key for success in our Mach-Zehnder development effort. The goal of this task was to demonstrate the feasibility of an integrated Mach-Zehnder all-optical switch for high-speed operation with adequate contrast ratio and transmission.

The high-speed test setup is shown in figure TS-5. The switching characteristics were evaluated in single wavelength operation. A pulsed beam from a Ti:Sapphire laser is divided into two beams, one for input signal and the other for control signal. The energy of the input signal is only a fraction of the control signal in order to avoid

29

any nonlinear effect due to the input signal. Input and control signals pass through an adjustable delay controlled by a prism placed on a micrometer stage. The adjustment of the control signal path length with respect to the input signal path length introduces a temporal delay between input and control signals. A difference of 300 microns in path length between two beams introduces 1-picosecond temporal delay with a 1-picosecond pulsed laser. The micrometer stage has 10-micron resolution--enough to measure sub-picosecond response. First, the delay was adjusted to match the path length of control and signal beams. Once input and control signals are spatially and temporally aligned, the test system is ready to evaluate an optical switch. Then, the output signal at given temporal delay was measured using a silicon detector. The switching speed and contrast ratio of an integrated Mach-Zehnder all-optical switch were extracted from the measurement.

An integrated Mach-Zehnder all-optical switch was evaluated with a pulsed Ti:Sapphire laser for high-speed operation. The pulsed Ti:Sapphire laser has 1-picosecond pulse width and a repetition rate of 82 MHz. The wavelength of control and signal beams was set near 905 nm for optimum transmission and switching contrast ratio.
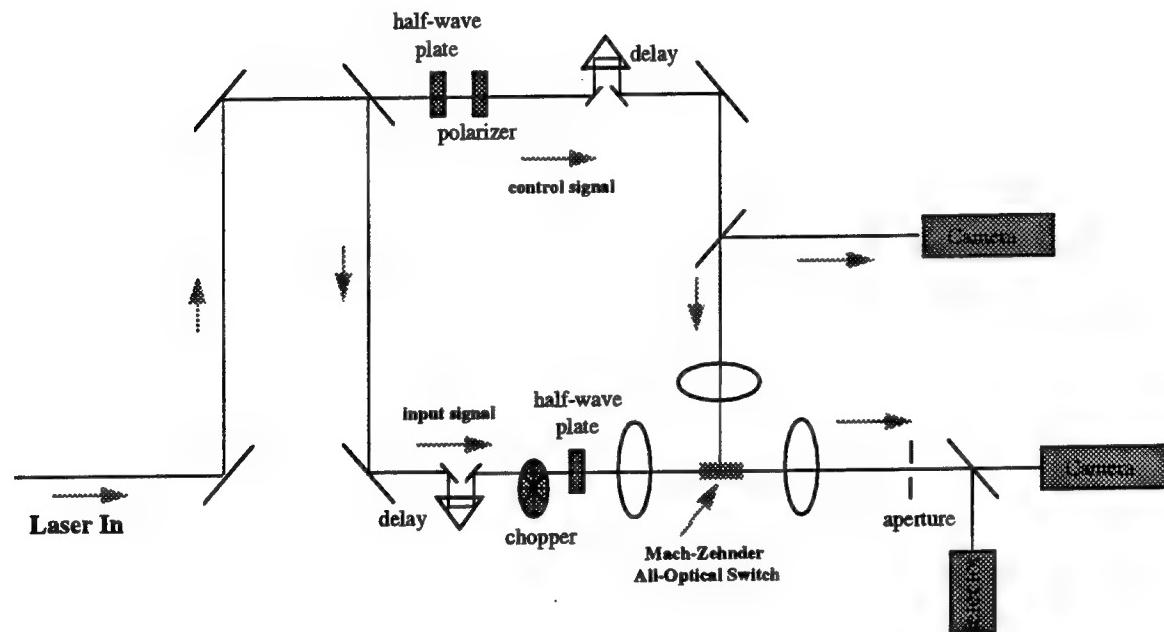


**Figure TS-5: High Speed Test Setup**

### 3.6 I-TOAD Design
#### 3.6.1    First Generation

**Wafer Growth:**

For our first generation devices, we grew 4 epitaxial structures by MBE. Each structure consisted of an intrinsic, absorptive region grown between p and n doped layers. This p-i-n structure allowed for voltage biasing of the absorptive region, thus allowing for DC tuning or slower timescale stabilization of the refractive index in each leg of the interferometer. In each wafer, the cladding material contained ~10% more aluminum than the average core composition. This resulted in a small difference in refractive index, used to guide the light. In the first wafer, the core material was 5 microns of bulk GaAs. The second wafer's core consisted of 0.5 microns of GaAs quantum wells. The third wafer's core consisted of 5 microns of GaAs quantum wells. The final wafer contained 0.5 microns of GaAs quantum wells in the core and 2.25 microns of nonabsorbing AlGaAs on each side of the wells (this was done with the hope that it would work better than using all quantum wells by only absorbing light, and thus changing the refractive index, in the center of the guide, where the optical intensity of the mode is at its peak). The

30

general structure of our wafers is shown in Figure FG-1. The refractive indices of the grown layers (determined from tables in the literature) were used in the simulation of the device.



n-type cladding, 2 microns
$Al_{0.2}Ga_{0.9}As$

intrinsic Core, 0.5-5 microns
GaAs/ $Al_{0.3}Ga_{0.7}As$ MQW

p-type cladding, 2 microns
$Al_{0.2}Ga_{0.9}As$

GaAs substrate
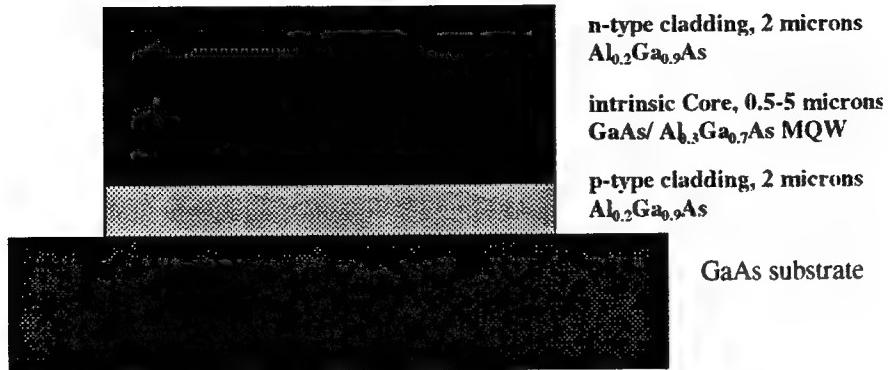
**Figure FG-1: Epitaxial structure of waveguide devices**

**Mask Design:**

The mask layout of our first generation devices included 3 types of structures: straight guides, Y-branches, and Mach-Zehnders. We varied the dimensions of each of these both to compare with simulations and to allow for optimization of switching contrast. These devices were also used to measure material parameters relevant for our designs. Comparison with simulations and the material parameter measurements were used to design our second-generation devices. A sample Mach-Zehnder mask layout is shown below (Figure FG-1) to indicate the relative dimensions involved. The total layout contained around 24 varieties of devices.
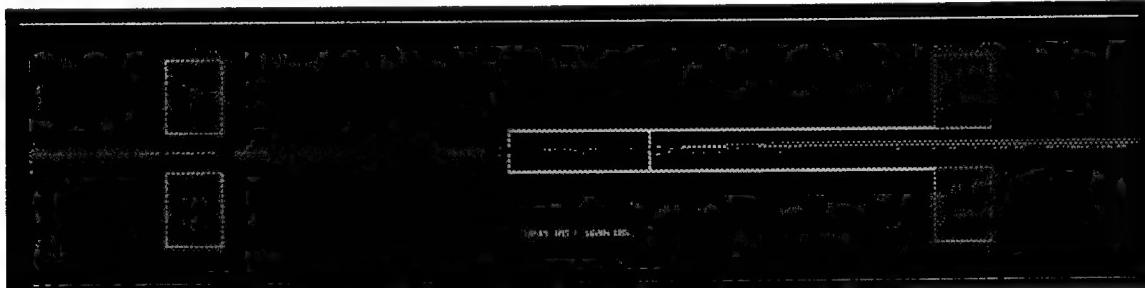


**Figure FG-2: Sample mask layout of Mach-Zehnder device**
**(~2.5 mm long and 20 microns wide, not including metal bonding pads)**

**Experimental Results:**
As described previously, there were three types of devices created in the first generation: straight waveguides, Y-branches, and Mach-Zehnder switches. Figure FG-3 shows the transmission through a 3-mm long waveguide along with the absorption of the guide versus wavelength. In order to have a device which operates at a single wavelength, we need absorption to generate carriers (and thus modulate the refractive index) but also desire high transmission of light. This tradeoff leads us to choose an operating wavelength between 890 and 905 nm (near the bandedge).

31

**Absorption and Transmission Spectrum**
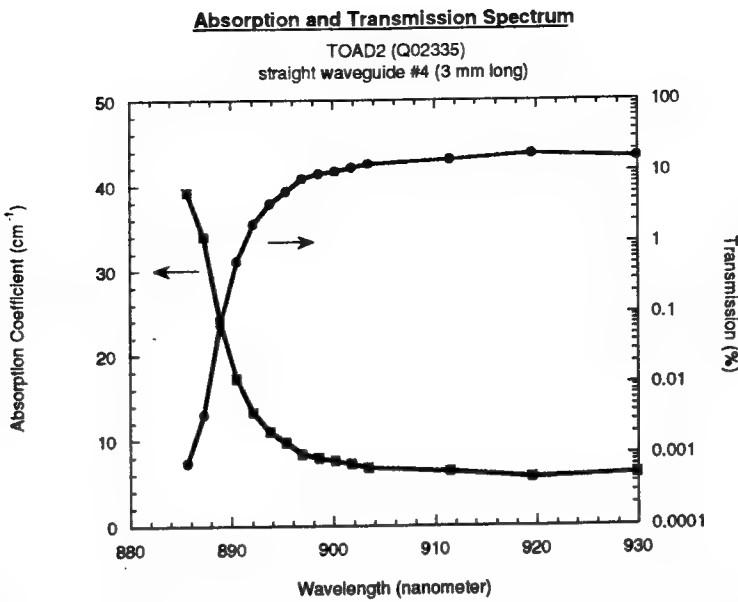


Figure FG-3: Absorption and transmission of straight waveguide vs. wavelength

The first step in our measurements was to use a straight waveguide in an external Mach-Zehnder interferometer to verify that we could obtain enough phase change to switch in an integrated switch. Figure FG-4 shows the results of this external configuration. Note the high contrast in the central spot of the pattern. This measurement is essentially the same setup as was used for Nakamura's results (i.e. external interferometer). High contrast is much easier to observe in this configuration. This external benchtop setup is very sensitive to vibrations, thus exact values of the contrast ratio are hard to obtain. What this experiment does show, however, was that using a single wavelength (905 nm) we could get the $\pi$ phase change necessary for switching. This measurement was done with a cw laser, however, and the mechanisms for changing the refractive index is quite different from that used in pulsed operation.
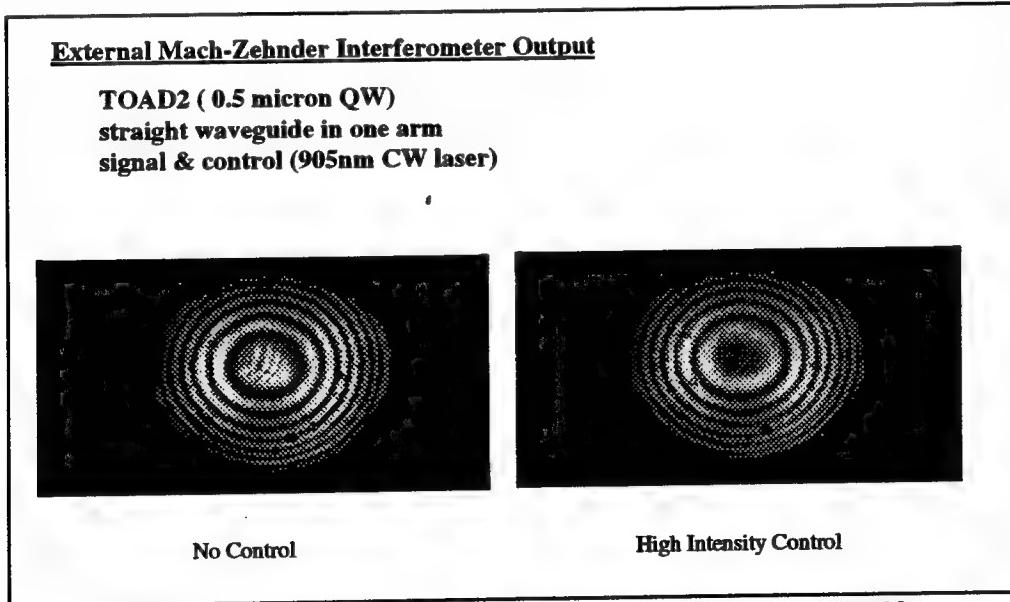


Figure FG-4: External Mach-Zehnder switch with straight waveguide

If we use two different wavelengths, with the control at a shorter wavelength where absorption is high, we can get up to 6*$\pi$ phase change, as shown in Figure FG-5. We observe similar amounts of phase change for bulk and quantum well devices when operating at equivalent distances in wavelength from the bandedge.

32

**Phase Change vs. Control Power**

Device: TOAD2 (Q02335)
CW Laser: 905nm (signal), 856nm (control)
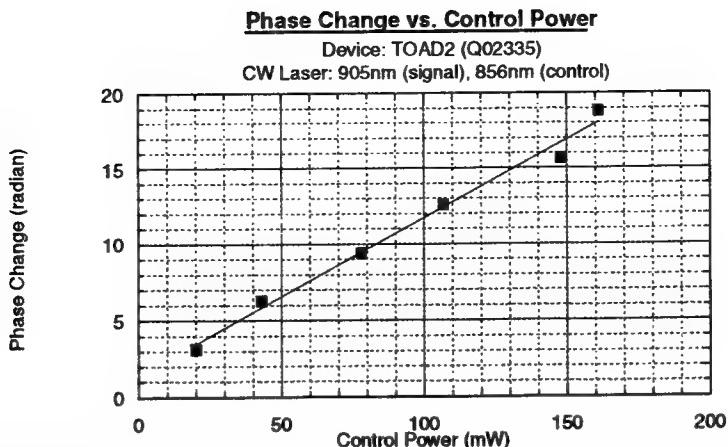


**Figure FG-5: Phase Change vs. Control Power, straight guide, showing 6\*π phase change**

After seeing the large phase changes we could obtain using two wavelengths, we mapped out the control power required to obtain π phase change vs. wavelength (Figure FG-6, signal at 905, varying the control). As expected, this curve varies with the absorption—more absorption implies less power to obtain the phase change. At 905 nm we need 4-5 times the power we need at shorter wavelengths.

**Required Control Power vs. Wavelength**
**for 180 degree phase change**
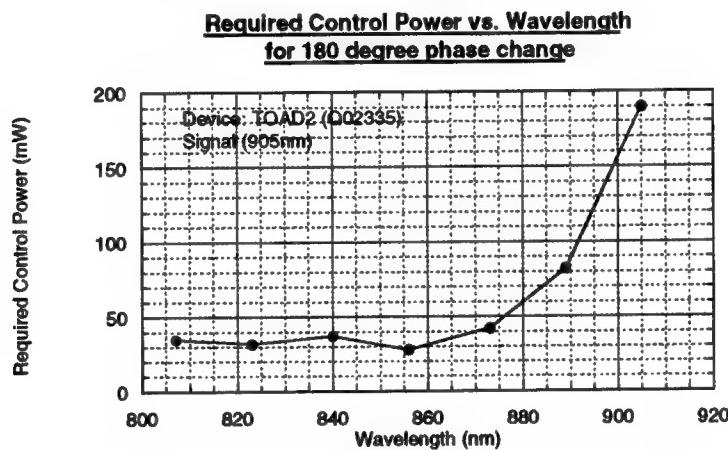


**Figure FG-6: Power for π phase change vs. wavelength**

Finally, we measured the phase change vs. control power at shorter wavelengths (Figure FG-7). The phase change increases linearly as expected. As mentioned previously, we measure differences between the bulk and quantum well materials (and combination of bulk and quantum well core) depending upon the wavelength of operation. The power required is in agreement with what others in the field have measured on similar structures and materials. The direction that the interference fringes move in all of these experiments indicate that the refractive index changes are dominated by thermal effects at cw operation.

33

## Phase Change vs. Control Power

**905nm CW Laser (signal)**
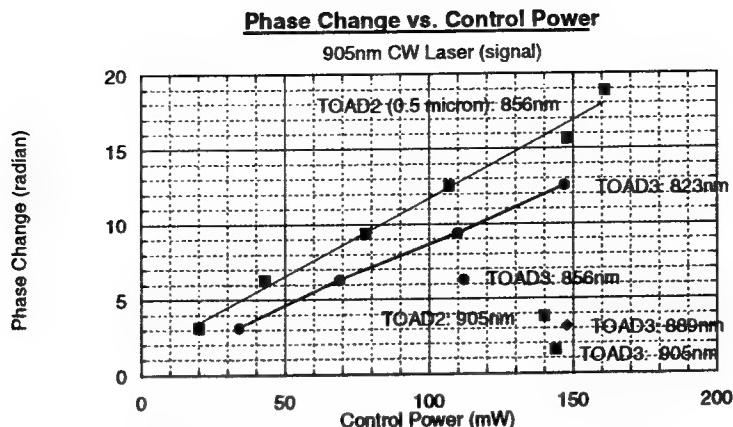


Figure FG-7: Phase change vs. control power

Our next set of measurements was performed on Y-branch waveguides (one waveguide is split into two). In particular we are interested in a 50/50 split between the guides. Figure FG-8 shows the results of one such measurement. In this case, the signal is at 905 nm and the control is at 823 (strong absorption). We observe close to 50/50 splitting between the two output guides. We also note that we can completely eliminate the light in one guide with the absorption changes induced by the control light at this wavelength (changes in absorption always accompany changes in index in refraction, as they are related by the Kramers-Kronig transformation--not always desirable, but sometimes useful). This again is only a thermally induced change and may not be a problem during pulsed operation. In the structures where the waveguides are close together, we see coupling effects from one guide to the other when control is applied. Experimentally (and in simulations) we observe that the guides need to be on the order of 15 microns apart to avoid this coupling.



### Near Field Intensity Profile: TOAD3 (Z1179B, 4 micron QW), Y-branch

**signal (905nm) & control (823nm)**

no control          control beam          control beam
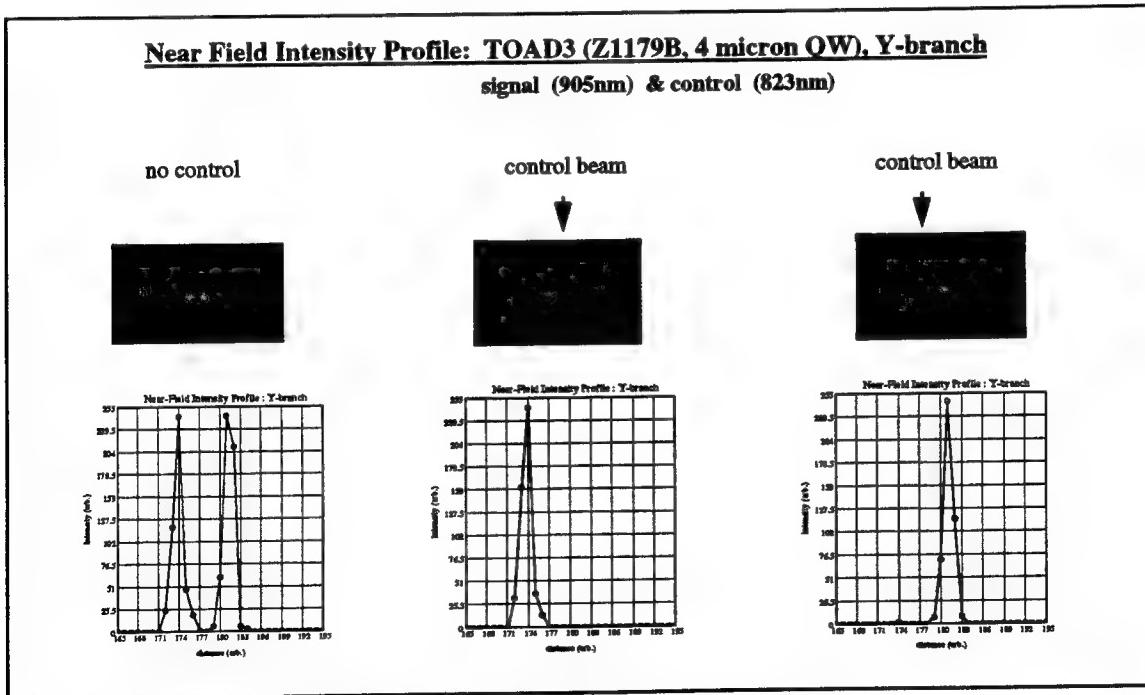
Figure FG-8: Y-branch measurements, optical control

We also measured the effects of applying electrical bias on the arms of the interferometers and Y-branches. Figure FG-9 shows how the output of a Y-branch varies under electrical bias. At 0 bias we have a 50/50 split. As we increase the reverse bias, the absorption increases and thus the output falls. This effect is useful for adjusting the splitting ratio between two arms of the interferometer to obtain optimum contrast.

**Figure FG-9: Y-branch measurement, electrical control**

Lastly, and most importantly, we move on to the results of our measurements of Mach-Zehnder (MZ) switches. Figure FG-10 shows a MZ switch with bulk GaAs in the core controlled electrically. The signal is at 893 nm (and pulsed, so no thermal effects were expected—in later measurements it was determined that this was in fact a thermal effect due to the high repetition rate of the laser) and there is no optical control in this case. As you can see, from the absorption and refractive index changes obtained by applying bias, we can obtain large contrast in a MZ switch. This contrast was determined to be a thermal effect however.

**Near field Intensity Profile: TOAD1 (6 micron bulk)**
**Mach-Zehnder device, bias on one arm**
**Laser: 892.67nm, 1ps @ 82MHz**
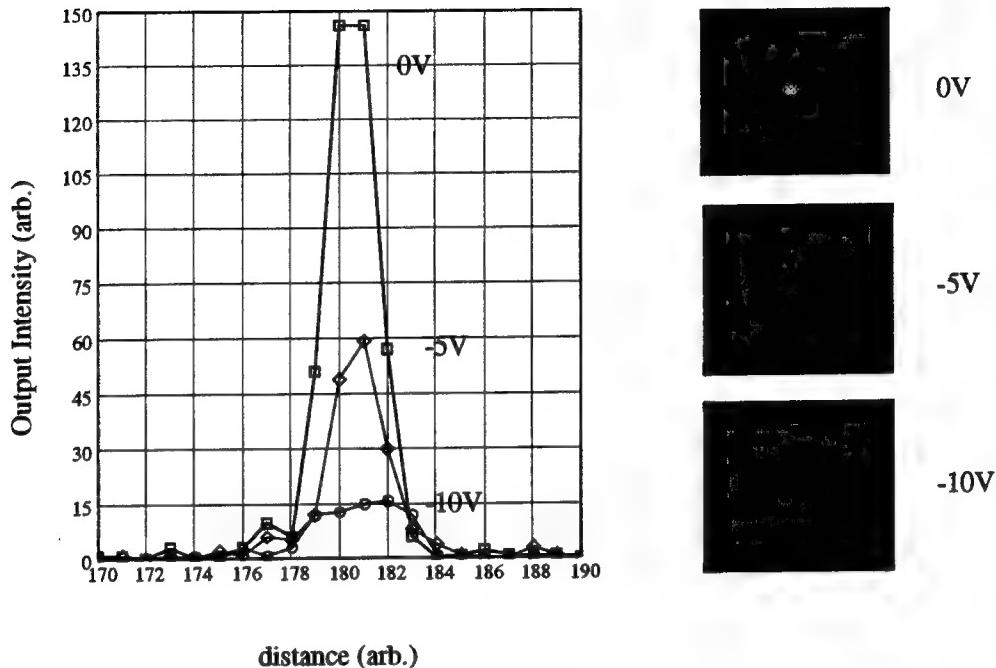
**Figure FG-10: Mach-Zehnder switch, electrical control**

Figure FG-11 exhibits this change in output signal vs. applied bias. Figure FG-12 shows what can be obtained when both electrical and optical control signals are applied. Note that in this figure, the signal begins to increase after decreasing, indicating that we have passed through the $\pi$ phase change point.
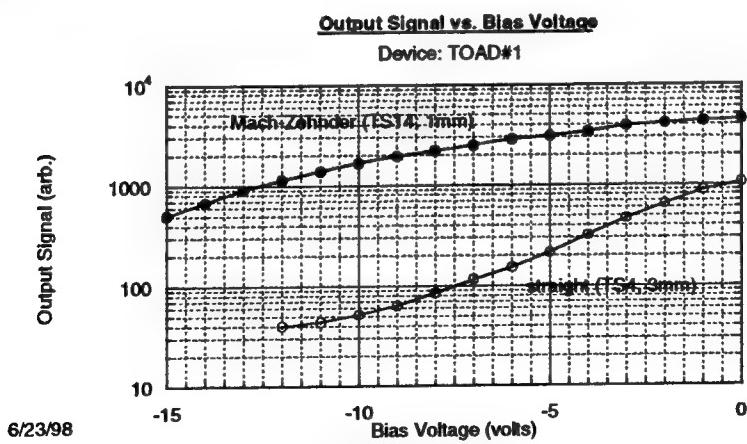


**Figure FG-11: Mach Zehnder output vs. electrical bias**
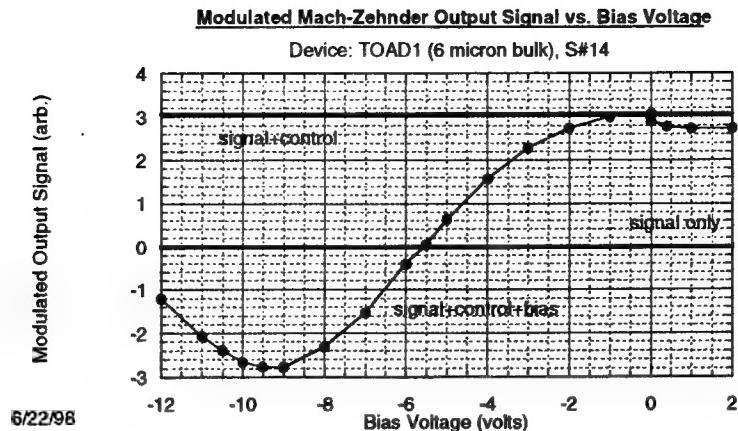
Figure FG-12: Mach Zehnder output vs. electrical bias with optical control

Figure FG-13 shows an oscilloscope trace of the output of a Mach Zehnder device switching under cw operation (chopped at 1 kHz). At cw operation we are dominated by thermally induced changes and thus cannot see high speed switching. Our contrast ratios have not been as high as the simulations have predicted them to be. This limited contrast seems to be due to an inability to collect only the signal light emitted from the waveguide (which should be correctable if using a fiber coupled to the guide at the output).
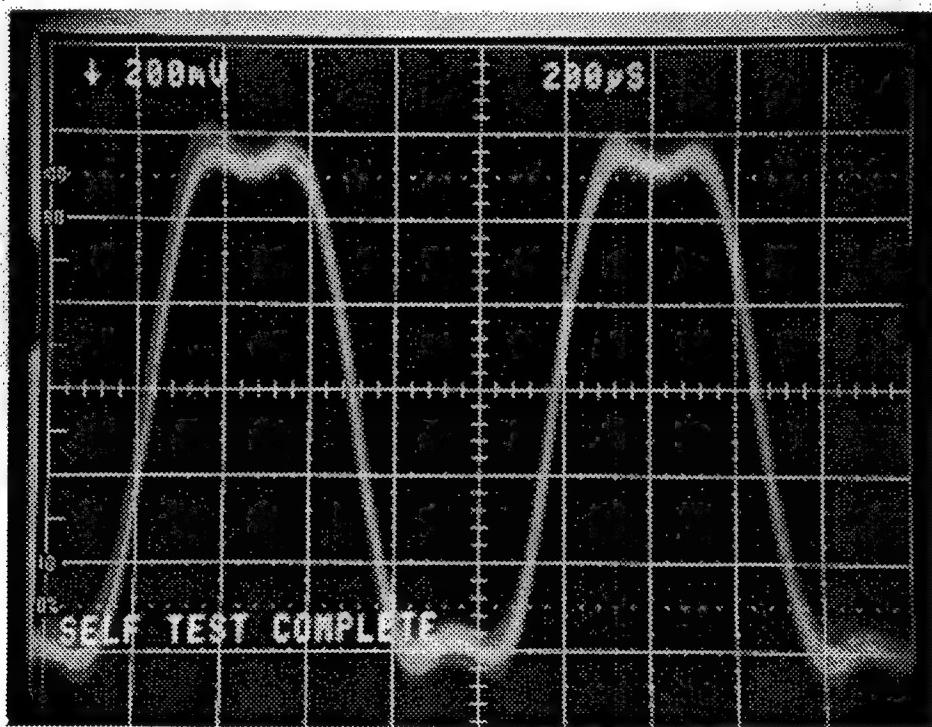


Figure FG-13: Mach Zehnder output, switching at 1 kHz, cw operation

Lastly, in this generation we performed high speed testing of our devices at Boston University using their pulsed Ti:Sapphire laser (both with and without electrical bias). In order to do this measurement, we had to build an adjustable delay between the signal and control paths. Under pulsed operation, we do see the high speed switching we expect (30 ps, possibly faster), as well as the slow recovery time we expect without a second control pulse to rebalance the two arms. The poor contrast ratios of our first generation devices complicated this measurement, as the exact placement of the detector could change the results significantly. Two-photon absorption also seems to play a role. Limited laboratory time and benchtop space for our measurements were difficulties. We did observe a high-speed phenomenon occurring, but it was unclear whether it was dominated by an absorptive change or a

37

refractive index change or some mix of the two because of the thermal effects also involved.   Figures FG-14 and 15 show some of the results of these measurements, which turned out to be the best results we observed in the program.

**Optical Switching in Mach-Zehnder Device**
Device: TOAD1 (6 micron bulk), TS#14
Laser: 892.67nm, 1ps @ 82 MHz
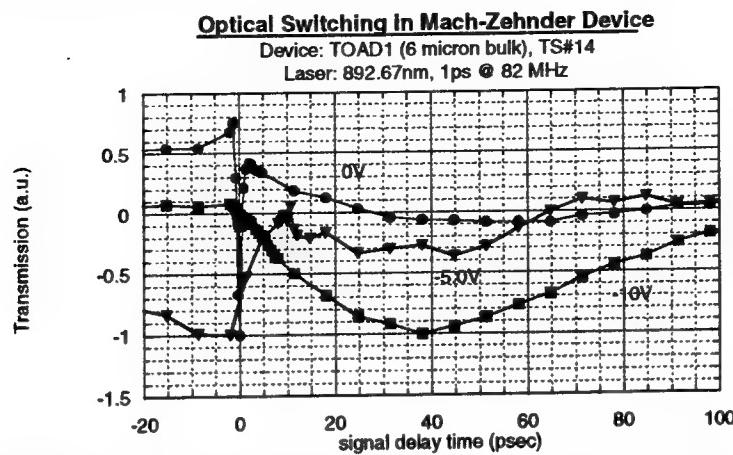


**Figure FG-14:  Pulsed switching of bulk GaAs device, with and without bias**

**Optical Switching in Mach-Zehnder device**
Device: TOAD3 (4 micron QW), TS#14
Laser: 880 nm, 1 ps @ 82MHz
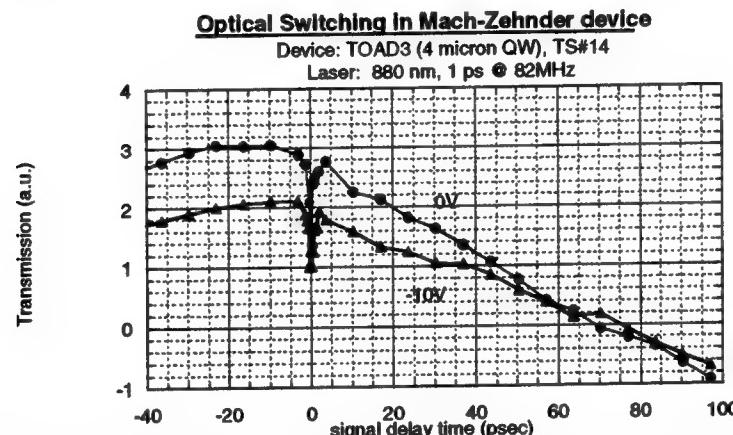


**Figure FG-15:  Pulsed switching of QW MZ device, with and without bias**

### 3.6.2    Second Generation:

**Wafer Growth:**

For our second-generation devices, we grew 3 epitaxial structures by MBE.  Each structure consisted of an intrinsic, absorptive region grown between p and n doped layers. In each wafer, the cladding material contains ~10% more Aluminum than the average core composition.  This results in a small difference in refractive index, used to guide the light in the vertical dimension.  The light is guided in the horizontal dimension by etching away the top n-layer of the device until the effective index of the etched region and that of the guide region differ by a small amount. This amount is chosen so that the light is only weakly guided and thus should be single mode  (there is a tradeoff between number of allowed modes and guiding strength of the waveguide).  The experimental results from our first generation devices as well as the 3-D simulations have indicated that structures in which the inner 0.5 microns is slightly higher index than the rest of the core guide light better than those in which the core is all the same material. Each of the three wafers for the second generation has a ~4 micron core with the central 0.5 microns as just described.  Thinner structures are more difficult to couple light into without any fiber coupling.  The first wafer is bulk material.  In the second the core is all quantum wells.  The third wafer has quantum wells only in the center 0.5 microns of the core.

**Mask Design:**

The mask layout again included 3 types of structures: straight guides, Y-branches, and Mach-Zehnders. The layout time and effort was greatly simplified by the simulation software we leased (Beamprop, from RSOFT), which can output mask layout GDS II format from the simulated structures. In the second generation, we focused on the devices yielding the best performance in the first generation (in terms of splitting angles, branch separations, waveguide widths, and device lengths).

**Experimental Results:**
CW Testing

We simplified the design, fabrication, and testing of waveguide structures by introducing a control signal from the top of a device. This approach should minimize the complexity of a optical system design and integration. The efficiency of this approach is compared with the side illumination method (where you must couple additional control signals into the arms of the interferometer) in Figure SG-1. This comparison is only valid for our specific testing conditions since no fiber pigtailing is used for coupling of the input signal. This reduces the coupling efficiency of input signal for side illumination approach. Figure SG-1 plots the control optical power needed to change the phase of signal by 180 degrees for a given control wavelength. It clearly demonstrates the similar effects on signal propagating through a straight waveguide device for both approaches. For this reason, all of our work is based on the top illumination approach, which has been researched by other groups as well.
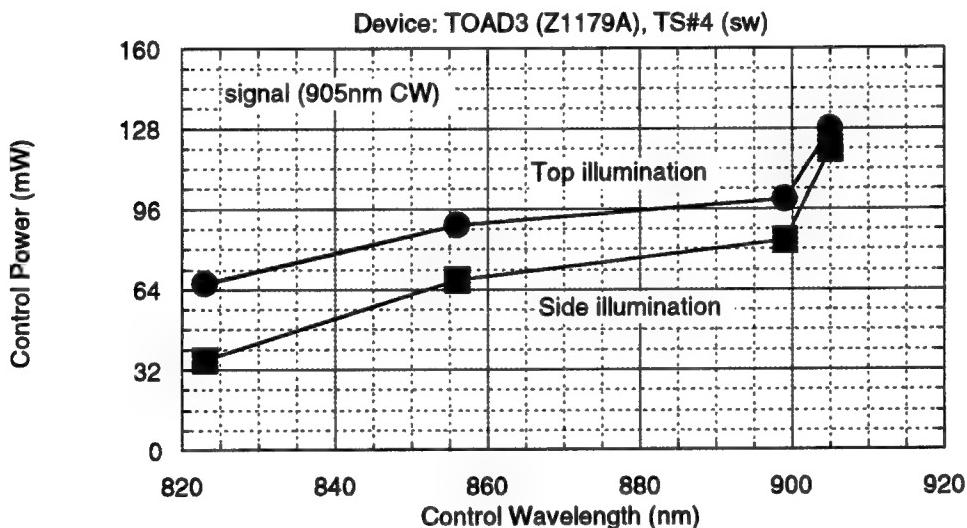


**Figure SG-1: Control optical power required for π phase change for a given wavelength.**

The output of the Mach-Zehnder waveguide device is initially in high transmission state as a result of constructive interference. For optical networking applications, the output of a device should be in low transmission state, if no control signal is applied. Then the output signal is switched up with a control signal leading to high transmission state, allowing only the data for your TDM channel to pass through. Initially, the signals in both arms of our Mach-Zehnder switch are in-phase and constructively interfered, being of same path length. It is difficult to fabricate a Mach-Zehnder device in which the signals in both arms are 180 degrees out of phase. This initial condition, low transmission state, can be achieved by applying bias voltages to the branches of a device.

We used a GaAs/AlGaAs multiple quantum well (MQW) based Mach-Zehnder waveguide switch to demonstrate switching behavior. First, we evaluated the device for a given bias voltage at the signal and control wavelengths of 905 nm and 823 nm, respectively. The output intensity profiles shown in Figure SG-2 clearly indicate that the output signal is the result of not only change in absorption but change in index of refraction. The output mode structure changes with a bias voltage, especially in side lobes. The modulation depth at the signal wavelength of 905nm is not large enough to obtain low transmission state with a bias voltage. This could be corrected by using a thinner intrinsic region in our devices. There is however a tradeoff between the thickness needed to generate enough

39

carriers within the mode profile of the waveguide and the smaller thickness needed for low voltage operation. We have focused our work on studying optically controlled switches, and thus did not optimize them for low switching voltages. Other work in the field has shown voltage-length products on the order of 3 V*mm.
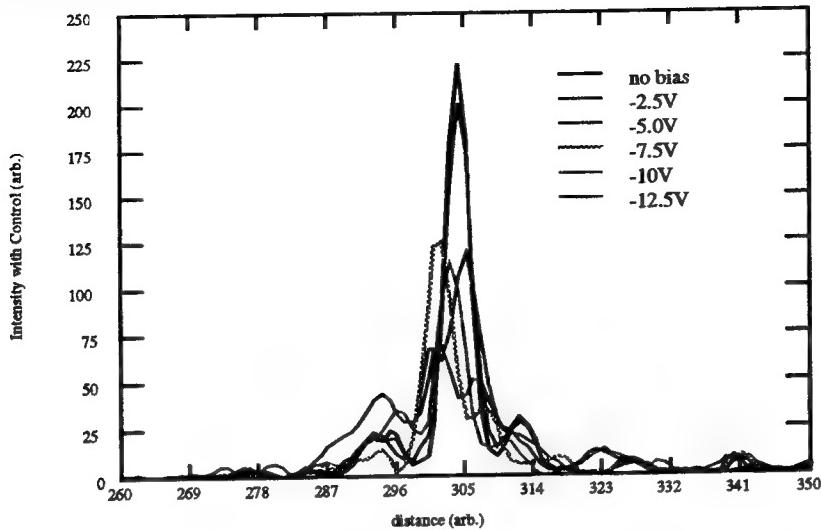


**Figure SG-2 Mach-Zehnder output, electrical bias**

We have evaluated the device with various signal wavelengths to achieve low initial transmission state with a bias voltage (Figure SG-3). The output signal of the device is monitored with respect to a biased voltage at a given wavelength of signal. In order to optimize the modulation of signal with a voltage, we chose the wavelength of input signal near the absorption edge of GaAs/AlGaAs MQW device (i.e. 856 nm).



**Figure SG-3: The output of electrically controlled Mach-Zehnder switch for a given wavelength**

Figure SG-4 shows the output intensity profiles of Mach-Zehnder waveguide device at the wavelength of 856 nm. The output is changed from high to low transmission state with 7.5 reverse biased voltage on one of the branches. Then optical control is applied to the other branch of the device. Up-switching with a very small contrast ratio is attained with 100 mW of optical control power. The change in absorption with an optical control may be responsible for the low switching contrast ratios we have observed.

40
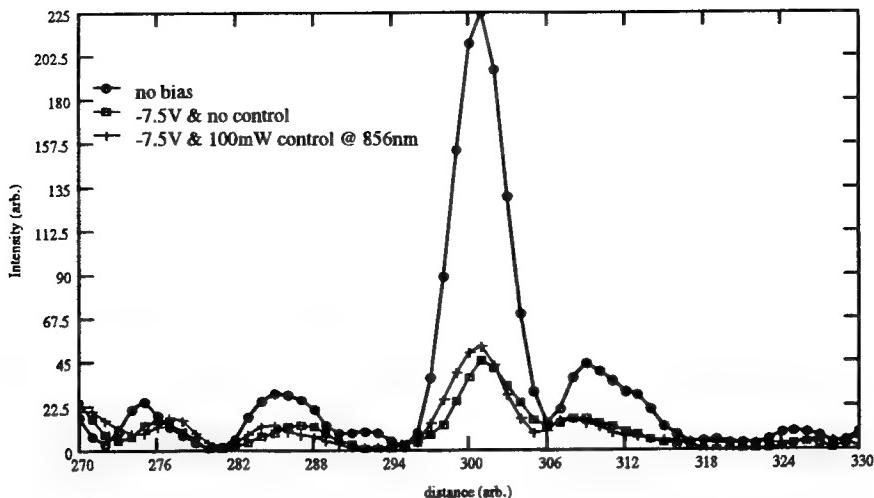
**Figure SG-4 Output intensity profiles versus optical and electrical controls**

Figure SG-5 shows the output intensity profiles of a Y-branch at a signal wavelength of 856 nm. The output signal of the Y-branches with respect to bias voltage is shown. The input signal is aligned and coupled into the waveguide resulting in a 50/50 split at the junction of Y-branches, if no bias voltage is applied. The output of the branch on which a bias voltage is applied shows strong modulation with a voltage. Since the output signals of Y-branches are not recombined in this structure, we can conclude that the modulated output signal is dominated by the change in absorption.
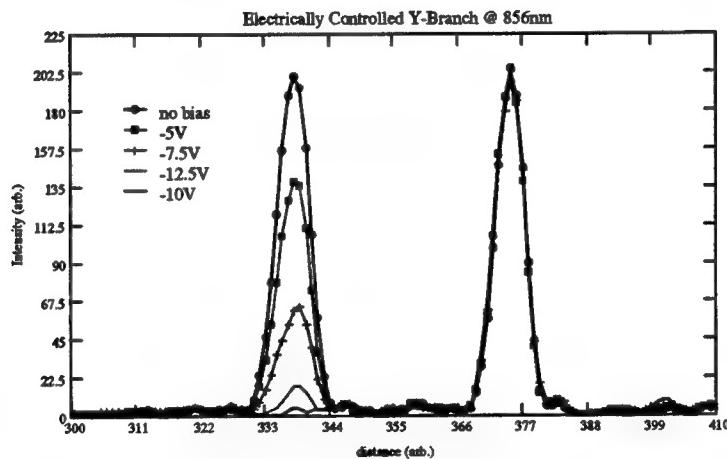


**Figure SG-5: Output intensity profiles of an electrically controlled Y-branch**

In contrast to Y-branches, the output of the Mach-Zehnder device (shown in Figure SG-6) is the result of the change in absorption and index of refraction. Figure SG-7 compares the dependence of output signals on bias voltages for Y-branches and Mach-Zehnder devices. The modulation depth is similar in both devices with a given bias voltage. This indicates that the modulation of signal in our Mach-Zehnder device (at a given wavelength) is also dominated by the change in absorption. We observed similar behavior in GaAs bulk structure at the wavelength of 893 nm. The difference in wavelength is due to the smaller bandgap of bulk material. This problem may be corrected by going to longer signal wavelength (and shorter control wavelength). At this point we do not feel that a single wavelength device is practical (i.e. using the same wavelength for signal and control). Absorptive changes will always dominate such a device.

41
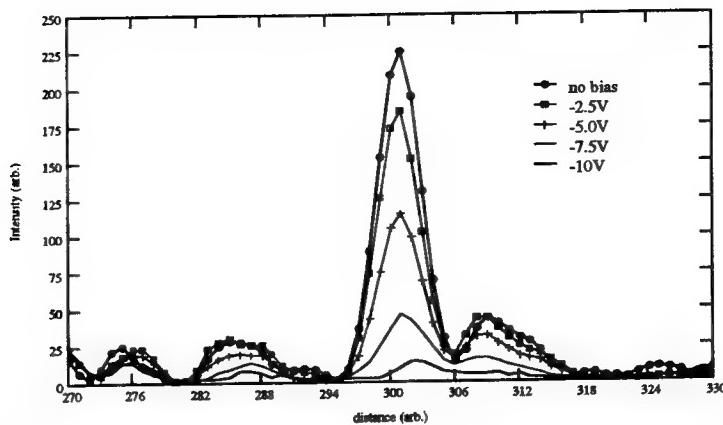
**Figure SG-6: Output intensity profiles of electrically controlled Mach-Zehnder device**
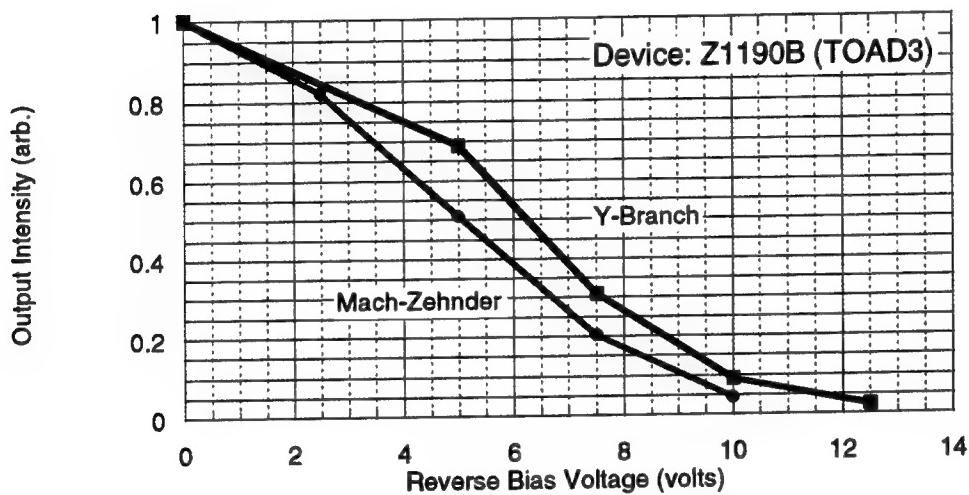


**Figure SG-7: Comparison of output intensity of electrically controlled Mach-Zehnder and Y-branches devices**

Figure SG-8 shows the symmetric nature of our integrated Mach-Zehnder device with respect to optical control. The change in output intensity profiles with an optical control in either branch is identical as shown in the Figure SG-9. The on-axis and integrated output signals are recorded as an optical control beam is scanned across two branches of the device.

**Output Signal Profile (Z1190A, MZ)**



control on bias side & no bias
control on other side od bias & no bias
no control & no bias
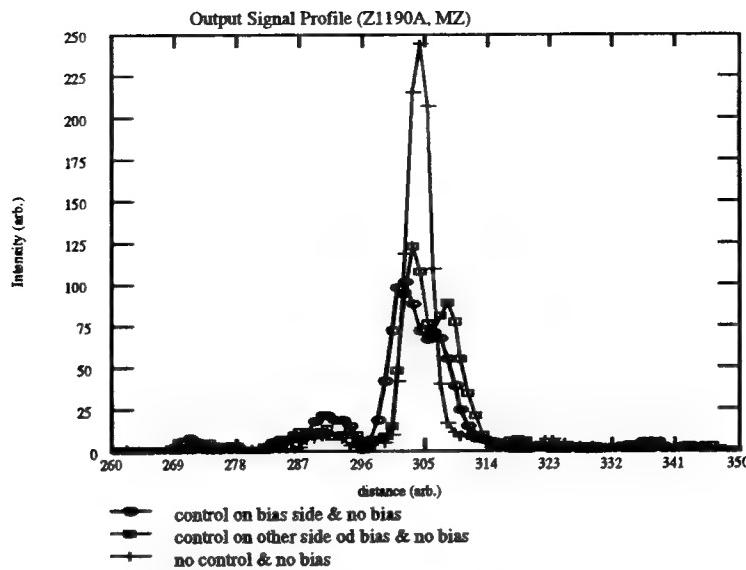
**Figure SG-8: Output intensity profile of Mach-Zehnder device with optical control on each arm, showing symmetric behavior**

**Control Beam Scan Between Two Branches
Device: Z1190A (TOAD3), TS#14**



11/04/98
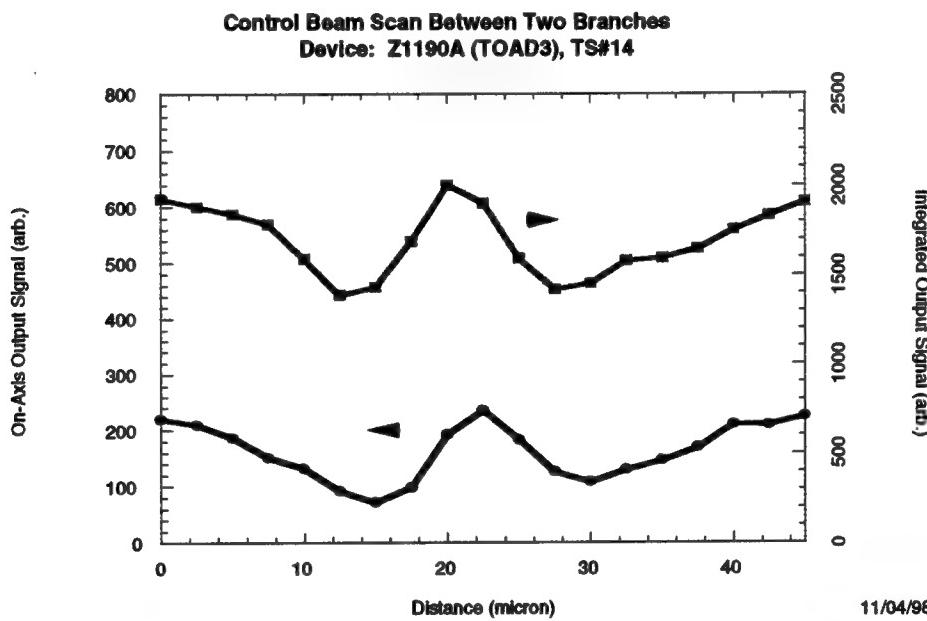
**Figure SG-9: Symmetry of Mach-Zehnder waveguide device: Optical control is scanned across both arms of the device**

## High Speed Testing

High-speed demonstration of an integrated Mach-Zehnder waveguide switch is the key for success in current Sanders' waveguide switch development effort. The goal of this task is to demonstrate the feasibility of an integrated Mach-Zehnder waveguide switch for high-speed operation with adequate contrast ratio and transmission. An integrated Mach-Zehnder waveguide switch was evaluated with a pulsed Ti:Sapphire laser for high speed operation at Boston University with limited access to the facility (~20 days). The pulsed Ti:sapphire laser has a 1~2 picosecond pulse width and a maximum repetition rate of 82 MHz.

The first phase of high-speed testing was focused on single wavelength switch operation because of the lack of high-speed detector and oscilloscope. The single wavelength operation makes the use of a device more practical for the system applications. A pulsed beam from a Ti:sapphire laser is divided into two beams, one for input signal and the

43

other for control signal. The energy of input signal is only a fraction of control signal in order to avoid the nonlinear effect due to the input signal. Input and control signals pass through the delay controlled by a prism placed on micrometer stage. The adjustment of control signal path length with respect to input signal path length introduces a temporal delay between input and control signals. A difference in 300 micron path length between two beams introduces 1-picosecond temporal delay with 1-picosecond pulsed laser. The micrometer stage has 10 micron resolution--enough to measure sub-picosecond response.

First, the delay is adjusted to match the path length of control and signal beams. Once input and control signals are spatially and temporally aligned, the test system is ready to evaluate an optical switch. The wavelengths of control and signal beams are set at 893 nm for optimum transmission and switching contrast ratio. The wavelength tuning range of Boston University's pulsed laser is limited to 900nm or below. A GaAs bulk based Mach-Zehnder device shows stronger effects on optical and electrical controls at 893 nm. The output signal of a device with respect to the temporal delay between input and control signals is recorded with an amplified silicon detector for a given bias voltage.

Initially our plan was to use cw signal light at 905 nm and pulsed control light at a shorter wavelength (tunable). The responsivity of the best high-speed detector we could obtain was 0.1 A/W with an output conversion gain of 5 V/W. The maximum signal power from our cw laser is 8 mW. Given 10% transmission through the device setup and 50% coupling losses into the fiber, this gives us a best case signal at the oscilloscope of 2 mV. The available high-speed scope had a 1 mV noise level, which therefore required that we include an amplifier before the scope to bring up our signal level. Even with the amplifier, we were unable to observe any change in the output signal due to the control signal. This observation is due to a combination of two things: 1. our change in signal (i.e. contrast ratio) was still limited to 10-20% (0.2-0.4 mV) and thus it was still hidden by the noise level, and 2. our coupling and transmission were less than the best case 50% and 10% respectively. There was another cw laser in the laboratory at 905 nm which would have given us higher power, however Boston University was using it for another experiment during the period of our experiment.

After not observing any change with the high-speed detector, we returned to attempting single wavelength operation. For this experiment, we did observe upswitching of our output signal by about 20% when the device was pre-biased to between 2.5 and 8 volts (depending on the alignment). This switching however was independent of the delay between the signal and control pulses, indicating that the repetition rate was too high, causing thermal effects to dominate. At this point, we inserted a pulse picker into the optical path to reduce the repetition rate. Alignment of a pulse picker is very time consuming. Given the limited time we had for our experiments at Boston University, we were only able to obtain extinction between selected and suppressed pulses of 20:1. This ratio was not sufficient to reduce the average power enough to eliminate thermal effects.

At this point, we decided to attempt to measure the nonlinear index of refraction ($n_2$) using the pulsed laser (previously measured with a cw laser). The optical table on which our setup was placed was not air-isolated from the floor and thus room vibrations caused our experimental error to be +/- $\pi/4$. This larger margin of error required that we use high average power to reliably observe any phase change at all. Again, the phase shifts observed were independent of the delay between signal and control and also in the same direction as would be indicated by thermal changes. The phase shift observed was linear with intensity, indicating that we were not saturating the background carrier concentration in the core of the waveguide (which could be a cause of slow response times and limited contrast). We then switched the pulsed laser to cw mode to measure $n_2$. The phase shifts observed were similar to those observed under pulsed operation, which led us to believe that the changes were due to average power and thus temperature effects. The bulk and quantum well devices behaved similarly at comparable distances (in wavelength) from the bandedge. The quantum well device was operated at 876 nm and the bulk device at 900 nm (with bandedges of 855 and 872 respectively)—i.e. both showed similar behavior approximately 20-30 nm above the bandedge. This new cw data is shown in Figure SG-10. We located a more recent paper in the literature in which $n_2$ was measured to be $10^{-10}$ cm²/W for pulsed operation similar to ours, but only at 5 kHz repetition rate. When the repetition rate was increased to 76 MHz (and the average power lowered to eliminate temperature effects), no significant phase change was observed.

### 3.7 Conclusions

Thus, we conclude (given the limited time and accessibility of a high-speed laser) that an integrated Mach-Zehnder cannot be operated at high repetition rate under single wavelength operation. Under single wavelength operation, the wavelength used must be near the bandedge --too close to the bandedge results in not enough transmission and

too far from the bandedge results in not enough absorption to generate carriers and thus change the refractive index. Because the device must be operated near the bandedge, absorption and temperature effects dominate the performance of the device. The single event switching time has been shown by other researchers to be quite fast (1 psec), however no one has conclusively reported continuous operation of such an integrated device at large repetition rate (although a few researchers have shown 3-4 continuous pulses). Other researchers who have worked on all-optical waveguide devices now have shifted their emphasis to asymmetric Fabry-Perot devices (see reference 77).



**signal & control: single wavelength**
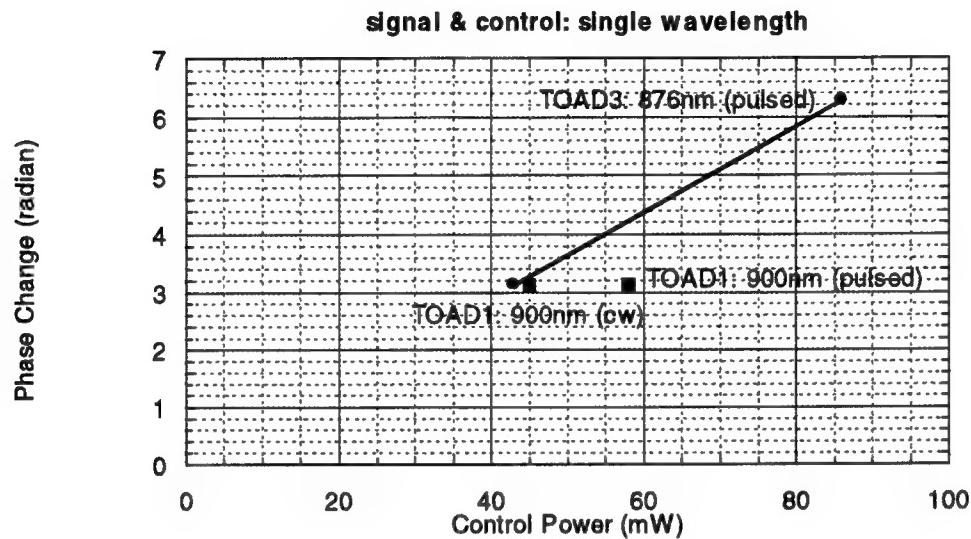
**Figure SG-10: Phase change versus average control power,
cw and pulsed single wavelength operation
(TOAD1 is bulk device, TOAD3 is a quantum well device)**

We continued to search the available literature for similar work in this field. This search coupled with what we observed in our measurements has led us to conclude that this device has limited practicality in the form envisioned by us (single wavelength operation). While we do see high speed switching (as do other groups), we are not able to observe this switching at high repetition rate (82 MHz). Other researchers have also observed this problem. The best results we could find only show evidence of 4 consecutive switching events at 82 MHz. In addition, this result was observed only in an external Mach-Zehnder configuration (where better contrast ratios are more easily observed).

# 4. Appendix A: Picosecond High PRF Lasers and Matching Detectors

By Jeff Odhner, Advanced Technology, Lasers and Electro-Optics Group, Sanders

The following is an industry survey of lasers with a very short pulsewidth. The application is short haul communications where the laser is supplying the clock for the rest of the system. The following are the basic requirements for the lasers studied.

## 4.1 Laser Requirements

| | |
|---|---|
| PW | <10 picoseconds |
| PRF | 1 GHz |
| Channels | 100 |
| Laser power out | more is better |
| Jitter | <femptoseconds |
| Stability | must be very stable |
| MTBF | > 2 years |
| Cost | < $60K required (<$10K desired) |
| Wavelength | not critical (1.3-1.5 micron is acceptable) |
| Size | smaller is better (<shoebox size is desirable) |

## Detector Requirements
Should match well to the laser.

## Calculations:
The cut-off frequency for the detectors seeing a sine wave is related to the rise time by:

$$tr = 0.35/fc$$

Where tr is the rise time and fc is the cut-off frequency.

For a detector with a 0.23 nsec rise time, the cut-off frequency is 1.5 GHz. However, this is accurate for a sine wave and is not entirely accurate for pulses.

## 4.2 Recommendation:

*In House Solution*
For a prototype system, the Sanders Lasers and Electro-optics group can make a laser to meet you needs. We actually have the laser diodes and neodynium vanadate to demonstrate a high rep rate short pulse laser. Hopefully we can find a GHz scope somewhere in the company. We actually have the resources (manpower and much of the material) to put something like this together right now.

*Low Cost Solution*
If you have more time than money, a prototype can be had from the University of Michigan Center for Ultra-fast Optical Science. They can certainly supply a short pulsewidth (John Neise, (734) 764-9271 or Tbor Uhauz at Intralase (949) 462-7195).

*Semi-Off the Shelf Solution*
Lightwave is the only company out there doing 10 psec 1 GHz lasers. They have a semi-off the shelf solution that seems to meet all of your requirements.

*Off the Shelf solution Close to Meeting Requirements*
Plenty of people out there come close but either the pulsewidth is too long or the PRF is too low. These are included because the concept definition may be possible with a system which has lower performance.

## 4.3 Summary of Industry Survey of Lasers which meet the requirements:

| Manfr (Location) | Model # | PW (psec) | PRF (Hz) | Wavelength (nm) | Energy/ Pulse (mJ) | Size (LxWxH mm) | Stability | MTBF (hours） | Cost per 1 unit |
|---|---|---|---|---|---|---|---|---|---|
| Ligthwave (Mt View, CA) Klaus Wit | 136-840-LSX100 (ss laser diode with passive mode locked saturable absorber) | <100 fsec | 100 MHz-2GHz | 840 nm | >35 mW @100 MHz <35 mW @ 1 GHz | 930 x 180 x 180 | | >10K | $84K |
| | Vanadate laser (Picalo) | 7 psec | 1 GHz | 1064 | 200 mW avg 0.2 nJ/pulse 20-30 W peak power | 100 x 130 x 250 | < 1 fsec pulse to pulse (250 fsec long term) | >10K | $50K |
| Sanders Lasers and EO Group | Custom | <10 psec | 1 GHz | Any | 0.2 nJ/pulse | 180 x 180 x 300 | < 1 fsec pulse to pulse | >10K | $50K |

The following is a list of short pulsewidth sources that are packaged well and may be useful but do not meet all the requirements in some area (either the PW is too long or the PRF is too low).

| Manfr (Location) | Model # | PW (psec) | PRF (Hz) | Wavelength (nm) | Energy/ Pulse (mJ) | Size (LxWxH mm) | Temporal Stability | Channels | Cost per 1 |
|---|---|---|---|---|---|---|---|---|---|
| Broadband Com-munications | 420B | 400 minimum | 3GHz | 1310 or 1550 | 0.63 mW | 257 x 264 x 115 | 0.005 UI RMS | | |
| | 400A | 500 minimum | 1GHz | 780-1550 | 0.5mW | 257 x 264 x 115 | | | |
| Spectra Physics | OPAL | <130 fsec | 82 MHz | | 1.3 &1.5 microns | >150 @ 1.3 and 1.5 microns | | | |
| Newport | L2010 | | 1GHz | 635-1750 | | | | | |
| Picosecond Pulse Labs | 4015C | 43 ps | 500KHz | Electrical pulse | | 965x213x 262 | <1ps | NA | |
| Picosecond Pulse | 4015 | <22 | 500 KHz | Electrical | | | 1 psec RMS | NA | |

| Labs | | | | pulse | | | | | |
|---|---|---|---|---|---|---|---|---|---|
| IntraAction | Standing wave AO device | 10 psec (threshold 1GHz sine wave | 1GHz | 780-1550 | High | Small | Function of RF source | | |
| Brimrose | Standing wave AO device | 10 psec (threshold 1GHz sine wave | 1GHz | 780-1550 | High | Small | Function of RF source | | |
| ILX Lightwave | 7900B | Sine wave out | 500KHz | 1310-1650 | | Rack mount | | | $5945/ laser source module  $3495/ basic rack unit |
| Santec | ECL-200 | | | 1520-1590 | 10 mW | 210x370x 110 | | 32 or 64 | |
| PicoQuant | PDL 800 | 40 | 80 MHz | 635 and 1060 | 500mW | Very small | | | |
| | Femtosecond Titanium sapphire laser | 20fs-200fs | 70-110 MHz | 740-950 | 1W | Shoebox Without power supply | | | |
| FiberVeiw | Subpicosecond fiber laser | 150 fs | 2 MHz | 1530-1560 | 100W peak | | | | |

## 4.4  Summary of Industry Survey of GHz detectors

| Manufacture (Location) | Model # | Active area (mm2) | Peak Wavelength (nm) | Responsivity (A/W) @ wavelength in nm | Package style (dimensions in mm) | NEP (w/sqrHz) | Rise time in nsec (f cutoff in Hz) | Temp range (operating) (°C) | Cost per 1 |
|---|---|---|---|---|---|---|---|---|---|
| UDT (Hawthorn CA) | PIN-UHS016 | .13 | 750 | 0.35 @ 830 nm | TO-18 | 7.2E-15 @ 830 nm | 0.25 (1.4 GHz) | -40-+100 | |
| | PIN-UHS016L | .13 | 750 | 0.35 @ 830 nm | TO-18 | 7.2E-15 @ 830 nm | 0.25 (1.4 GHz) | -40-+100 | |
| Hammamatsu (Bridge-water, NJ) | S5973 | 0.12 | 760 (320-1000) | 0.51 @ 780 nm | TO-18 | 1.5E-15 | 0.23 (1.5 GHz) | -40-+100 | |
| | S5973-01 | 0.12 | 760 (320-1000) | 0.51 @ 780 nm | TO-18 | 1.5E-15 | 0.23 (1.5 GHz) | -40-+100 | |
| Newport | PX-D7 | - | (400-900) | 0.05 @ 670 nm | Package with amp | 1x10-12 | 0.0058 (60 GHz) | Lab | $5900.00 |
| | 818-BB-31 | 0.44 | (1000-1600) | 0.8 @ 1300 | packaged | <1x10-13 | <0.2 | Lab | $579.00 |
| Fermionics (20 GHz in Simi Valley CA) | HSD-30 | - | 1300/1550 | 0.7 | Packaged (11x40x14) | - | 0.012 | 0-55 | |
| Sumitomo (transceiver) | SDM7604-XC | - | 830 | - | Packaged | - | - | - | - |
| Broadband Communications | 330A | | 1530-1565 | | | | (3 GHz) | | |

# 5. Appendix B: List of literature collected

1. A.M. Kan'an and P. Likamwa, "Ultrafast all-optical switching not limited by the carrier lifetime in an integrated multiple-quantum-well Mach-Zehnder interferometer," J. Opt. Soc. Am. B, Vol. 14, No. 11, pp. 3217-3223.

2. Z.Y. Cheng and C.S. Tsai, "Optically activated integrated optic Mach-Zehnder interferometer on GaAs," Applied Phys. Let., Vol. 59, No. 18, pp. 2222-2224.

3. Stegeman, G.I., Wright, E.M., Finlayson, N., Zanoni, R., and Seaton, C.T., "Third Order Nonlinear Integrated Optics," Journal of Lightwave Technology, Vol. 6, No. 6, pp. 953-970.

4. K. Al-hemyari, C.N. Ironside, and J.S. Aitchison, "Resonant nonlinear optical properties of GaAs/GaAlAs single quantum well waveguide and an integrated asymmetric Mach-Zehnder interferometer," IEEE Journal of Quantum Electronics, Vol. 28, No. 10, pp. 2051-2056.

5. M. Renaud, M. Bachmann, and M. Erman, "Semiconductor optical space switches," IEEE Journal of Selected Topics in Quantum Electronics, Vol. 2, No. 2, pp. 277-288.

6. P.A. Besse and H. Melchior, "All-optical switches based on Mach-Zehnder configuration with improved extinction ratios," IEEE Photonics Technology Letters, Vol. 9, No. 1, pp. 55-57.

7. R. Jin, C.L. Chuang, H.M. Gibbs, S.W. Koch, J.N. Polky, and G.A. Pubanz, "Picosecond all-optical switching in single-mode GaAs/AlGaAs strip-loaded nonlinear directional couplers," Applied Physics Letters, No. 53, Vol. 19, pp. 1791-1793.

8. S. Ohke, T. Umeda, and Y. Cho, "Analysis on waveguiding property of GaAs-AlGaAs MQW nonlinear optical waveguide," Electronics and Communications in Japan, Part 2, Volume 74, No. 4, pp. 12-20.

9. J. Leuthold, P.A. Besse, J. Eckner, E. Gamper, M. Dulk, and H. Melchior, "All-optical space switches with gain and principally ideal extinction ratios," IEEE Journal of Quantum Electronics, Vol. 34, No. 4, pp. 622-633.

10. S.T. Ho, C.E. Soccolich, M.N. Islam, W.S. Hobson, A.F.J. Levi, and R.E. Slusher, "Large nonlinear phase shifts in low-loss AlGaAs waveguides near half-gap," Applied Physics Letters, Vol. 59, No. 20, pp. 2558-2560.

11. S. Nakamura and K. Tajima, "Ultrafast all-optical gate switch based on frequency shift accompanied by semiconductor band-filling effect," Applied Physics Letters, Vol. 70, No. 26, pp. 3498-3500.

12. P. LiKamWa, A. Miller, C.B. Park, J.S. Roberts, and P.N. Robson, "All-optical switching of picosecond pulses in GaAs quantum well waveguide coupler," Applied Physics Letters, Vol. 57, No. 18, pp. 1846-1848.

13. K.W. DeLong and G.I. Stegeman, "Two-photon absorption as a limitation to all-optical waveguide switching in semiconductors," Applied Physics Letters, Vol. 57, No. 20, pp. 2063-2064.

14. R. Hess, M. Caraccia-Gross, W. Vogt, E. Gamper, P.A. Besse, M. Dulk, E. Gini, H. Melchior, B. Mikkelsen, M. Vaa, K.S. Jepsen, K.E. Stubkjaer, and S. Bouchoule, "All-optical demultiplexing of 80 to 10 Gb/s signals with monolithic integrated high-performance Mach-Zehnder interferometer," IEEE Photonics Technology Letters, Vol. 10, No. 1, pp. 165-167.

15. W. Hwang, M.Oh, H. Lee, H. Park, and J. Kim, "Polymeric 2x2 electrooptic switch consisting of asymmetric Y junctions and Mach-Zehnder interferometer," IEEE Photonics Technology Letters, Vol. 9, No. 6, pp. 761-763.

16. X. Leijtens, G. Yoffe, J. Haverkort, F. Karouta, J. Brubach, T. Eijkemans, L.M.F. Kaufmann, M.K. Smit, J.A.A. Stegemann, Y.C. Zhu, and J.H. Wolter, "2x2 Mach-Zehnder interferometric switch based on hetero-n-i-p-i quantum wells," Applied Physics Letters, Vol. 66, No. 20, pp. 2736-2738.

17. W. Bardyszewski, D. Yevick, Y. Liu, C. Rolland, and S. Bradshaw, "Theoretical and experimental analysis of Mach-Zehnder quantum-well modulators," Journal of Applied Physics, Vol. 80, No. 2, pp. 1136-1141.

18. A. Sneh, J.E. Zucker, and B.I. Miller, "Compact, low-crosstalk, and low-propagation-loss quantum-well Y-branch switches," IEEE Photonics Technology Letters, Vol. 8, No. 12, pp. 1644-1646.

19. P. LiKamWa and A.M. Kan'an, "Ultrafast all-optical switching in multiple quantum-well Y-junction waveguides at the band gap resonance," IEEE Journal of Selected Topics in Quantum Electronics, Vol. 2, No. 3, pp. 655-660.

20. Y. Silberberg and B.G. Sfez, "All-optical phase- and power-controlled switching in nonlinear waveguide junctions," Optics Letters, Vol. 13, No. 12, pp. 1132-1134.

21. A.M. Kan'an, P. LiKamWa, M. Dutta, and J. Pamulapati, "1.7 ps consecutive switching in an integrated multiple quantum-well Y-junction optical switch," IEEE Photonics Technology Letters, Vol. 8, No. 12, pp. 1641-1643.

22. J.S. Aitchison, D.C. Hutchings, J.U. Kang, G.I. Stegeman, and A. Villeneuve, "The nonlinear optical properties of AlGaAs at the half band gap," IEEE Journal of Quantum Electronics, Vol. 33, No. 3, pp. 341-348.

23. Y.H. Lee, A. Chavez-Pirson, S.W. Koch, H.M. Gibbs, S.H. Park, J. Morhange, A. Jeffery, N. Peyghambarian, L. Banyai, A.C. Gossard, and W. Wiegmann, "Room-temperature optical nonlinearities in GaAs," Physical Review Letters, vol. 57, No. 19, pp. 2446-2449.

24. D.S. Chemla, D.A.B. Miller, and P.W. Smith, "Nonlinear optical properties of GaAs/GaAlAs multiple quantum well material: phenomena and applications," Optical Engineering, Vol. 24, No. 4, pp. 556-564.

25. R.S. Grant, "Effective nonlinear coefficients of optical waveguides," Optical and Quantum Electronics, Vol. 28, pp. 1161-1173.

26. D. Campi, P.J. Bradley, R. Calvani, and R. Caponi, "Modeling of nonlinear absorption and refraction in quantum-well structures for all-optical switching," IEEE Journal of Quantum Electronics, Vol. 29, No. 4, pp. 1144-1157.

27. S. Nakamura, K. Tajima, and Y. Sugimoto, "Cross-correlation measurement of ultrafast switching in a symmetric Mach-Zehnder all-optical switch," Applied Physics Letters, Vol. 67, No. 17, pp. 2445-2447.

28. P. Gunning, J.K. Lucek, D. Nesset, J.V. Collins, C.W. Ford, D. Pitcher, K. Smith, D. Cotter, E. Jahn, N. Agrawal, and A.S. Siddiqui, "Optical TDMA LAN incorporating packaged integrated Mach-Zehnder interferometer channel selector," Electronics Letters, Vol. 33, No. 16, pp. 1404-1406.

29. J. Bell, K. Al-hemyari, J.S.Aitchison, C.N. Ironside, G.T. Kennedy, and W. Sibbett, "Demonstration of all-optical switching in a symmetric Mach-Zehnder interferometer," Electronics Letters, Vol. 31, No. 24, pp. 2095-2097.

30. P.A. Besse and H. Melchior, "All-optical switches based on Mach-Zehnder configuration with improved extinction ratios," IEEE Photonics Technology Letters, Vol. 9, No. 1, pp. 55-57.

31. N.S. Patel, K.L. Hall, and K.A. Rauschenbach, "Interferometric all-optical switches for ultrafast signal processing," Applied Optics, Vol. 37, No. 14, pp. 2831-2842.

32. H. Kobayashi, R. Takahashi, Y. Matsuoka, and H. Iwamura, "1 Tbit/s demultiplexing using low temperature grown InGaAs/InAlAs multiple quatum wells," Electronics Letters, Vol. 34, No. 9, pp. 908-910.

33. S.D. Lau, J.P. Donnelly, C.A. Wang, R.B. Goodman, and R.H. Rediker, "Optical phase difference measurement and correction using AlGaAs integrated guided-wave components," IEEE Photonics Technology Letters, Vol. 3, No. 10, pp. 902-904.

34. N. Agrawal, C.M. Weinert, H.J. Ehrke, G.G. Mekonnen, D. Franke, C. Bornholdt, and R. Langenhorst, "Fast 2x2 Mach-Zehnder optical space switches using InGaAsP-InP multiquantum-well structures," IEEE Photonics Technology Letters, Vol. 7, No. 6, pp. 644-645.

35. J.E. Zucker, K.L. Jones, B.I. Miller, and U. Koren, "Miniature Mach-Zehnder InGaAsP quantum well waveguide interferometers for 1.3 μm," IEEE Photonics Technology Letters, Vol. 2, No. 1, pp. 32-34.

36. R.P. Espindola, M.K. Udo, D.Y. Chu, S.L. Wu, S.T. Ho, R.C. Tiberio, P.F. Chapman, and D. Cohen, "All-optical switching with low-peak power in microfabricated AlGaAs waveguides," IEEE Photonics Technology Letters, Vol. 7, No. 6, pp. 641-643.

37. C. Amano, S. Matsuo, T. Kurokawa, and H. Iwamura, "20 dB contrast GaAs/AlGaAs multiple quantum-well nonresonant modulators," IEEE Photonics Technology Letters, Vol. 4, No. 1, p. 31-33.

38. J.E. Zucker, K.L. Jones, G.R. Jacobovitz, B. Tell, K. Brown-Goebeler, T.Y. Chang, N.J. Sauer, M.D. Divino, M. Wegener, and D.S. Chemla, "InGaAs-InAlAs quantum well intersecting waveguide switch operating at 1.55 μm," IEEE Photonics Technology Letters, Vol. 2, No. 11, pp. 804-806.

39. M. Fetterman, C.P. Chao, and S.R. Forrest, "Fabrication and analysis of high-contrast InGaAsP-InP Mach-Zehnder modulators for use at 1.55 μm wavelength," IEEE Photonics Technology Letters, Vol. 8, No. 1, pp. 69-71.

40. J.E. Zucker, T.Y. Chang, M. Wegener, N.J.Sauer, K.L. Jones, and D.S. Chemla, "Large refractive index changes in tunable-electron-density InGaAs/InAlAs quantum wells," IEEE Photonics Technology Letters, Vol. 2, No. 1, pp. 29-31.

41. W.S. Rabinovich, G. Beadie, and D.S. Katzer, "Intersubband X3 in coupled InGaAs-AlGaAs multiple quantum wells," IEEE Journal of Quantum Electronics, Vol. 34, No. 6, pp. 975-981.

42. J.S. Aitchison, A. Villeneuve, and G.I. Stegeman, "All-optical switching in a nonlinear GaAlAs X junction," Optics Letters, Vol. 18, No. 14, p. 1153-1155.

43. S. Nakamura, K. Tajima, and Y. Sugimoto, "High repetition operation of a symmetric Mach-Zehnder all-optical switch," Applied Physics Letters, Vol. 63, No. 19, pp. 2457-2459.

44. K. Al-hemyari, A. Villeneuve, J.U. Kang, J.S. Aitchison, C.N. Ironside, and G.I. Stegeman, "Ultrafast all-optical switching in GaAlAs directional couplers at 1.55 μm without multiphoton absorption," Applied Physics Letters, Vol. 63, No. 26, pp. 3562-3564.

45. A. Villeneuve, P. Mamyshev, J.U. Kang, G.I. Stegeman, J.S. Aitchison, and C.N. Ironside, "Efficient time-domain demultiplexing with separate signal and control wavelengths in an AlGaAs nonlinear directional coupler," IEEE Journal of Quantum Electronics, Vol. 31, No. 12, pp. 2165-2172.

46. K.I. Kang, T.G. Chang, I. Glesk, and P.R. Prucnal, "Comparison of Sagnac and Mach-Zehnder ultrafast all-optical interferometric switches based on a semiconductor resonant optical nonlinearity," Applied Optics, Vol. 35, No. 3, pp. 417-426.

47. Z. Xiang, P. Ye, K.J. Guan, and J.T. Lin, "A novel OTDM frame synchronization scheme based on a terahertz optical asymmetric demultiplexer with feedback," IEEE Photonics Technology Letters, Vol. 11, No. 1, pp. 125-127.

48. E.J. Murphy, T.F. Adda, W.J. Minford, R.W. Irvin, E.I. Ackeman, and S.B. Adams, "Guided-wave optical time delay network," IEEE Photonics Technology Letters, Vol. 8, No. 4, pp. 545-547.

49. S. Kawanishi, "Ultrahigh-speed optical time-division-multiplexed transmission technology based on optical signal processing," IEEE Journal of Quantum Electronics, Vol. 34, No. 11, pp. 2064-2079.

50. C.H. Wang, A.D. Lloyd, and B.S. Wherrett, "Design ad modeling of asymmetric Fabry-Perot electrooptic modulators containing a polymeric film," IEEE Journal of Quantum Electronics, Vol. 30, No. 3, pp. 724-731.

51. T. Fujiwara, A. Watanabe, and H. Mori, "Measurement of uniformity of driving voltage in Ti:LiNbO3 waveguides using Mach-Zehnder interferometers," IEEE Photonics Technology Letters, Vol. 2, No. 4, pp. 260-261.

52. K. Wakita, I. Kotaka, and H. Asai, "High-speed InGaAlAs/InAlAs multiple quantum well electrooptic phase modulators with bandwidth in excess of 20 GHz," IEEE Photonics Technology Letters, Vol. 4, No. 1, pp. 29-31.

53. W. Wang, D. Chen, H.R. Fetterman, Y. Shi, W. H. Steier, and L.R. Dalton, "40 GHz polymer electrooptic phase modulators," IEEE Photonics Technology Letters, Vol. 7, No. 6, pp. 638-640.

54. S. Nakamura, Y. Ueno, and K. Tajima, "Ultrafast (200-fs switching, 1.5 Tb/s demultiplexing) and high-repetition (10 GHz) operations of a polarization-discriminating symmetric Mach-Zehnder all-optical switch," IEEE Photonics Technology Letters, Vol. 10, No. 11, pp. 1575-1577.

55. M. Cada, R.C. Gauthier, B.E. Paton, and J. Chrostowski, "Nonlinear guided waves coupled nonlinearly in a planar GaAs/GaAlAs multiple quantum well structure," Applied Physics Letters, Vol. 49, No. 13, pp. 755-757.

56. P.R. Berger, Y. Chen, P. Bhattacharya, J. Pamulapati, and G.C. Vezzoli, "Demonstration of all-optical modulation in a vertical guided-wave nonlinear coupler," Applied Physics Letters, Vol. 52, No. 14, pp. 1125-1127.

57. R. Jin, C.L. Chuang, H.M. Gibbs, S.W. Koch, J.N. Polky, and G.A. Pubanz, "Picosecond all-optical switching in single-mode GaAs/AlGaAs strip-loaded nonlinear directional couplers," Applied Physics Letters, Vol. 53, No.19, pp. 1791-1793.

58. T. Huang, Y. Chung, L.A. Coldren, and N. Dagli, "Field-induced waveguides and their application to modulators," IEEE Journal of Quantum Electronics, Vol. 29, No. 4, pp. 1131-1143.

59. U. Das, Y. Chen, and P. Bhattacharya, "Nonlinear effects in coplanar GaAs/InGaAs strained-layer superlattice directional couplers," Applied Physics Letters, Vol. 51, No. 23, pp. 1679-1681.

60. K. Tajima, "All-optical switch with switch-off time unrestricted by carrier lifetime", Japanese Journal of Applied Physics, Vol. 32, No. 12A, pp. L1746-L1749.

61. S. Nakamura, K. Tajima, and Y. Sugimoto, "Experimental investigation on high-speed switching characteristics of a novel symmetric Mach-Zehnder all-optical switch," Applied Physics Letters, Vol. 65, No. 3, pp. 283-285.

62. S. Nakamura, K. Tajima, and Y. Sugimoto, "High-repetition operation of a symmetric Mach-Zehnder all-optical switch," Applied Physics Letters, Vol. 66, No. 19, pp. 2457-2459.

63. E. Jahn, N. Agrawal, M. Arbert, H.J. Ehrke, D. Franke, R. Ludwig, W. Pieper, H.G. Weber, and C.M. Weinert, "40 Gb/s all-optical demultiplexing using a monolithically integrated Mach-Zehnder interferometer with semiconductor laser amplifiers," Electronics Letters, Vol. 31, No. 21, pp. 1857-1858.

64. E. Jahn, N. Agrawal, H.Jehrke, R. Ludwig, W. Pieper, and H.G. Weber, "Monolithically integrated asymmetric Mach-Zehnder interferometer as a 20 Gbit/s all-optical add/drop multiplexer for OTDM systems," Electronics Letters, Vol. 32, No. 3, pp. 216-217.

65. S. Nakamura, K. Tajima, and Y. Sugimoto, "Cross-correlation measurement of ultrafast switching in a symmetric Mach-Zehnder all-optical switch," Applied Physics Letters, Vol. 67, No. 17, pp. 2445-7.

66. K. Al-hemyari, J.S. Aitchison, C.N. Ironside, G.T. Kennedy, R.S. Grant, and W. Sibbett, "Ultrafast all-optical switching in GaAlAs integrated interferometer in 1.55 µm spectral region," Electronics Letters, Vol. 28, No. 12, pp. 1090-1092.

67. I. Glesk, J.P. Sokoloff, and P.R. Prucnal, "Demonstration of all-optical demultiplexing of TDM data at 250 Gbit/s," Electronics Letters, Vol. 30, No. 4, pp. 339-341.

68. S.D. Benjamin, A. Othonos, and P.W.E. Smith, "Large ultrafast optical nonlinearities in As-rich GaAs," Electronics Letters, Vol. 30, No. 20, pp. 1704-1706.

69. K.I. Kang, I. Glesk, T.G. Chang, P.R. Prucnal, and R.K. Boncek, "Demonstration of all-optical Mach-Zehnder demultiplexer," Electronics Lettes, Vol. 31, No. 9, pp. 749-750.

70. B. Broberg and S. Lindgren, "Refractive index of InGaAsP layers and InP in the transparent wavelength region," J. Appl. Physics, Vol. 55, No. 9, pp. 3376-3381.

71. C. Lawetz, J.C. Cartledge, C. Rolland, and J. Yu, "Modulation characteristics of semiconductor Mach-Zehnder optical modulators," J. Lightwave Technology, Vol. 15, No. 4, pp. 697-703.

72. G.J.M. Krijnen, A. Villeneuve, G.I. Stegeman, O. Lambeck, and H. Hoekstra, "A versatile all-optical modulator based on nonlinear Mach-Zehnder interferometers" Proceedings of 1994 Nonlinear Optics: Materials, Fundamentals and Applications. Held: Waikoloa, HI, USA 25-29 July 1994. 1994 IEEE Nonlinear Optics: Materials, Fundamentals, and Applications, pp. 412-14.

73. J.S. Aitchison, "All-optical switching using AlGaAs waveguide devices at 1.55 mu m" Held: London, UK 3 Nov. 1993. IEE Colloquium on 'Ultra-Short Optical Pulses' pp. 8/1-5.

74. P. LiKamWa, J.E. Sitch, N.J. Mason, J.S. Roberts, and P.N. Robson, "All-optical multiple-quantum-well waveguide switch," Electronics Letters, Vol. 21, No. 1, pp. 26-28.

75. H.S. Loka, S.D. Benjamin, and P.W.E. Smith, "Optical characterization of low-temperature-grown GaAs for ultrafast all-optical switching devices," IEEE Journal of Quantum Electronics, vol. 34, No. 8, pp. 1426-37.

76. A. Villeneuve, K. Al-hemyari, J.U. Kang, C.N. Ironside, J.S. Aitchison, and G.I. Stegeman, "Demonstration of all-optical demultiplexing at 1555 nm with an AlGaAs directional coupler," Electronics Letters, Vol. 29, No. 8, pp. 721-2.

77. H.S. Loka and P.W.E. Smith, "Ultrafast all-optical switching in an asymmetric Fabry-Perot device using low-temperature-grown GaAs," IEEE Photonics Technology Letters, vol. 10, No. 12, pp. 1733-5.

78. W. Wang, D. Chen, H.R. Fetterman,, Y. Shi, W.H. Steier, and L.R. Dalton, "40 GHz polymer electrooptic phase modulators," IEEE Photonics Technology Letters, Vol. 7, No. 6, pp. 638-40.

79. M. A. Fisher, H. Wickes, G.T. Kennedy, R.S. Grant, and W. Sibbett, "Ultrafast nonlinear refraction in an active MQW waveguide," Electronics Letters, Vol. 29, No. 13, pp. 1185-6.

80. W.J. Dally, M.-J. E. Lee, F.-T. R. An, J. Poulton, and S. Tell, "High Performance Electrical Signaling", MPPOI98, 1998. [postscript, 749KB] [zip'ed postscript, 277KB] [PDF, 110KB]

# 6. Appendix C: Simulation and Result

```
===========================================
```

Library Name: Optical-Net
Physical Location: /usr/home/hpc/lawrence/oand/
Owner: clawrenc
Version: 3.6
Current Access: read
Allowed Access: write


Data Structure
   Basic Bit Message
   cm-mod-cmd
   cm-npe-msg
   cm-rvd-cmd
   cm-tvd-cmd
   Control States
   det-cm-msg
   fdr-mod-msg
   fdr-rvd-msg
   fdr-toad-msg
   fiber-fdr-msg
   fiber-pps-msg
   mll-pps-msg
   mod-tvd-msg
   npe-cm-msg
   npe-cm-pkt-hdr
   PPS-Combiner-O1
   pps-fiber-msg
   rvd-toad-msg
   toad-det-msg
   tvd-fiber-msg

Module
   16 Node Network
   16-Port PPS
   4 Node Net
   4 Node Net 2
   4 Node Net 3
   4 Node Net 4
   4 Node Net 4 Plus
   4 Node Net 4 Plus 2
   4 Node Net Active
   4 Node Net Active 4
   4 Node Net Active 4 New
   4-Node Optical Network
   4-Port HUB
   4-Port PPS
   4-Port PPS/Combiner
   4-Port PPS/Splitter
   A-Bit Buffer Control
   A-Bit Buffer Control II
   ABC Test
   Bit Message Maker
   Buffer Reset Module

Module (Continued)
    Communications Manager (CM)
    Communications Manager (CM) 2
    Communications Manager (CM) 5
    Communications Manager (CM) 6
    Communications Manager (CM) 7
    Communications Manager (CM) 8
    Complete Optical Node
    Complete_Optical_Node_Test
    Control States
    Da Test
    Detector
    Detector Data - Filler / Filter
    Detector Data - Filler / Filter 2
    Feeder (Fdr)
    Fiber HO
    Fiber OH
    HUB
    HUB-test
    HUB2
    ILA Rank Memory
    Mod Cmd Generator
    Mode Locked LASER
    Modulator
    Node & NIC Test
    Node - Processor Host
    Node O-Queue Mgr
    Node Processing Elements (NPE)
    NPE Msg Generator
    NPE Msg Generator 2
    NPE-CM-test
    NPE_Test
    One Node Net Test
    One Node Net Test 2
    ONIC
    ONIC 2
    ONIC 3
    ONIC 4
    ONIC 5
    ONIC 6
    Optical Network
    Packet Bit-Generator
    PPS/Combiner
    PPS/Splitter
    PPS/Splitter2
    Protocol Control
    Protocol Control 2
    Protocol Control Proto
    Random Int Generator
    Random Int Generator 2
    Random Int Generator 3
    Rch_Cmd_Generator
    RCVR A-Bit Disposition
    RCVR D-Bits Disposition

Module (Continued)
RCVR Packet Segment Cycle Handler
RCVR S-Bit Disposition
Receiver Variable Delay Element (RVD)
Receiver-test
RIG 2000
Seed Tester
Synch Pulse Generator
Synch Test 1
Synchronizer
Tch_Cmd_Generator
TOAD
TOAD2
Transceiver Test
Transceiver Test-HUB&Fibers
Transceiver Test-TOAD
Transceiver Test-TOAD'n HUB
Transceiver Variable Delay Element (TVD)
Transceiver-test
Uniform Pulse
U[0,1) Rangen 2
XCVR A-Bit Disposition
XCVR D-Bits Disposition
XCVR Handler Test
XCVR Packet Segment Cycle Handler
XCVR S-Bit Disposition

Plot
16 Node Network: I/O
2C: Detector Data Inputs
2C: Nodes Output
2C: Node 1: Packets Generated
2C: Node 1: All Output
4-Node ON: Plot
4-Node ON: Plot 2
Delays
Delays2
IO
N1_Host Pkt Trans
Node 1: Analysis
Node 1: Detector Vs. Filler/Filter
Send & Receive
Send & Receive: 500ns
Send & Receive: Synchronization
Two Nodes: Input
Two Nodes: Output
Two Nodes: Output 1500

Simulation
16 Nodes; 1 Sender
4 Node Net Sim
4 Node ONet 2
4 Node Optical Network - DB
4 Nodes; 1 Sender

Simulation (Continued)
    4-Node-1
    ABC Test 1
    Ahtah Time
    Complete-Node-Test
    D98_4_Node_Net
    Eye-on-ONIC
    Gutta Go
    Hub-test-sim
    Node & NIC Test 1
    Node & NIC Test 2
    NPE-CM-test-sim
    NPE_test
    One More Time
    One Node & No Net
    One Node - One Prayer
    One Node Net Test 1
    One Node Net Test II
    ONIC-debug-sim
    RIG 2
    RIG 2000 TEST 1
    RTest 1
    Seed Test 1
    Star Wars Returns
    Synch Test 1A
    The Empire Strikes Back
    The New Hope
    The Return of the Jedi
    TOAD/Transceiver-Test
    Two Contenders
    URNG
    Wing and a Prayer
    XCVR Handler Test 1
    XCVR Handler Test 3
    XCVR Handler Test 4
    XCVR Handler Test 5

Symbol
    PPS
    test
    test2

# 4 Node Optical Network

Mode Locked LASER

4-Port PPS

Fiber OH

Fiber OH

Fiber OH

Fiber OH

ONIC 5

ONIC 5

PROCESSOR HOST

PROCESSOR HOST

Node 2
100

Node 1
110

<-- Optical Network Interface Card

<-- Optical Network Interface Card

⇑P LASER Pulse Rate

⇑P Start Time
⇑P Stop Time

⇑P Number of Channels

⇑P M_Fbr_Len
⇑P n_Fbr_Len

⇑P fiber_length_in_meters
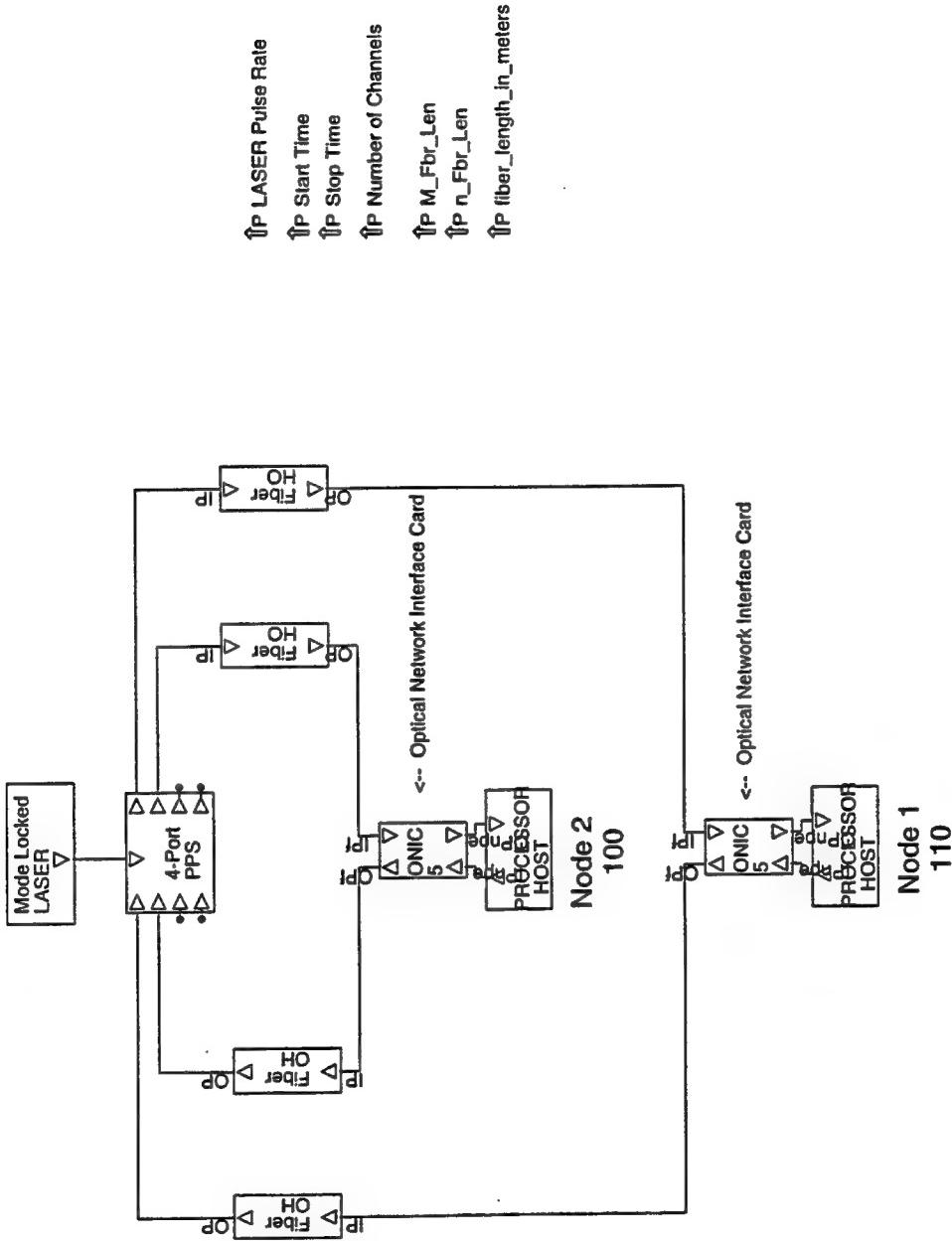
# 16 Node Optical Network

# 4 Node Optical Network

# 4-Port HUB

# Mode Locked LASER

# 4-Port PPS

IPL

IP

4-Port
PPS/Combiner

IP1
IP2
IP3
IP4

IP1
IP2
IP3
IP4

mOP1 mIP1
mOP2 mIP2

4-Port
PPS/Splitter

OP1
OP2
OP3
OP4

OP1
OP2
OP3
OP4
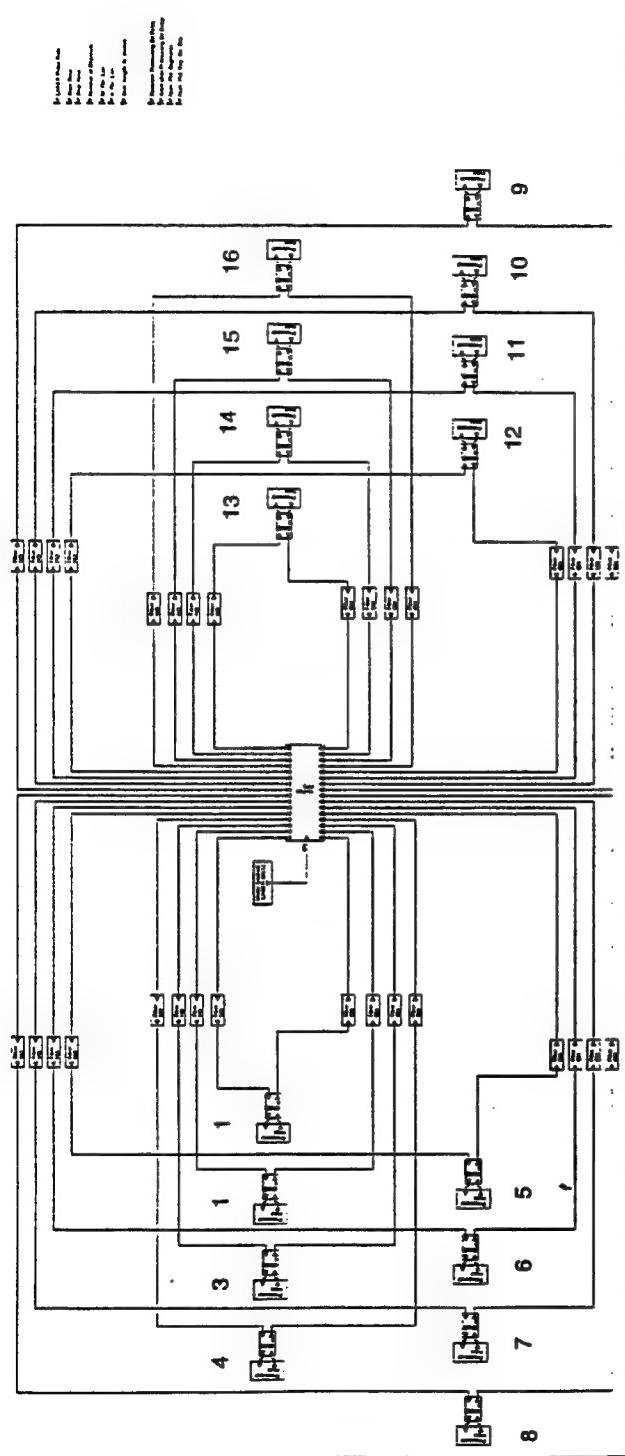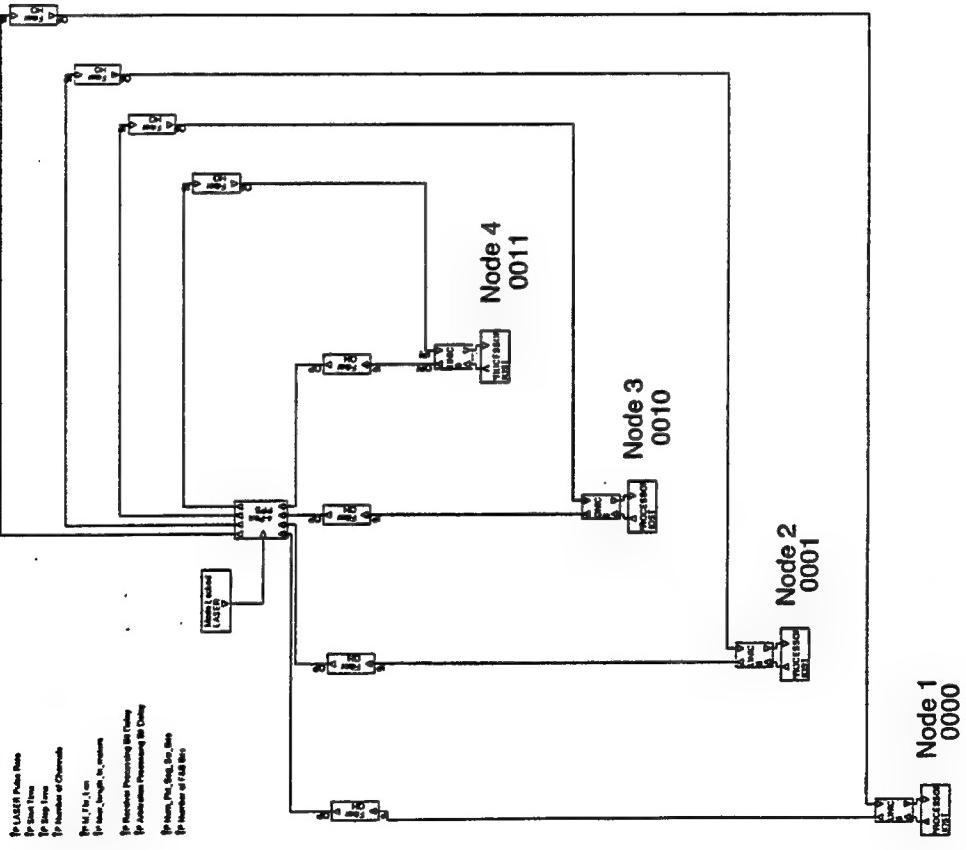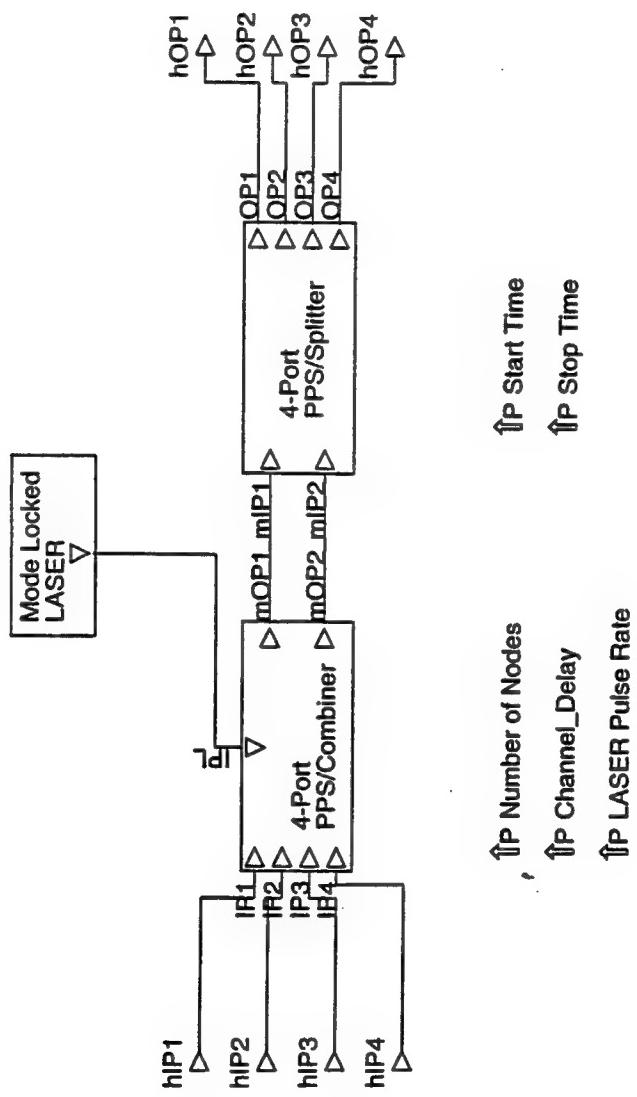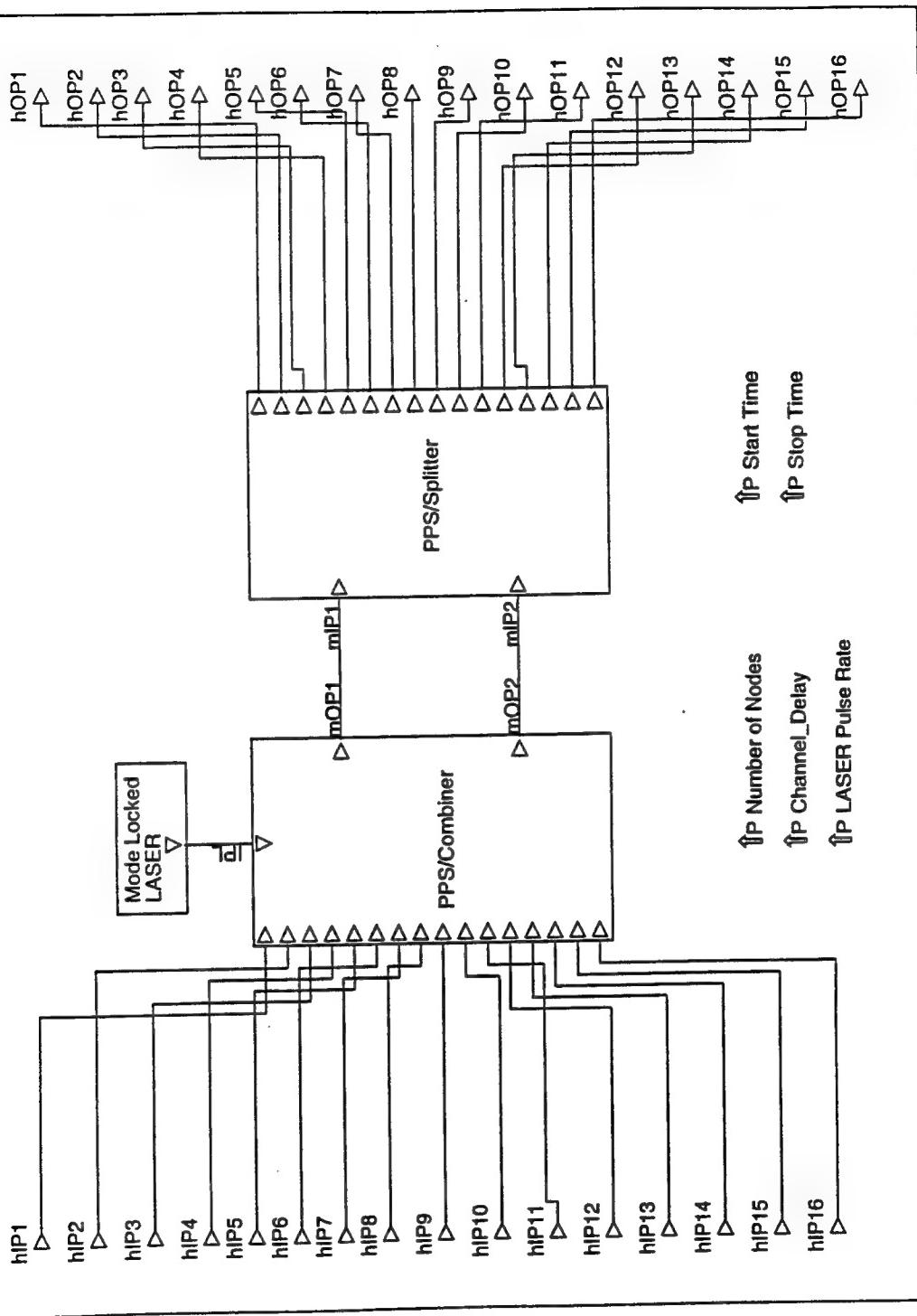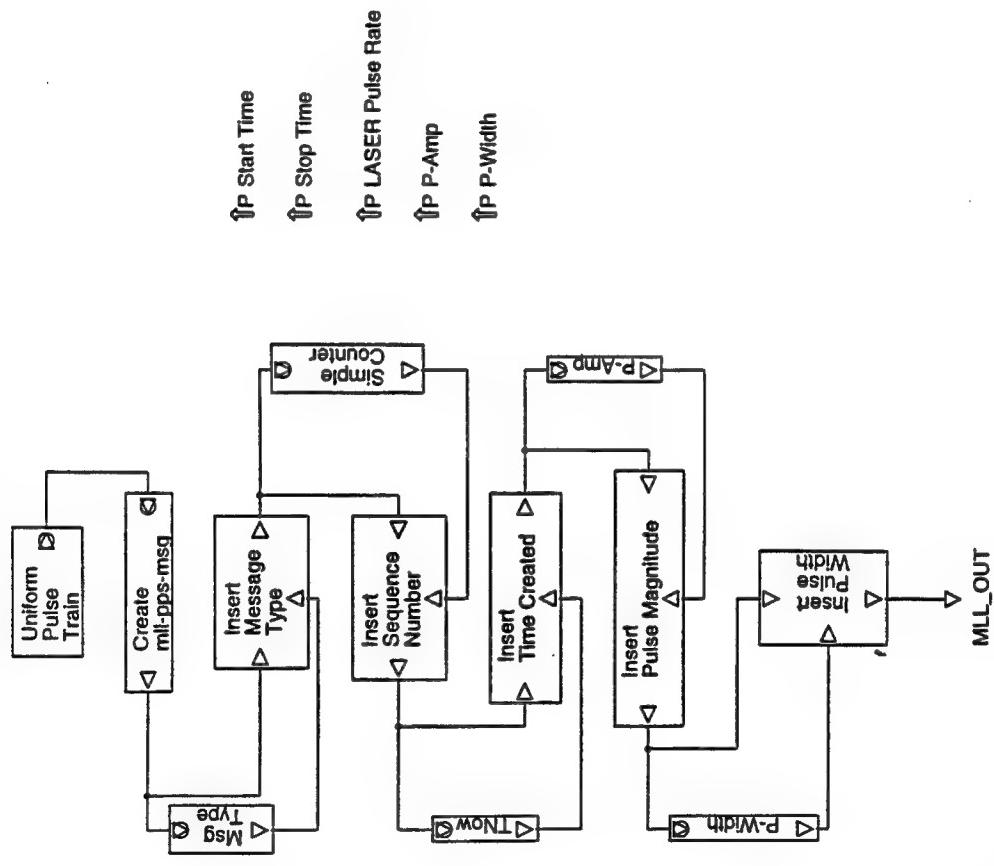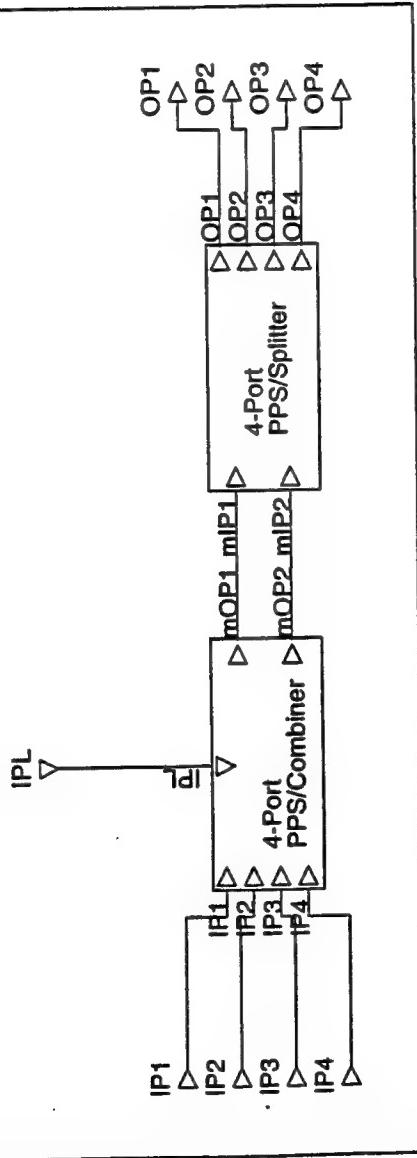
# 16-Port PPS

# PPS/Combiner

⇧P Number of Nodes
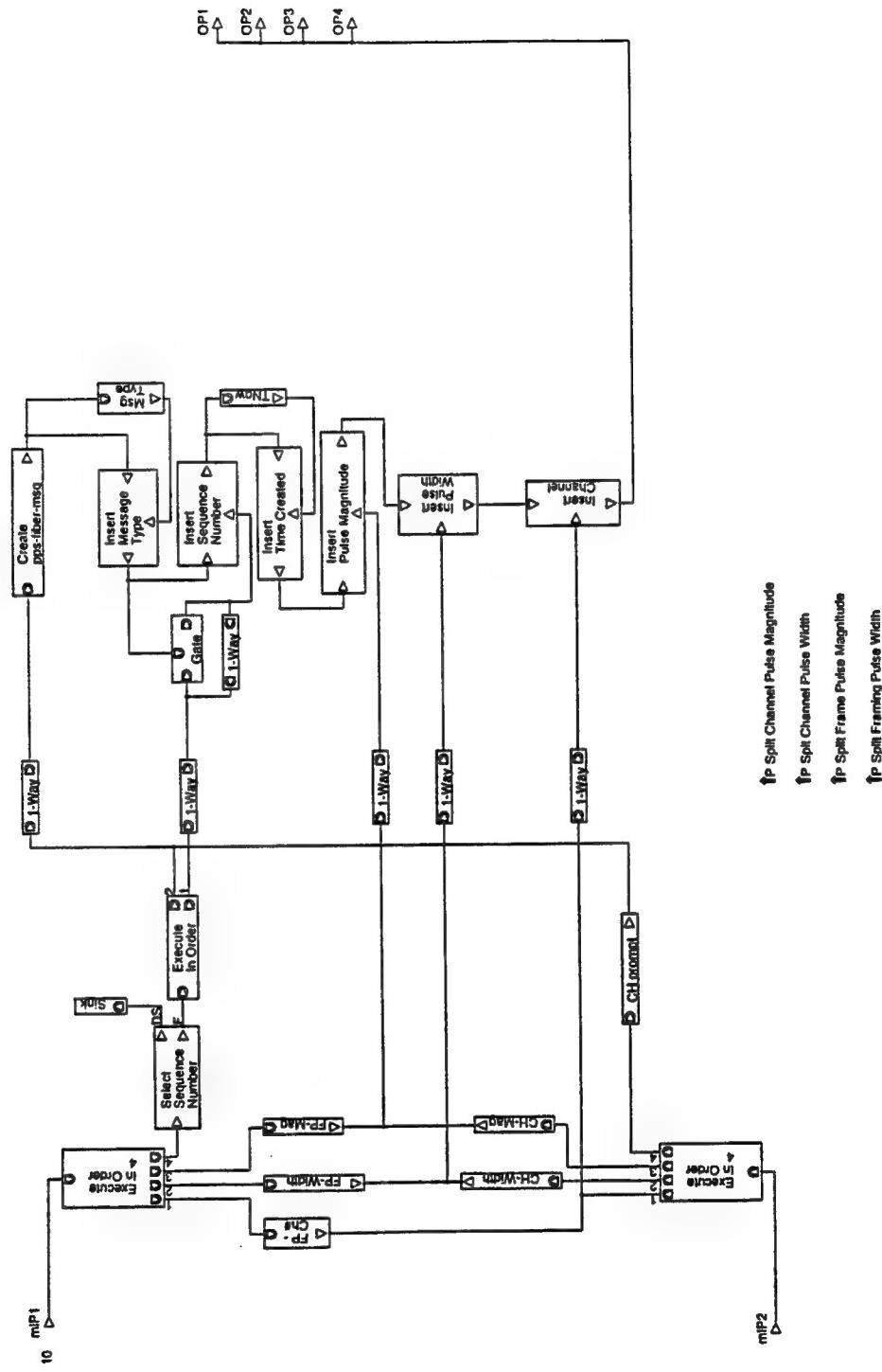
⇧P Channel_Delay

IPL

Unit Pulse

mOP1    10

CH-TSlot Cntr

CH-TSlot > 0

OPEN Post FP Delay

OPEN Channel Delay

CH == #Nodes

Sink

Execute in Order

RESET

Accumulator

Send CH No.

Chnl Data?

mOP2    Integer

Terminate Simulation

Not NULL

Sink

R-Channel Pulse

IP1

IP2

IP3

IP4

68

PPS/Splitter

4-Port PPS/Splitter    [ 31-Mar-1999 9:02:07 ]

69

PPS/Combiner

70
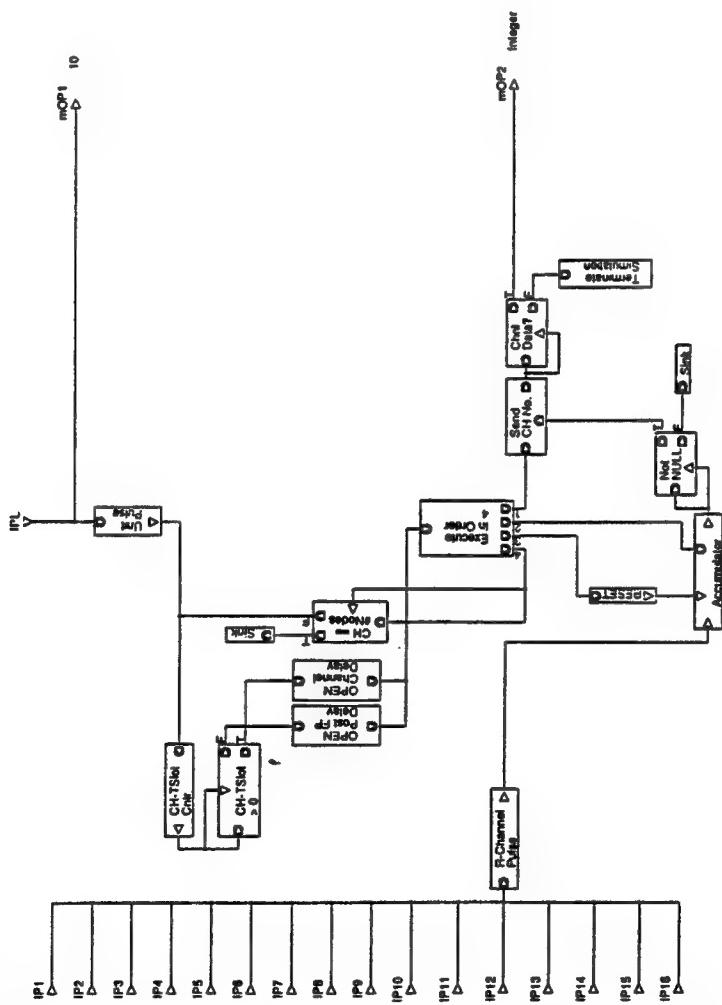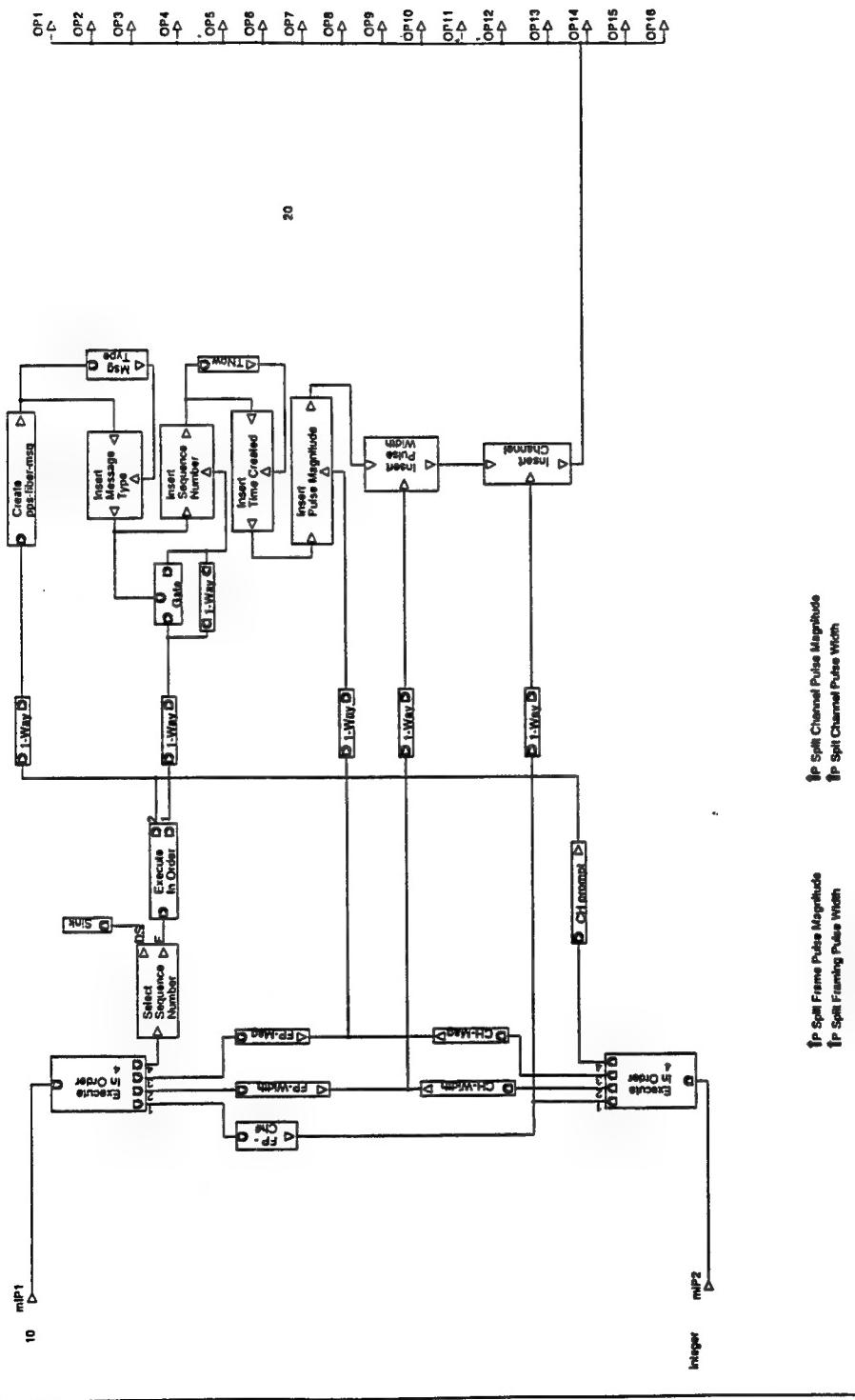
PPS/Splitter

PPS/Splitter
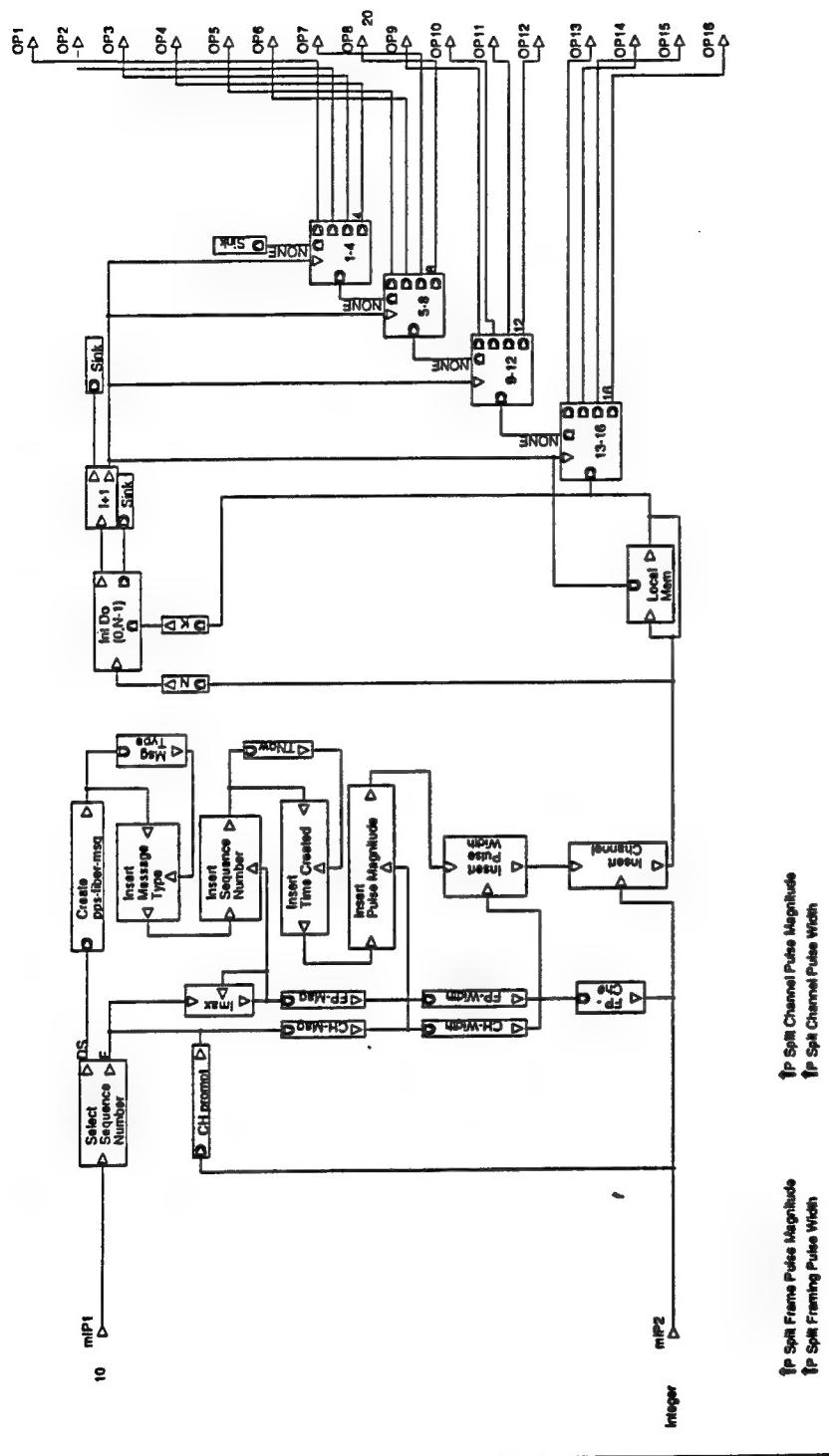
# Optical Fiber O-H
# (FIBER O-H)

**IP**

**Coerce
to fiber-pps-msg**

**Fixed
Abs Delay**

**Insert
Time
Sent**

**OP**

**TNow**
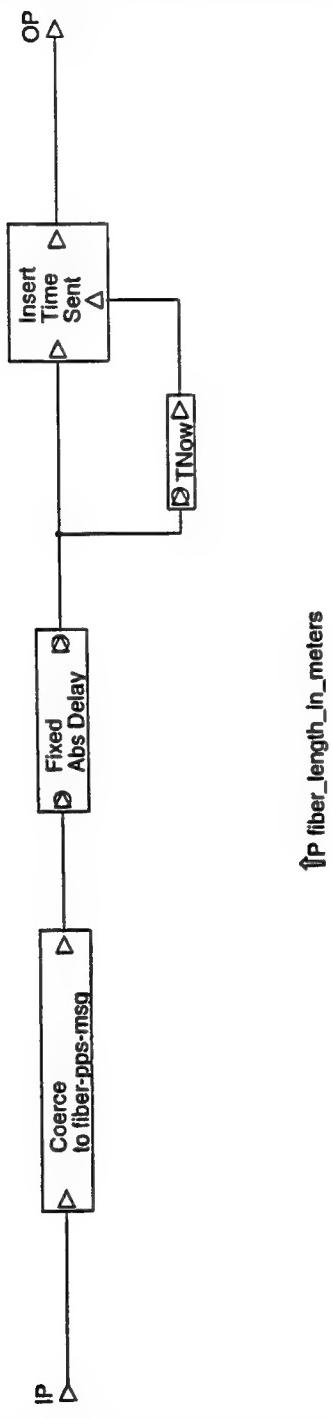
⇑**P fiber_length_in_meters**

# Optical Fiber H-O
# (FIBER H-O)

IP

Coerce
to fiber-ldr-msg

Fixed
Abs Delay

Insert
Time
Sent

OP

TNow

IP fiber_length_in_meters

# ONIC: Optical Network Interface Card

Transceiver Variable Delay Element (TVD)

Feeder (Fdr)

Modulator

Receiver Variable Delay Element (RVD)

TOAD

Detector

Communications Manager (CM) 8

IPFiber 30
OPFiber 90
OPnpe 116
IPnpe 120

IP Node ID

IP Num_Pkt_Seg_Sw_Bits
P Num_Pkt_Segments
P Num_Pkt_Seg_Bits
P Num_Pkt_Seg_D_Bits
IP Number of F&B Bits

IP Bit 1 A
IP Bit 2 A
IP Bit 3 A
IP Bit 4 A
IP Bit 1 B
IP Bit 2 B
IP Bit 3 B
IP Bit 4 B

IP Default Receive Channel

IP Stop Time
IP CM Clock Period
IP CM Clock Init
IP Bit Period
IP Receiver Processing Bit Delay
IP Arbitration Processing Bit Delay
IP Number of Channels

P M_Fbr_Del
P M_Synch_Del
IP M_Fbr_Len
P n_Fbr_Del
P n_Synch_Del
IP n_Fbr_Len

P RCVR Synch Offset
P XCVR Synch Offset

# ONIC: Transceiver Variable Delay Element (TVD)

# ONIC:  Transceiver Modulator
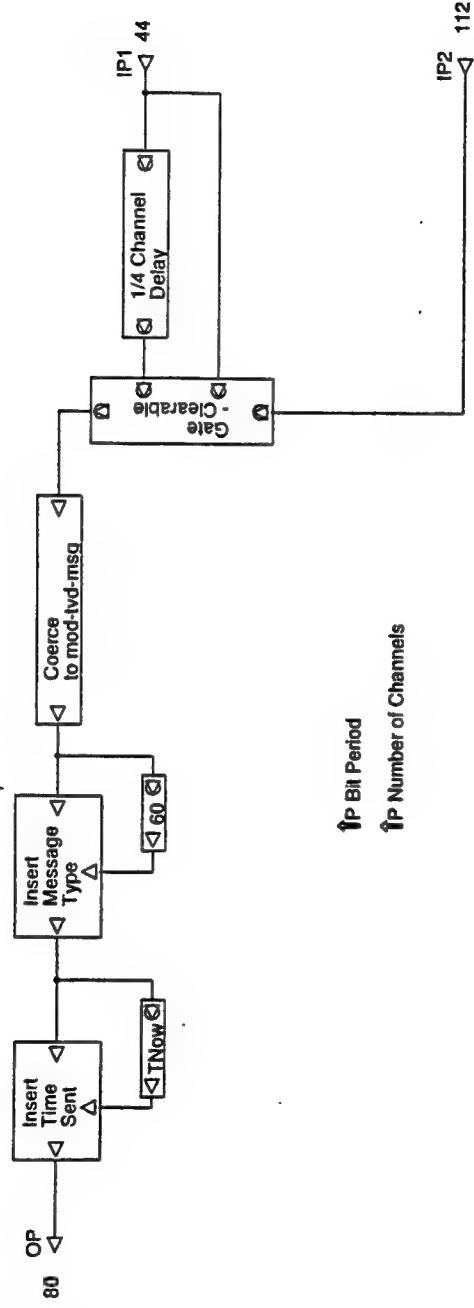
# ONIC: Feeder (Fdr)
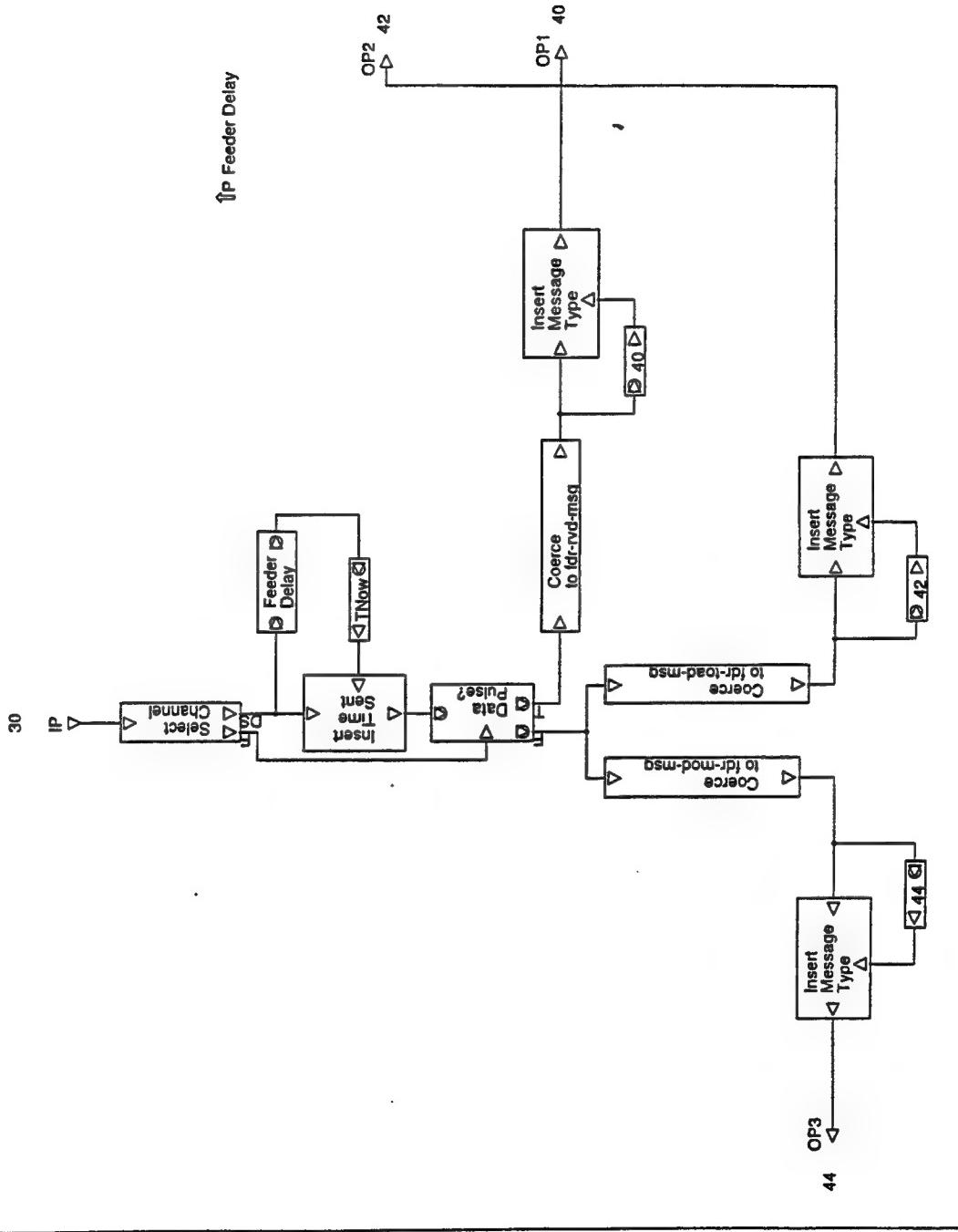
# ONIC: Receiver Variable Delay Element (RVD)
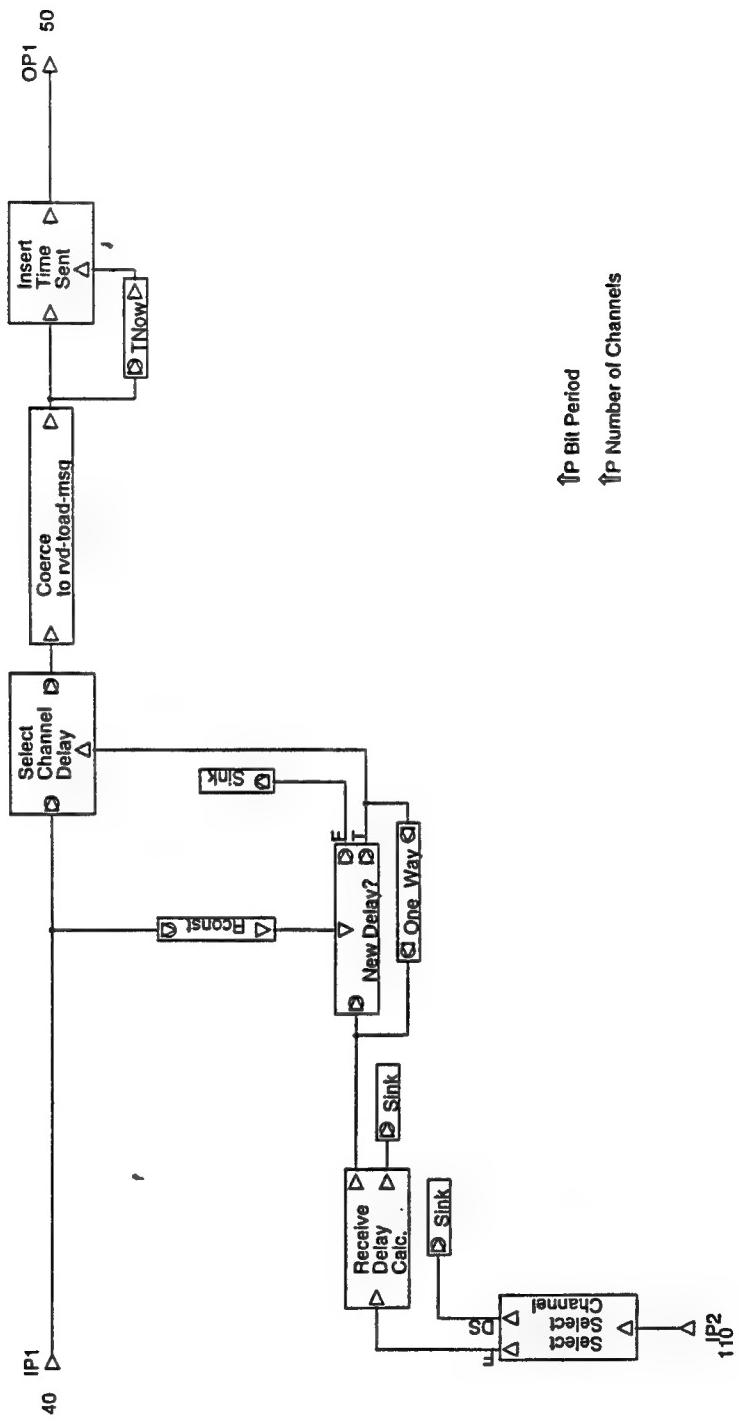
# ONIC: Receiver TOAD

# ONIC: Receiver Detector (Det)
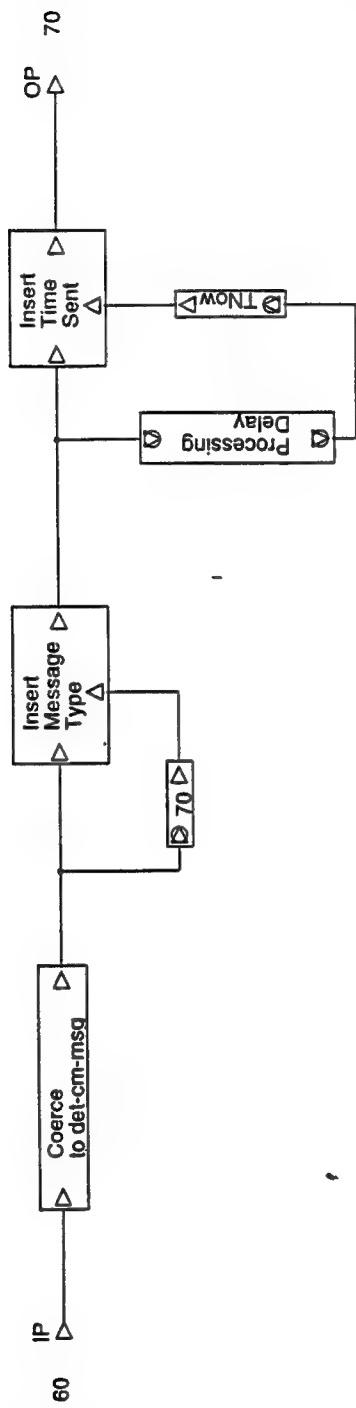
# ONIC - Communications Manager

# Tch_Cmd_Generator

Otch_set

Simple
Counter

Insert
Sequence
Number

Insert Destination
Channel

Create
cm-tvd-cmd

Itch_set
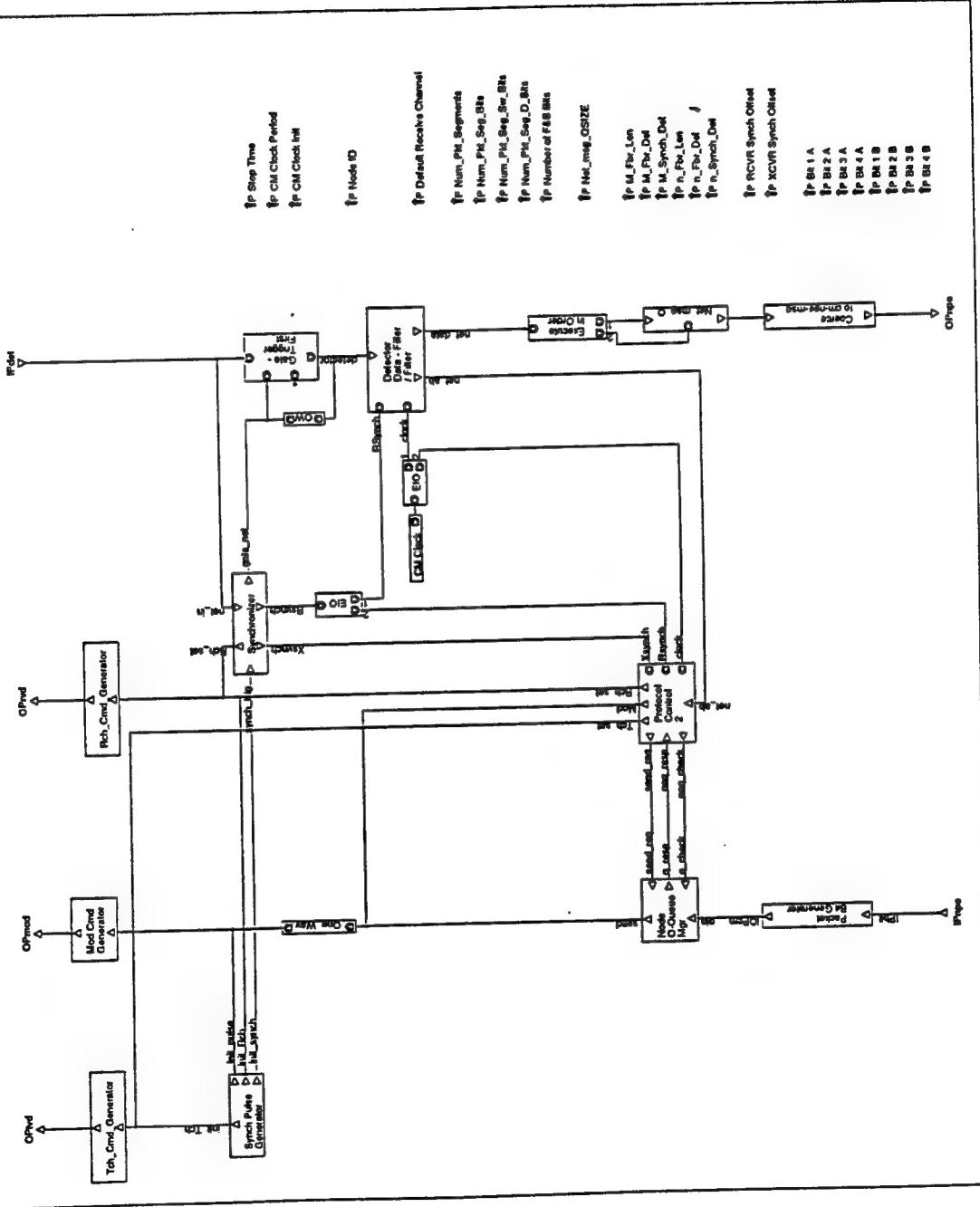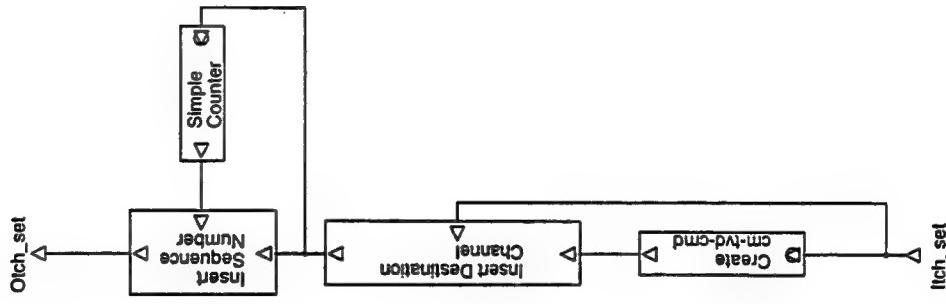
# Modulator Command Generator
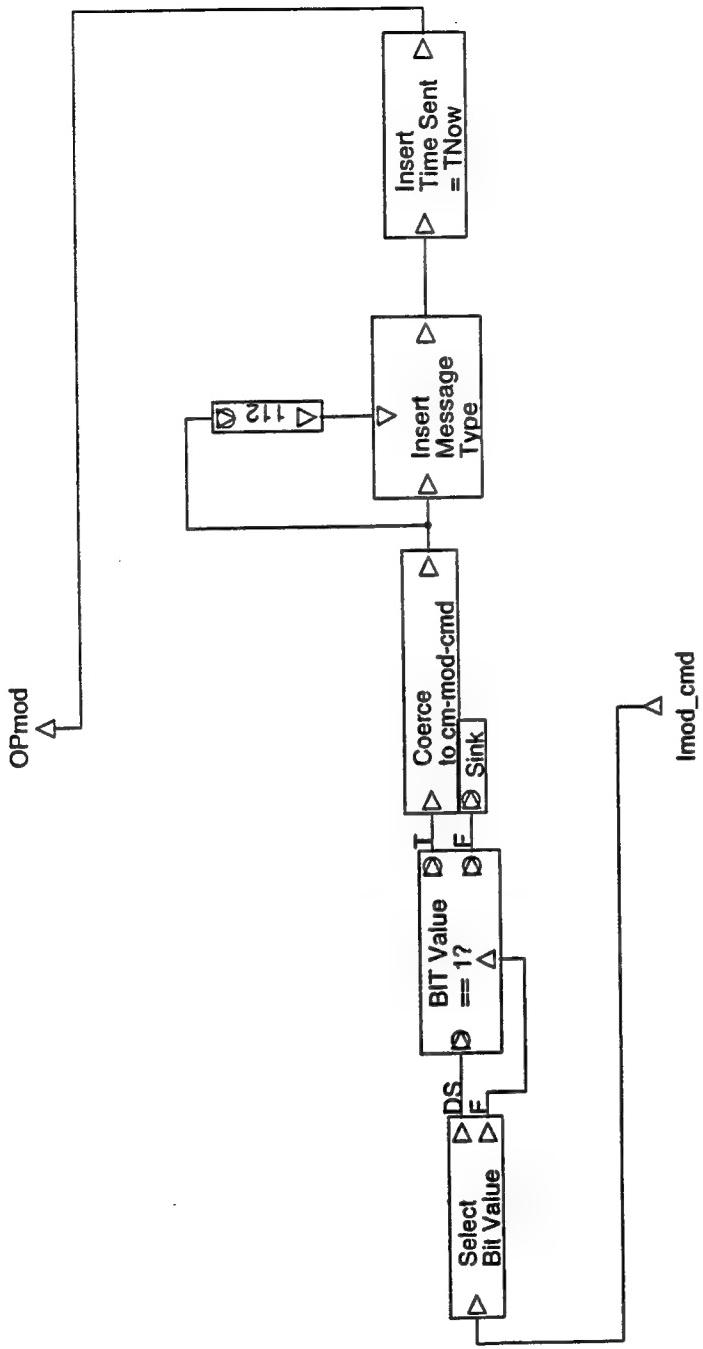
# Rch_Cmd_Generator

# Synch Pulse Generator



86
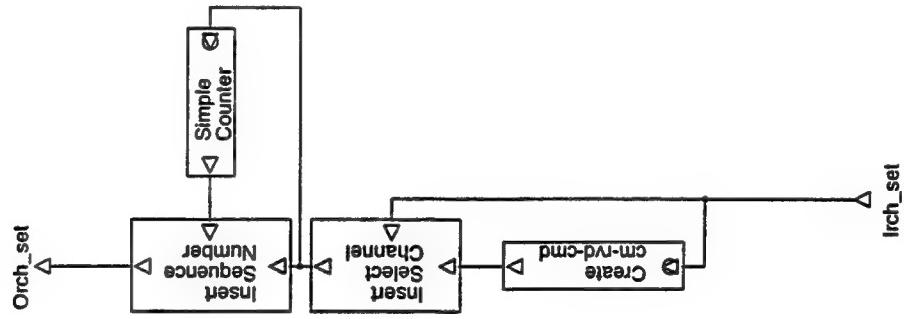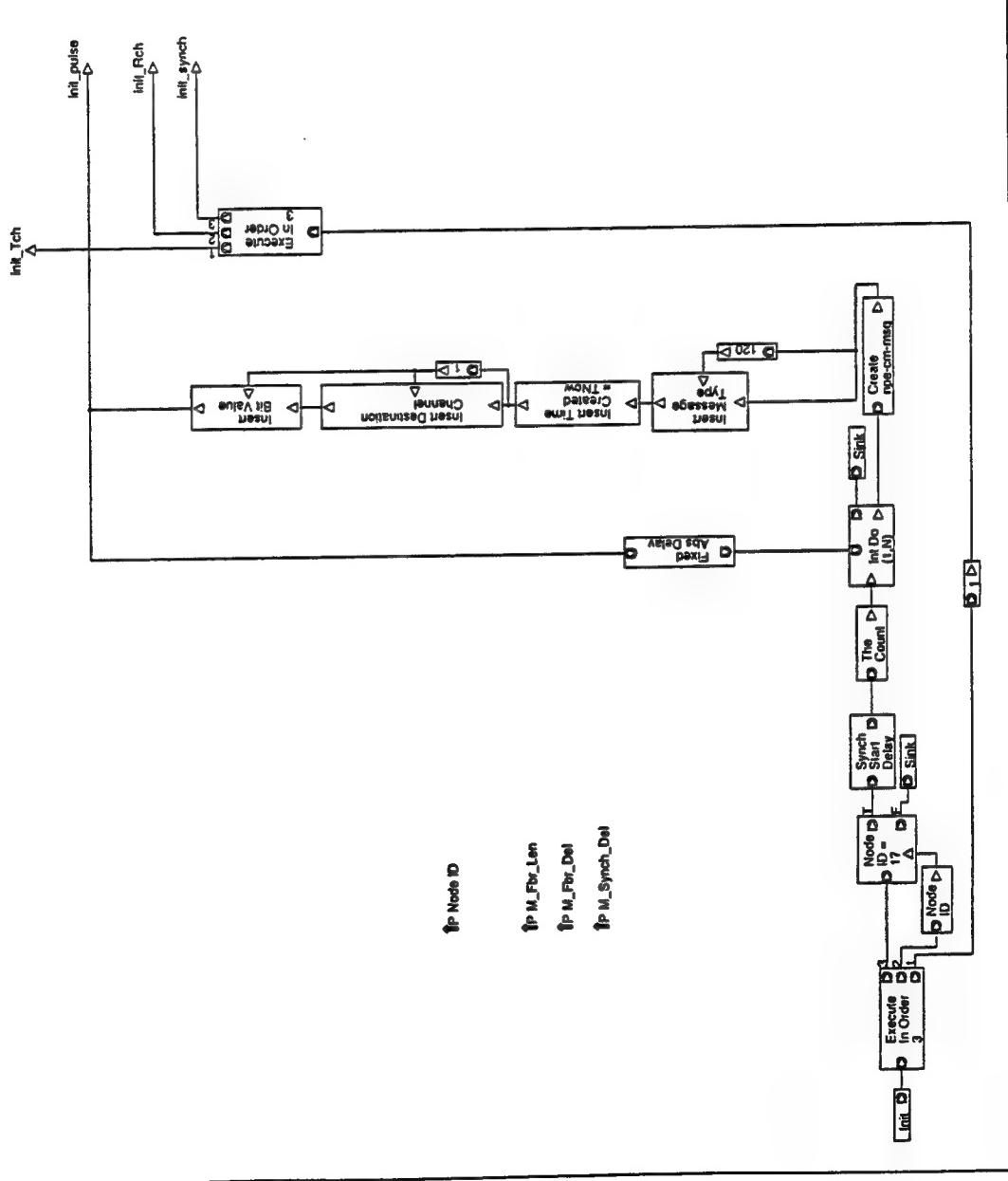
Synchronizer
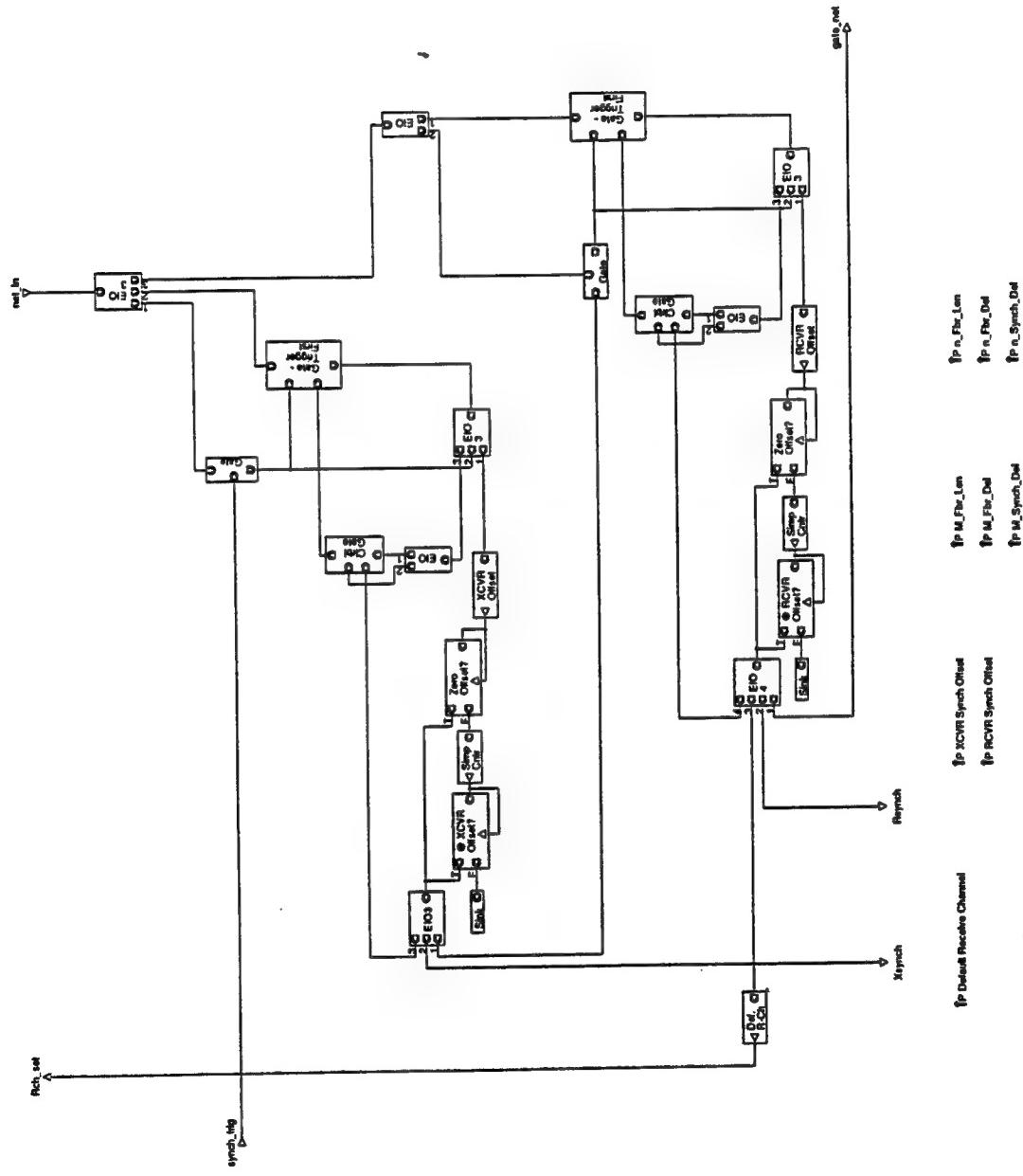
# Node Output Queue Manager



₽ Node_Output_OSIZE
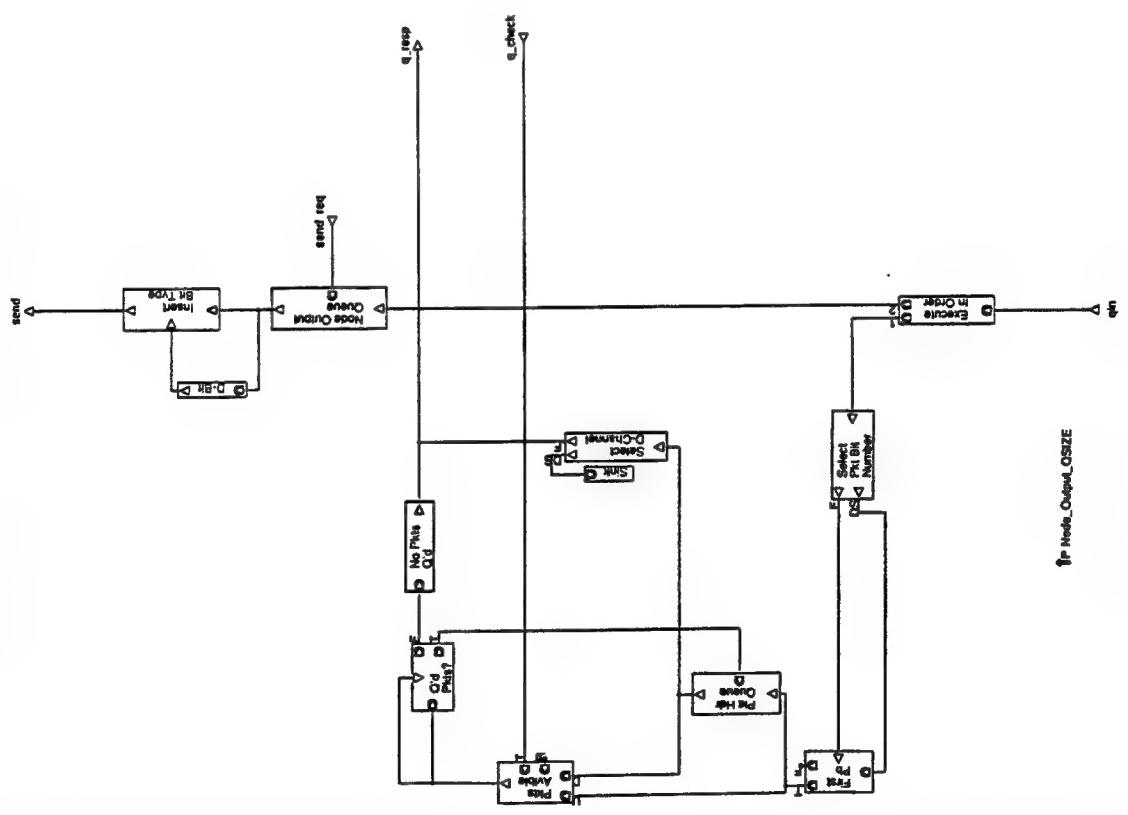
# Packet Bit Generator
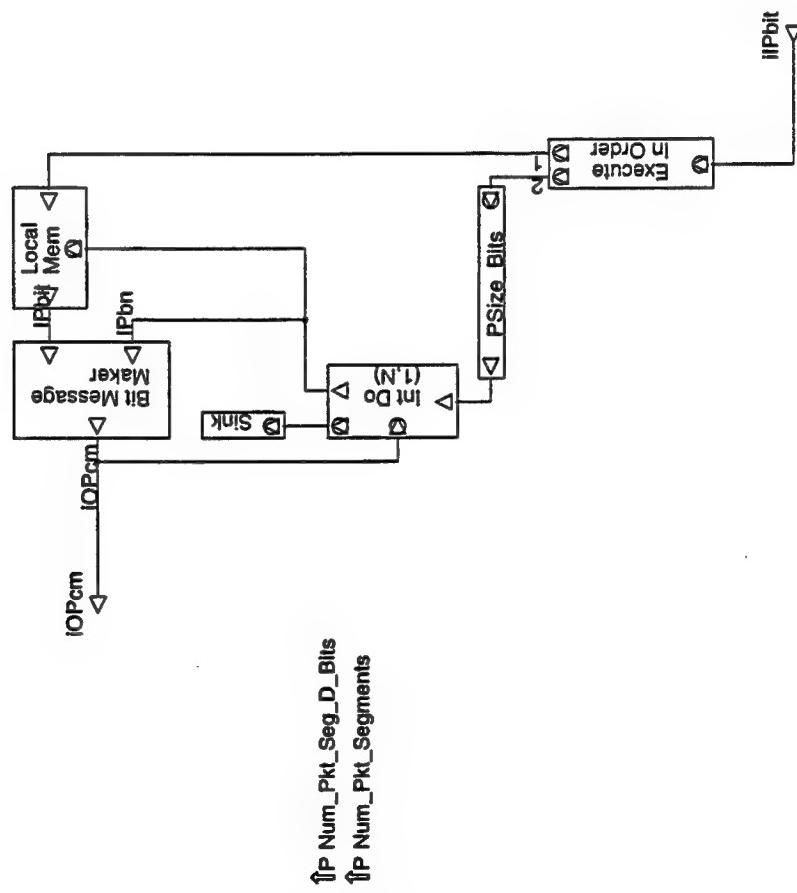
# Detector Data - Filler / Filter

Protocol Control

91
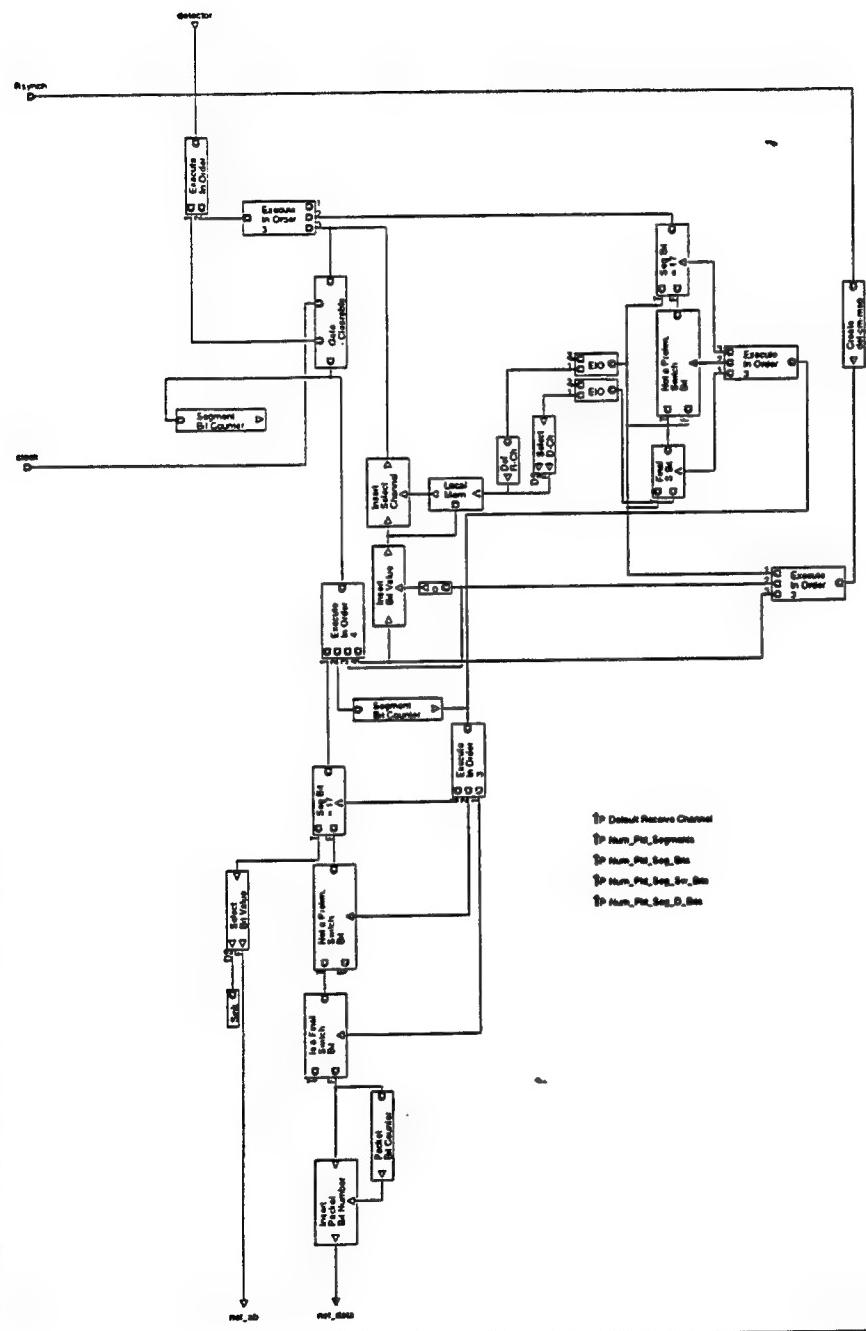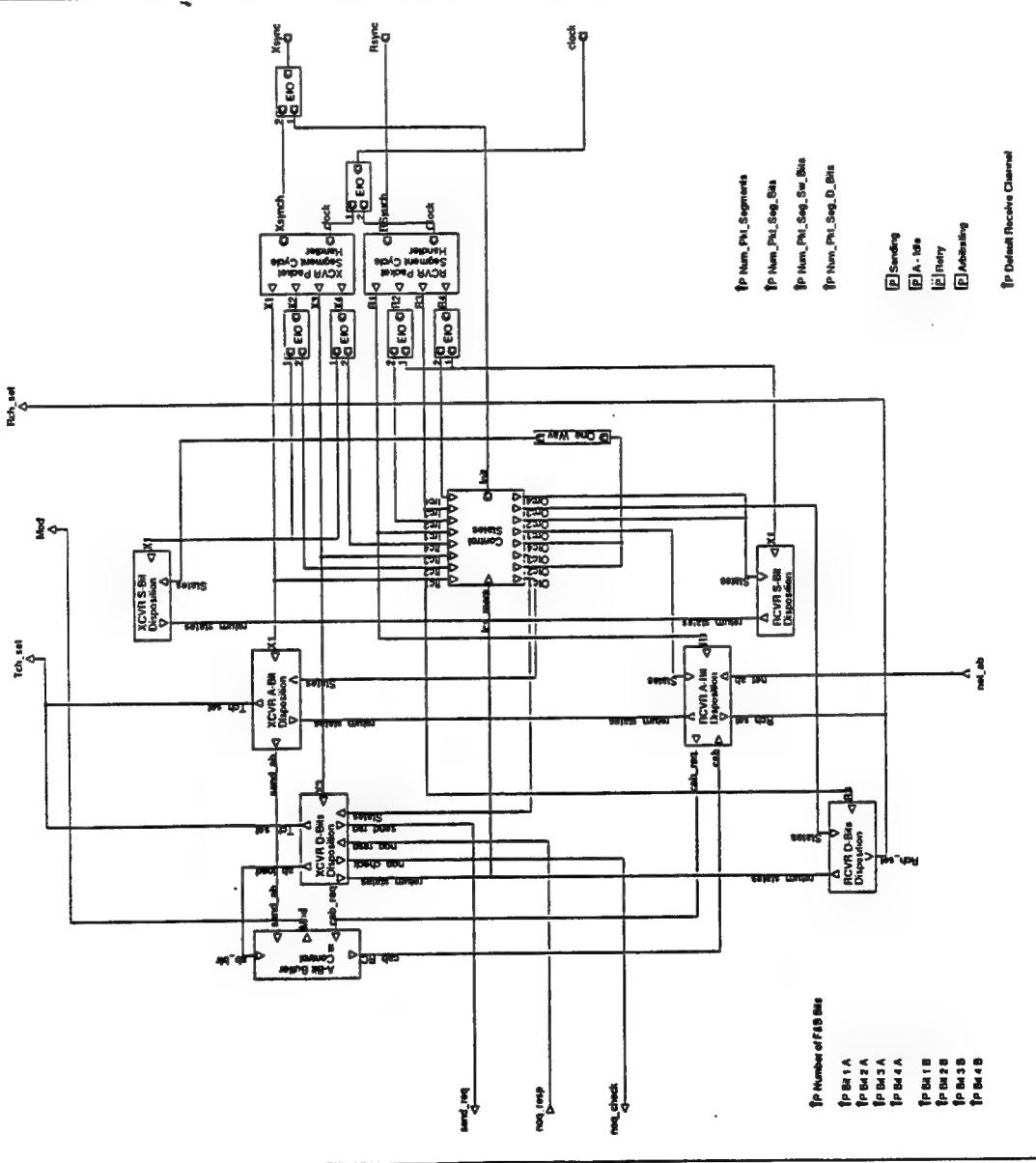
# XMTR Packet Segment Cycle Handler
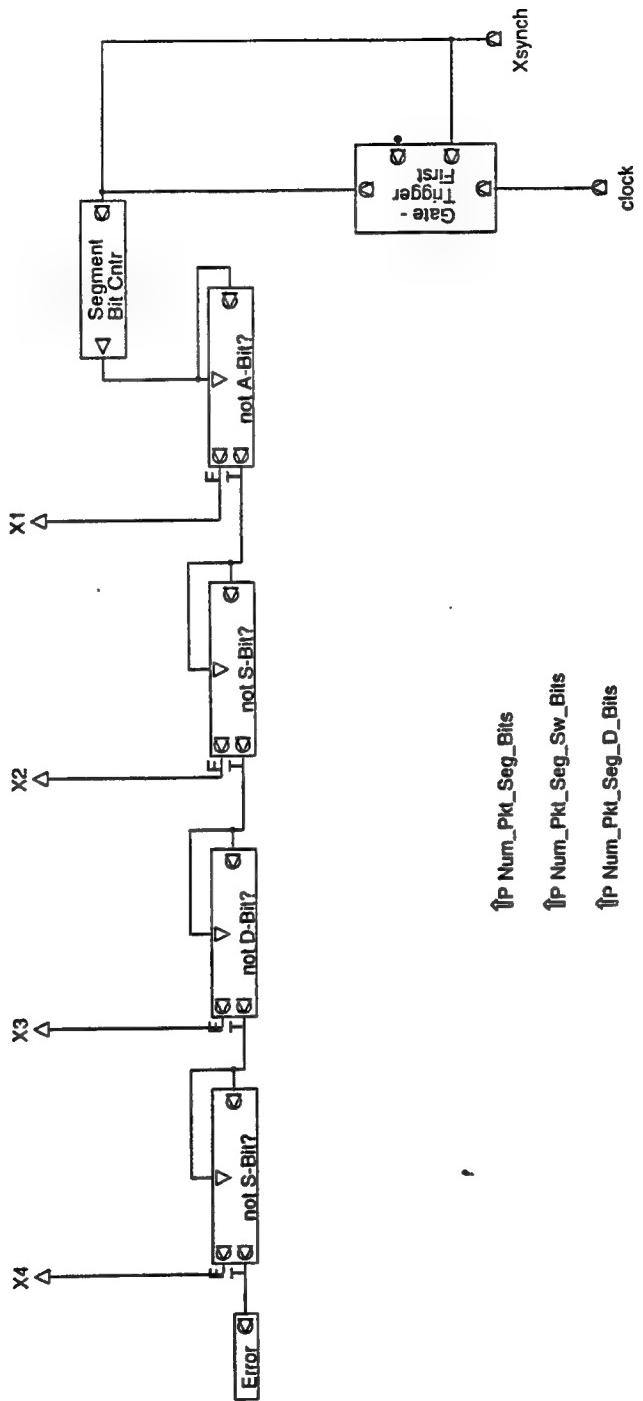
# XMTR A-Bit Disposition

# XMTR S-Bit Disposition

states

X1

Insert
Xseg_bit_count

return_states
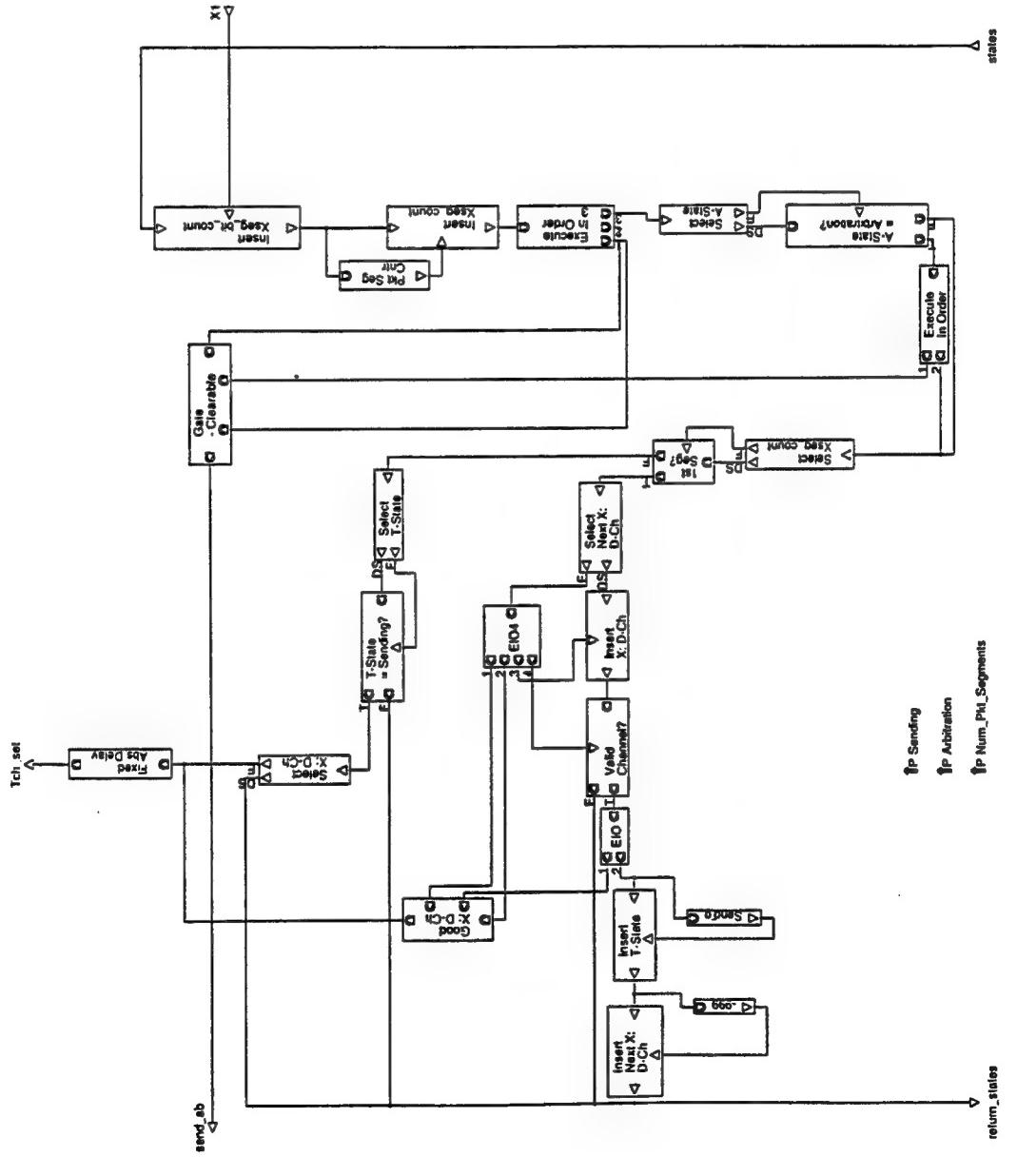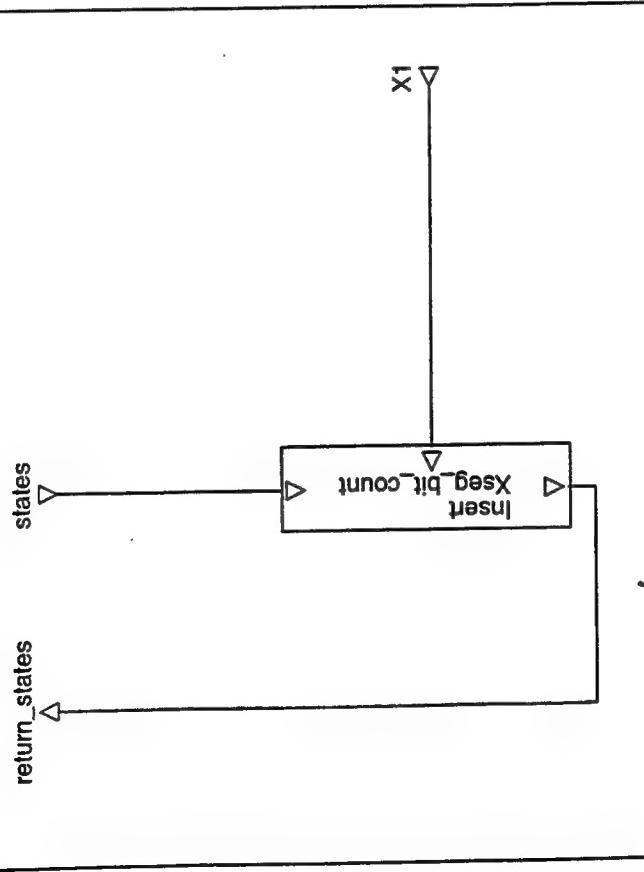
# XMTR D-Bits Disposition
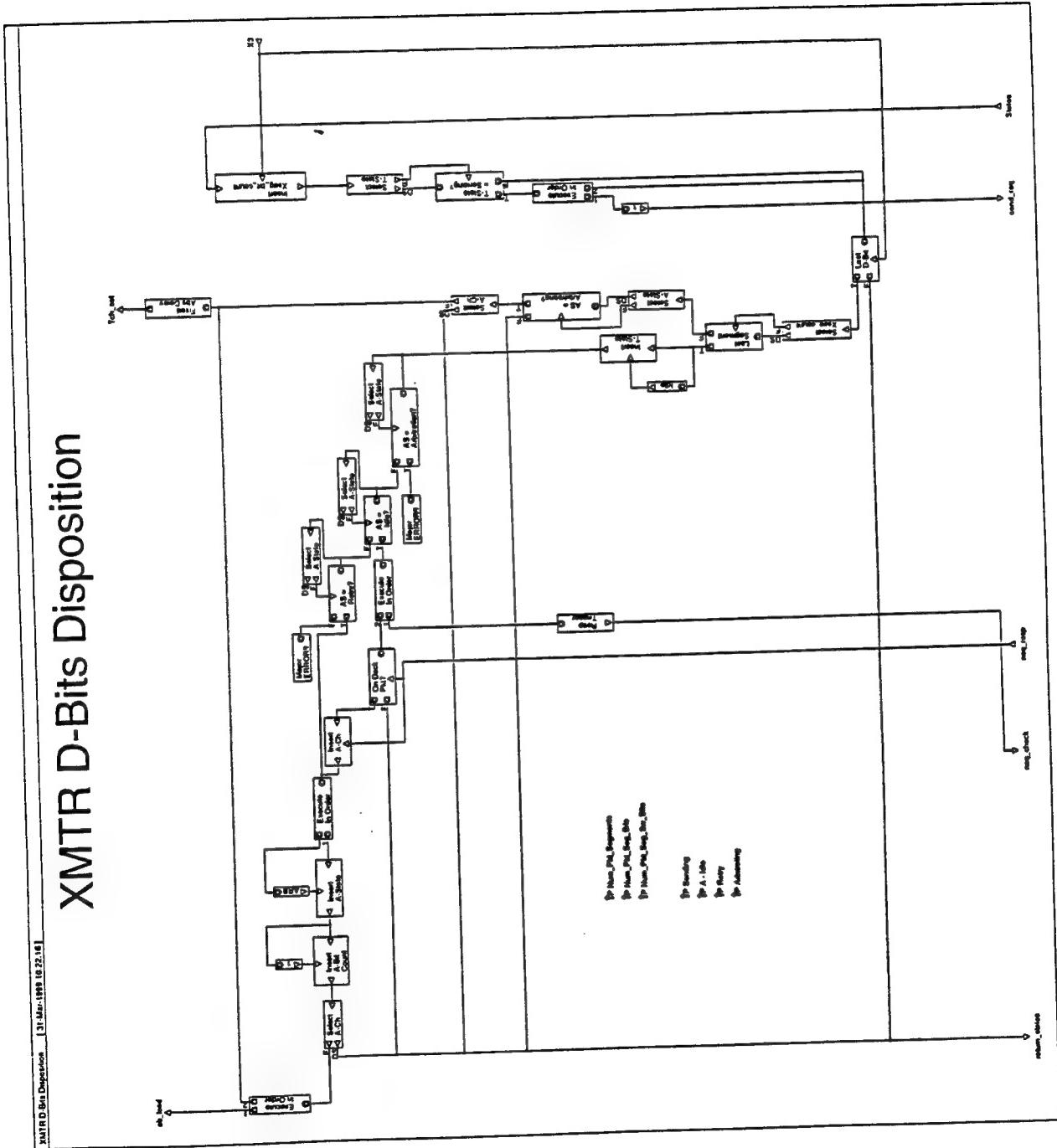
# RCVR Packet Segment Cycle Handler

# RCVR A-Bit Disposition
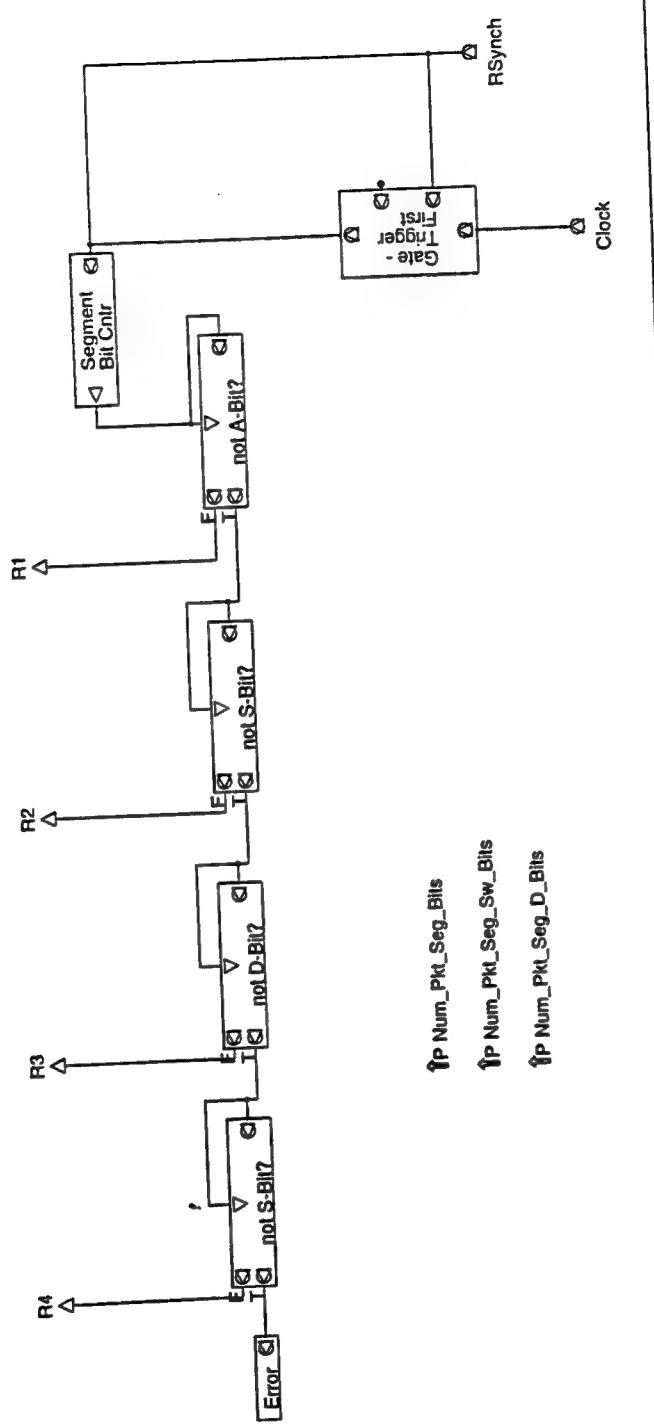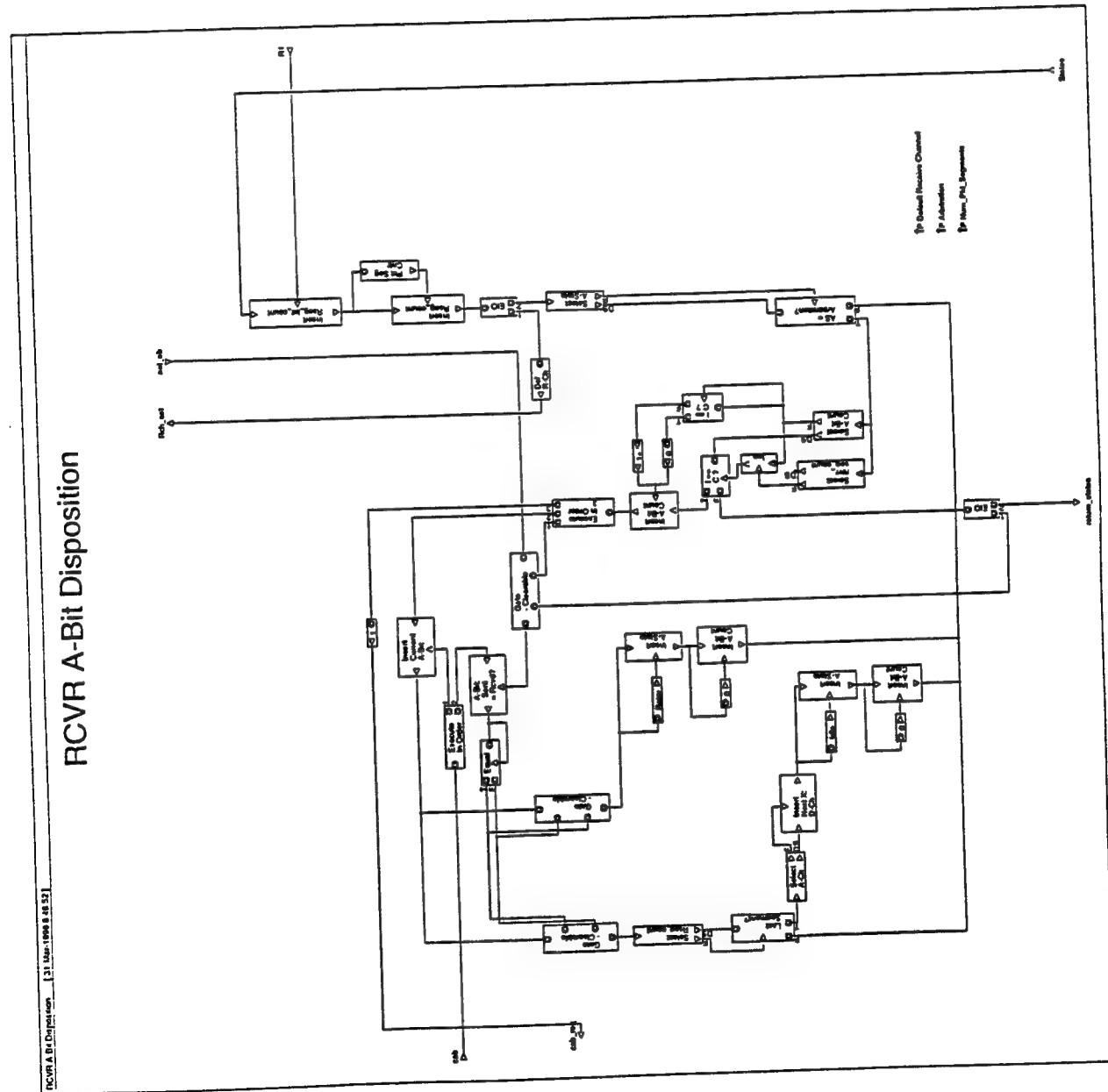


RCVR A-Bit Disposition

# RCVR S-Bit Disposition

states

return_states

Insert
Rseg_bit_count

X1

# RCVR D-Bits Disposition

States

R3

Insert
Rseg bit count

Last
D-Bit

Select
A-State

AS =
Arbitrating?

Select
A-Ch

P Arbitrating

P Num_Pkt_Seg_Bits

P Num_Pkt_Seg_Sw_Bits

return_states

Rch_set
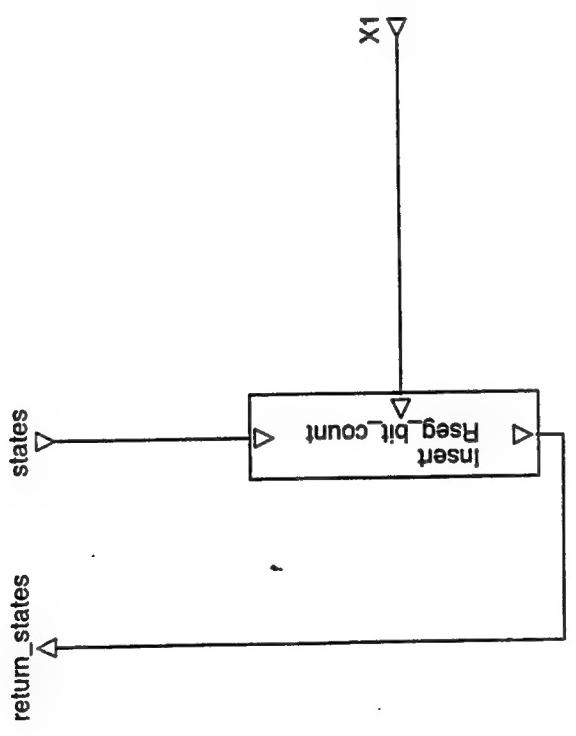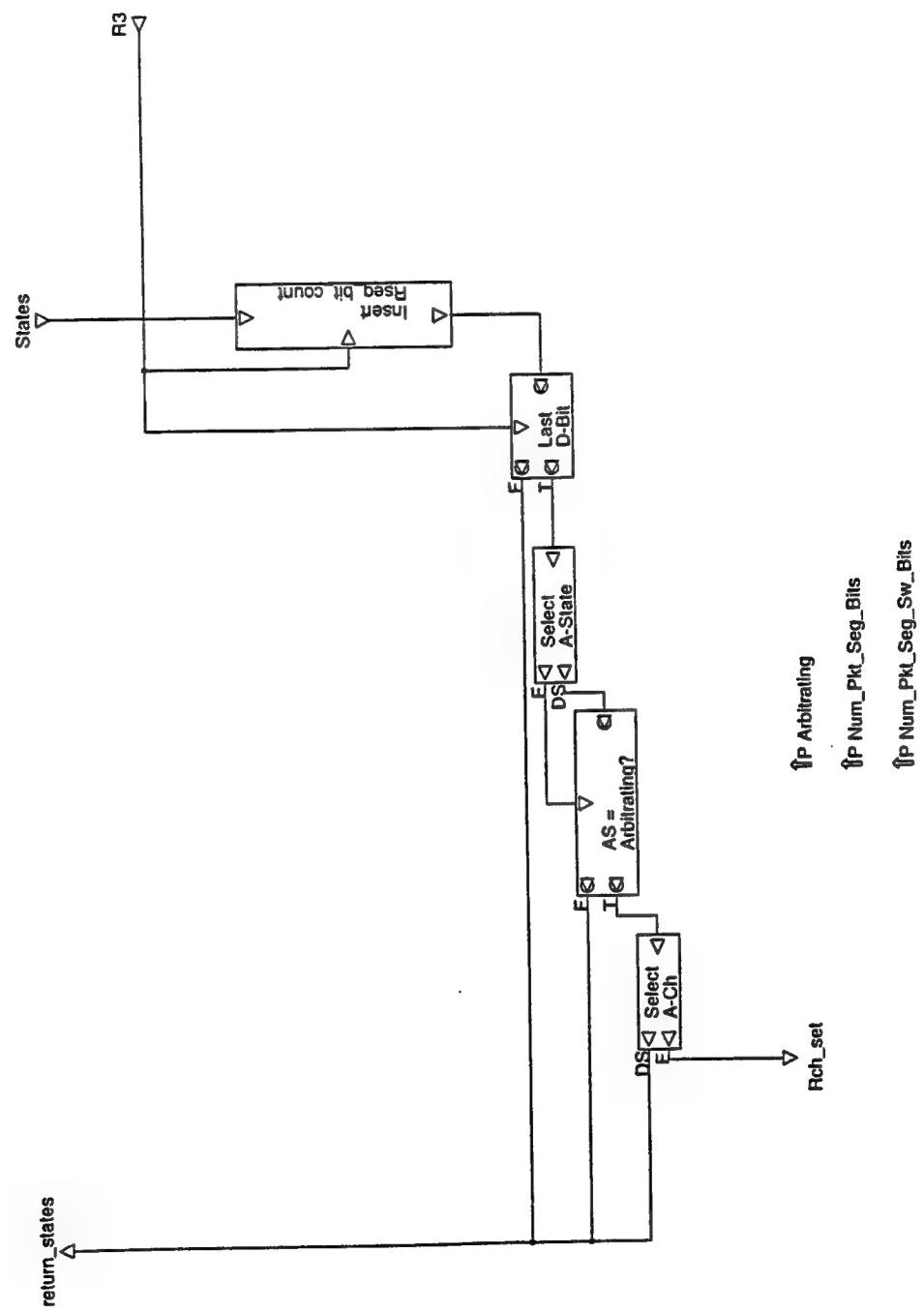
# Control States
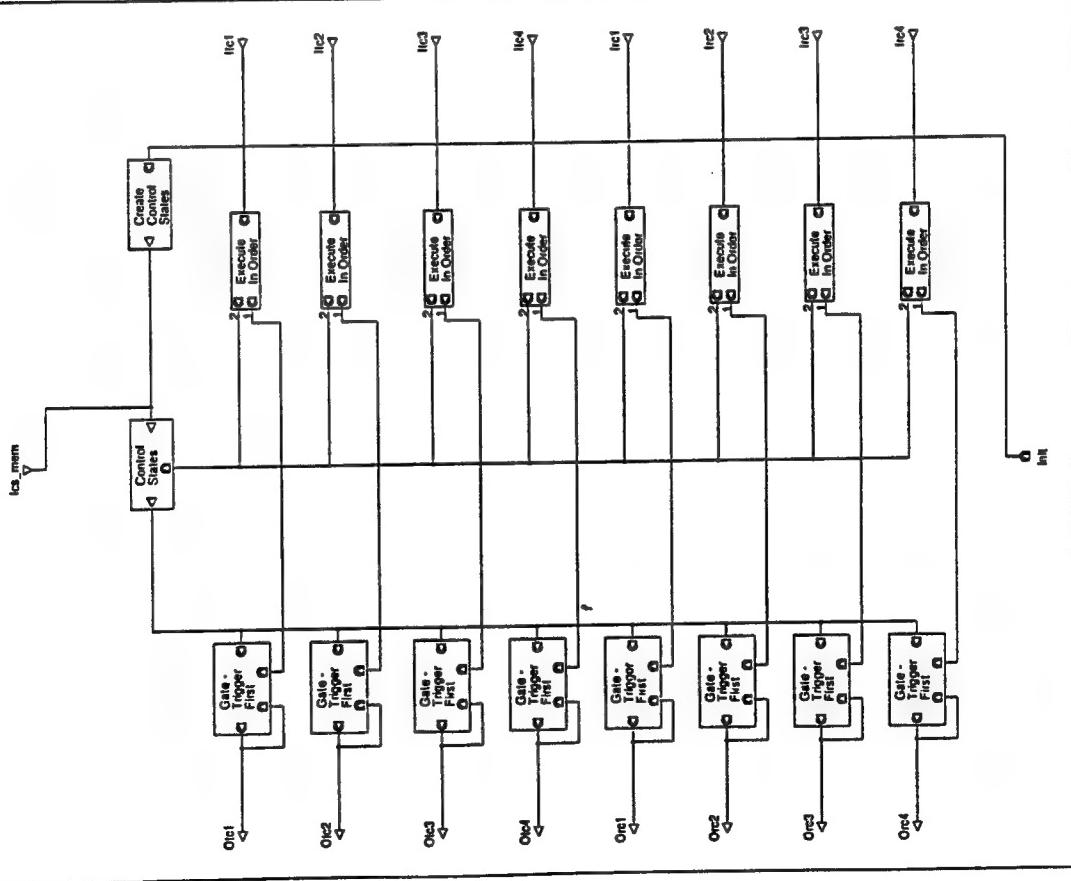
# A-Bit Sequence Buffer Control
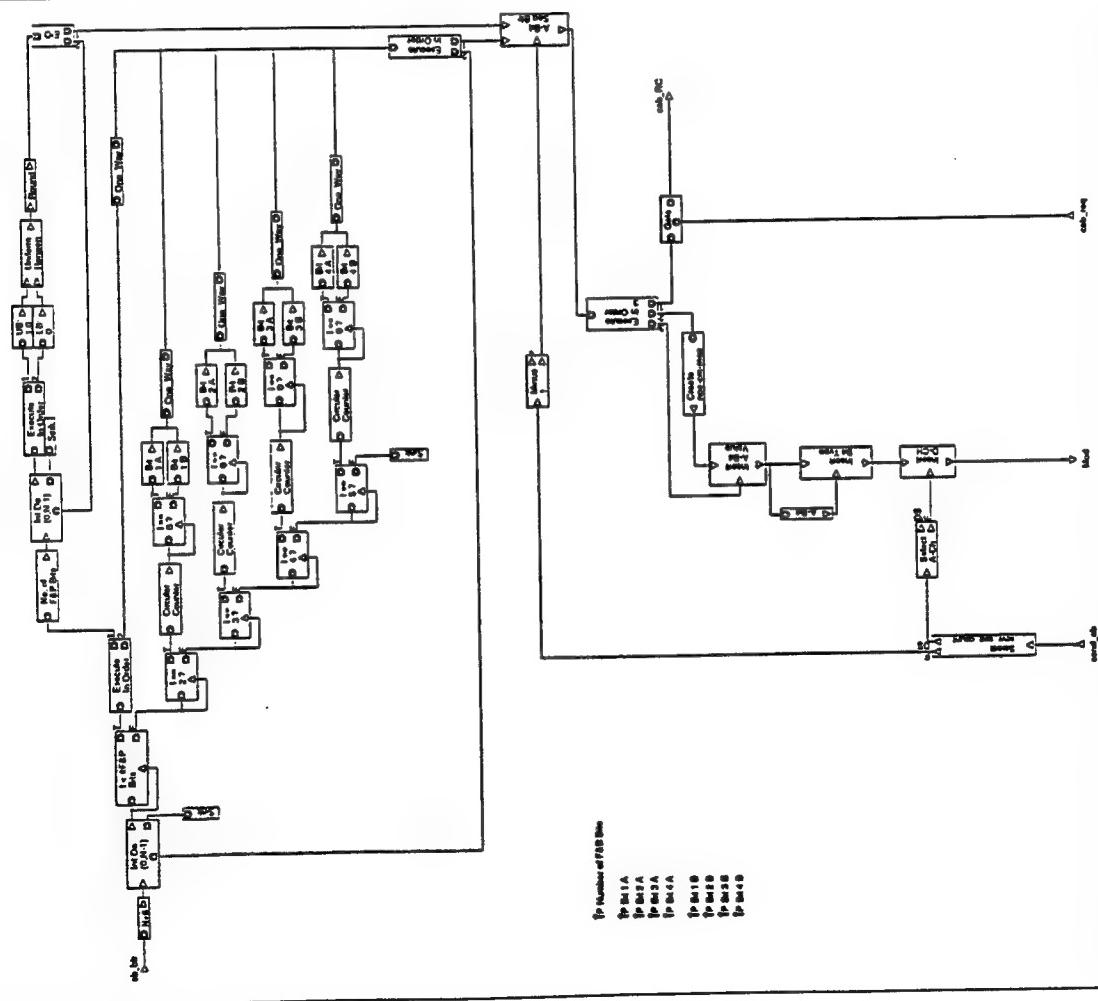
# NPE - Bit Message Generator

# Node or Node Processing Elements



↑P Start Time

↑P Stop Time

↑P Node Enable

↑P Node Pulse Period

↑P Number of Channels

↑P Test Mode

↑P Default X-mit Channel

# Node ONIC Bit Transmissions



**Transceiver Channel** vs. **'TNOW'**

4.0  3.5  3.0  2.5  2.0  1.5  1.0

0.    500.    1000.    1500.

+ Host 1: Output
+ Host 2: Output

△ Node 1: Output
○ Node 2: Output

# Node ONIC Bit Transmissions



'TNOW'

Transceiver Channel

+ Host 1: Output
+ Host 2: Output

▲ Node 1: Output
○ Node 2: Output

105

## Two Nodes:  Input



'Select Channel'

'TNOW'

□ Node 1: Input

▲ Node 2: Input

## Detector Vs. Filler/Filter Data

Receiver Channel

4.0  3.5  3.0  2.5  2.0  1.5  1.0

0.    500.    1000.    1500.

'TNOW'

O Node 1:  Detector          . Node 1: Input
o Node 2:  Detector          . Node 2:  Input

# Node 1:  Analysis



'TNOW'

• N1: Input

• N1: Output

'Select Channel'

2C: Nodes Output    [ 14-Oct-1998 14:31:22 ]

# Node ONIC Bit Transmissions
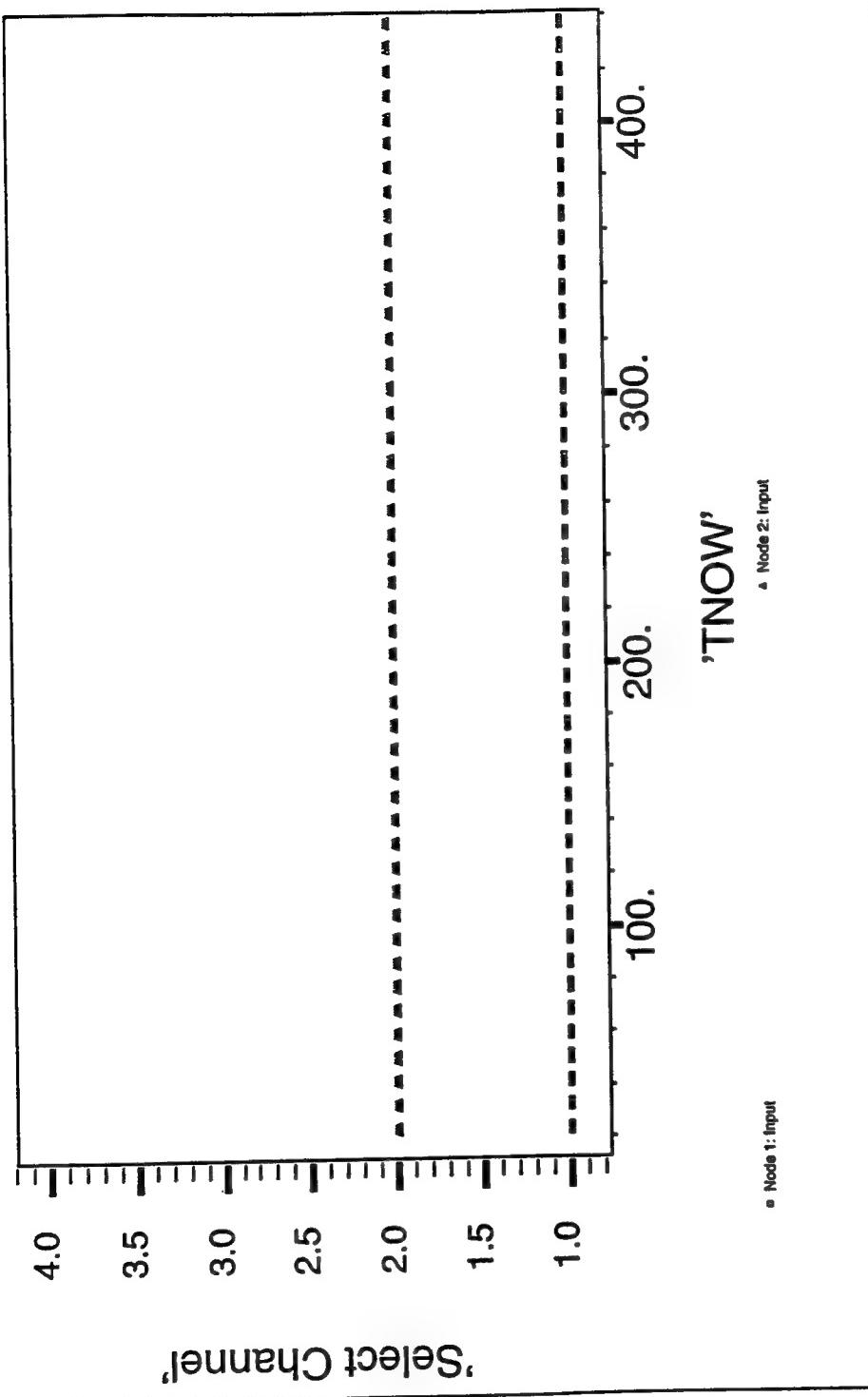


'TNOW'

+ Host 1: Output
+ Host 2: Output

▲ Node 1: Output
○ Node 2: Output

Transmitter Channel
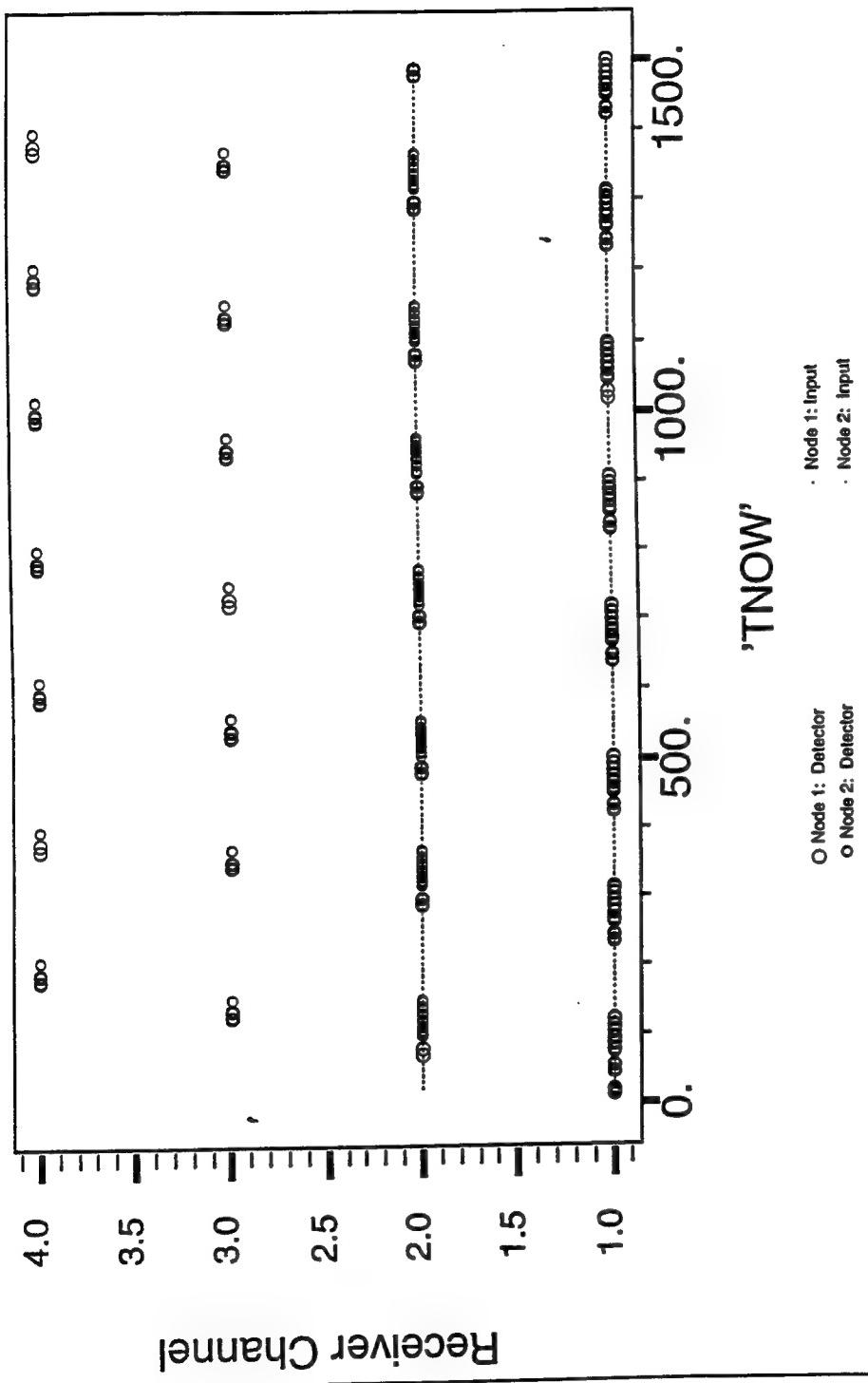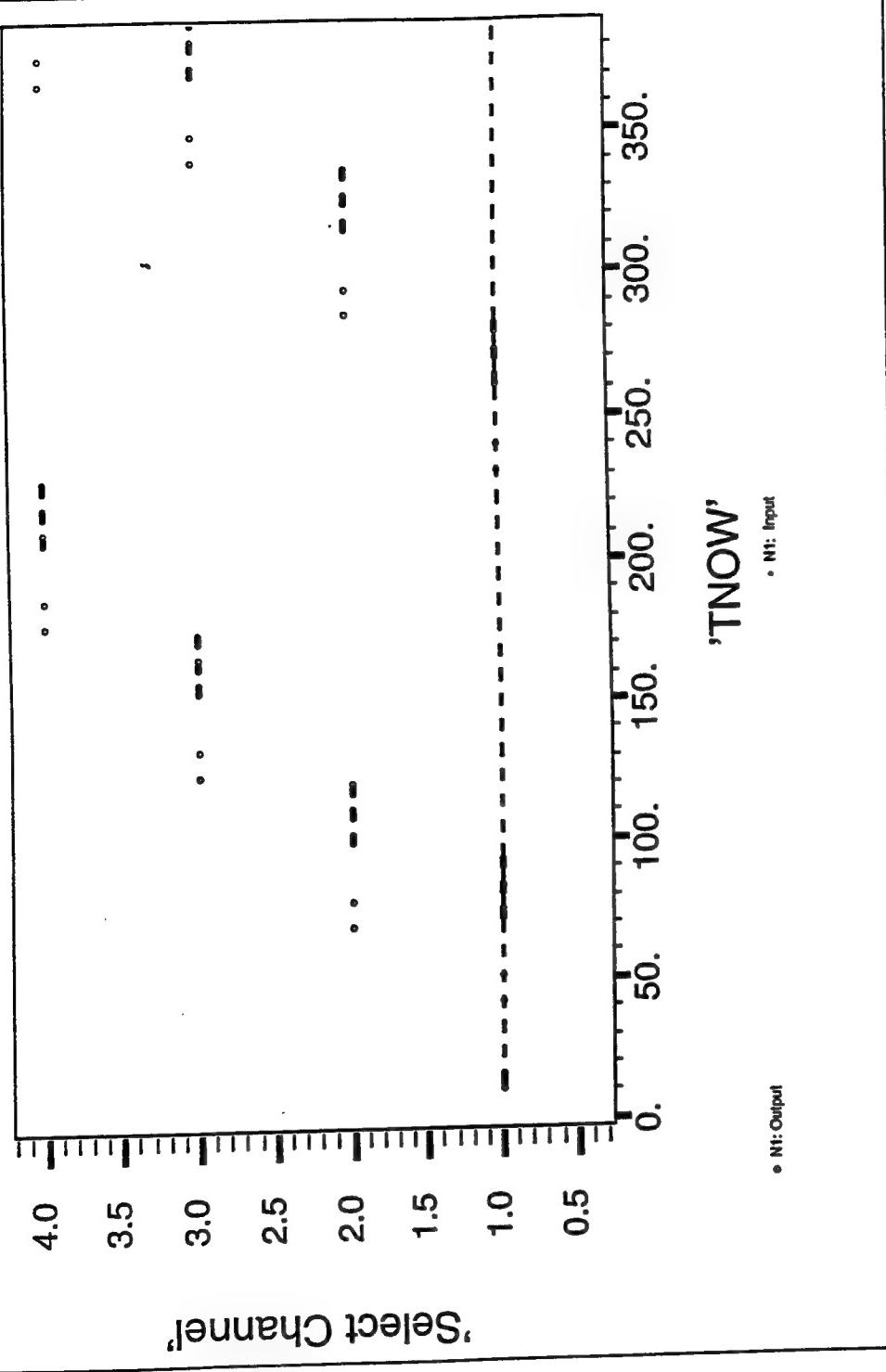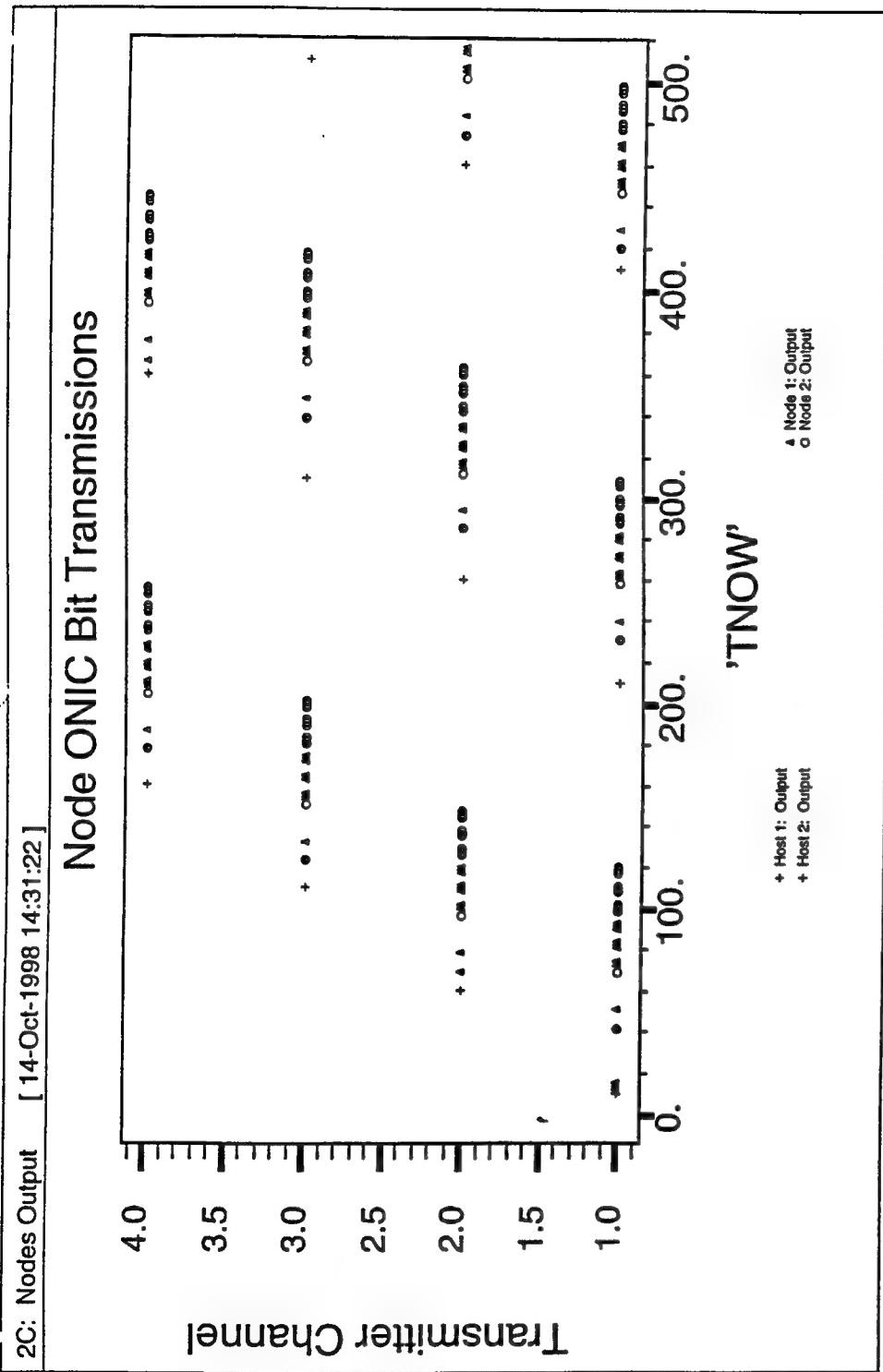
2C: Node 1: All Output    [ 21-Dec-1998 11:17:07 ]
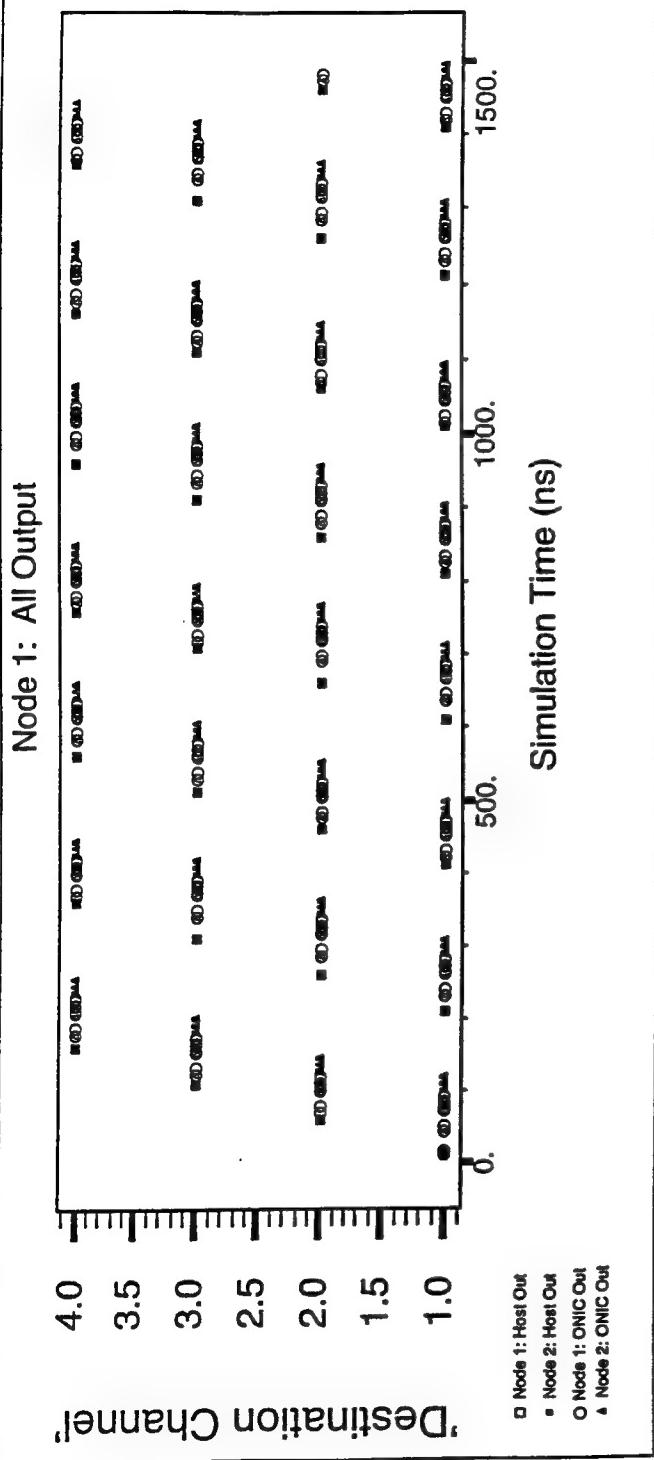
Node 1:  All Output

Destination Channel

Simulation Time (ns)

□ Node 1: Host Out
■ Node 2: Host Out
○ Node 1: ONIC Out
▲ Node 2: ONIC Out

## 2C: Node 1: Packets Generated



'Destination Channel'

'TNOW'

⊙ Node 1: Host Out

O Node 2: Host Out
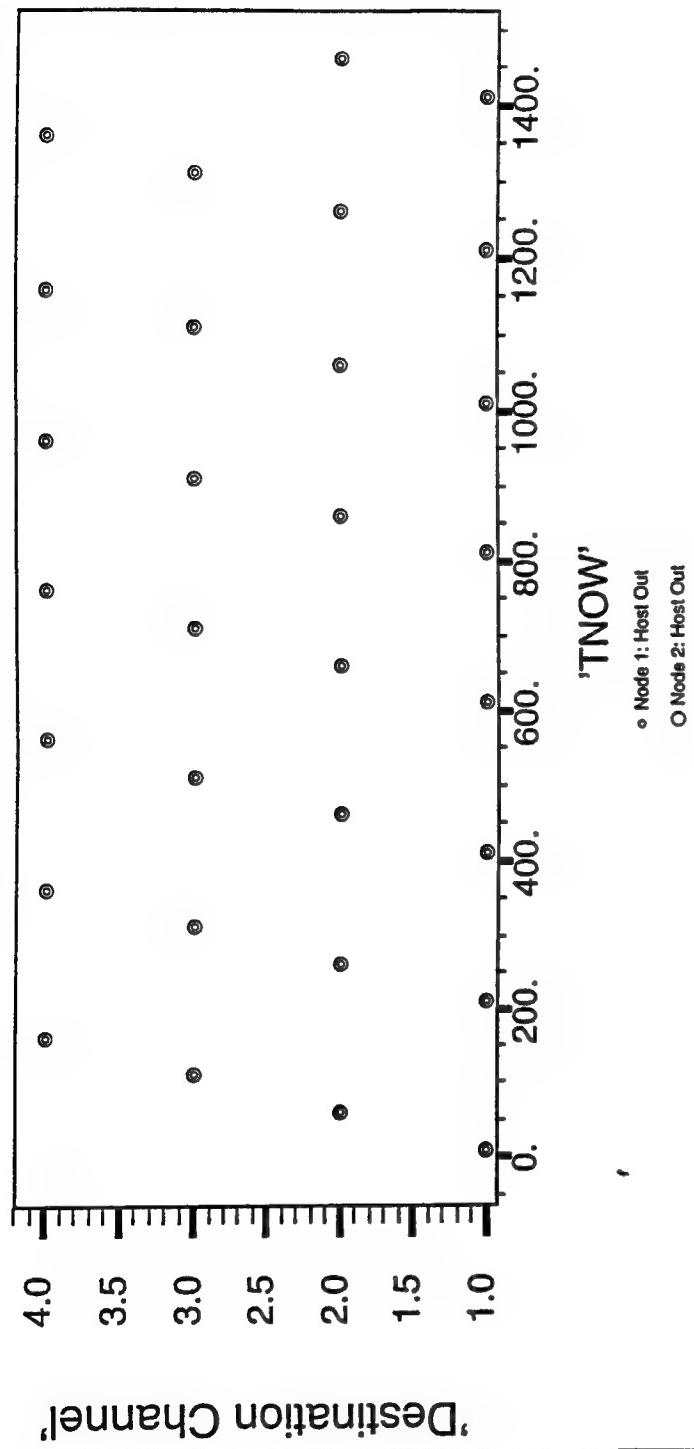
2C: Detector Data Inputs   [ 21-Dec-1998 11:17:07 ]

Detector Inputs

'Select Channel'

'TNOW'

○ Node 1: Inputs
○ Node 2: Inputs

112
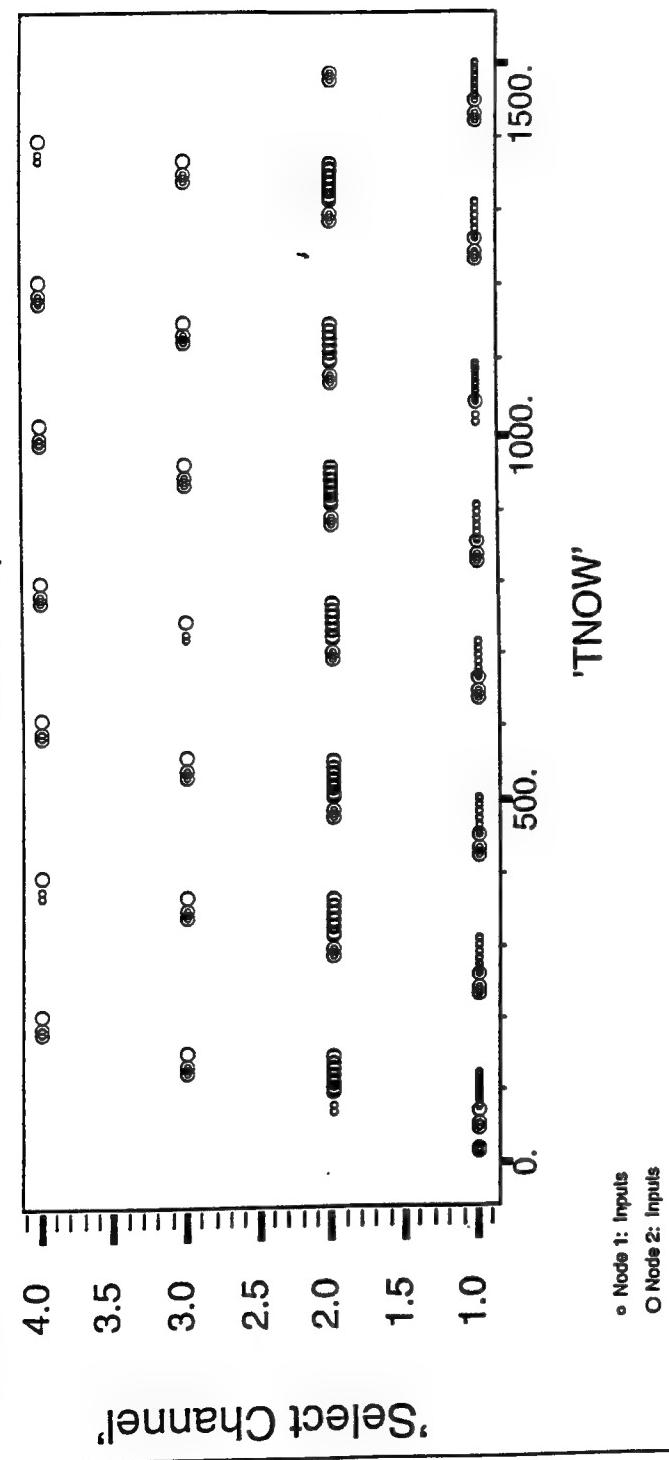
Send & Receive: 500ns    [ 21-Dec-1998 11:39:47 ]

Send & Receive

'TNOW'

Send and Receive Channels

△ Node 1:  Detector
+ Node 2:  Detector
□ Node 3:  Detector
· Node 4:  Detector

+ Host Transmit
○ Node 1: Send
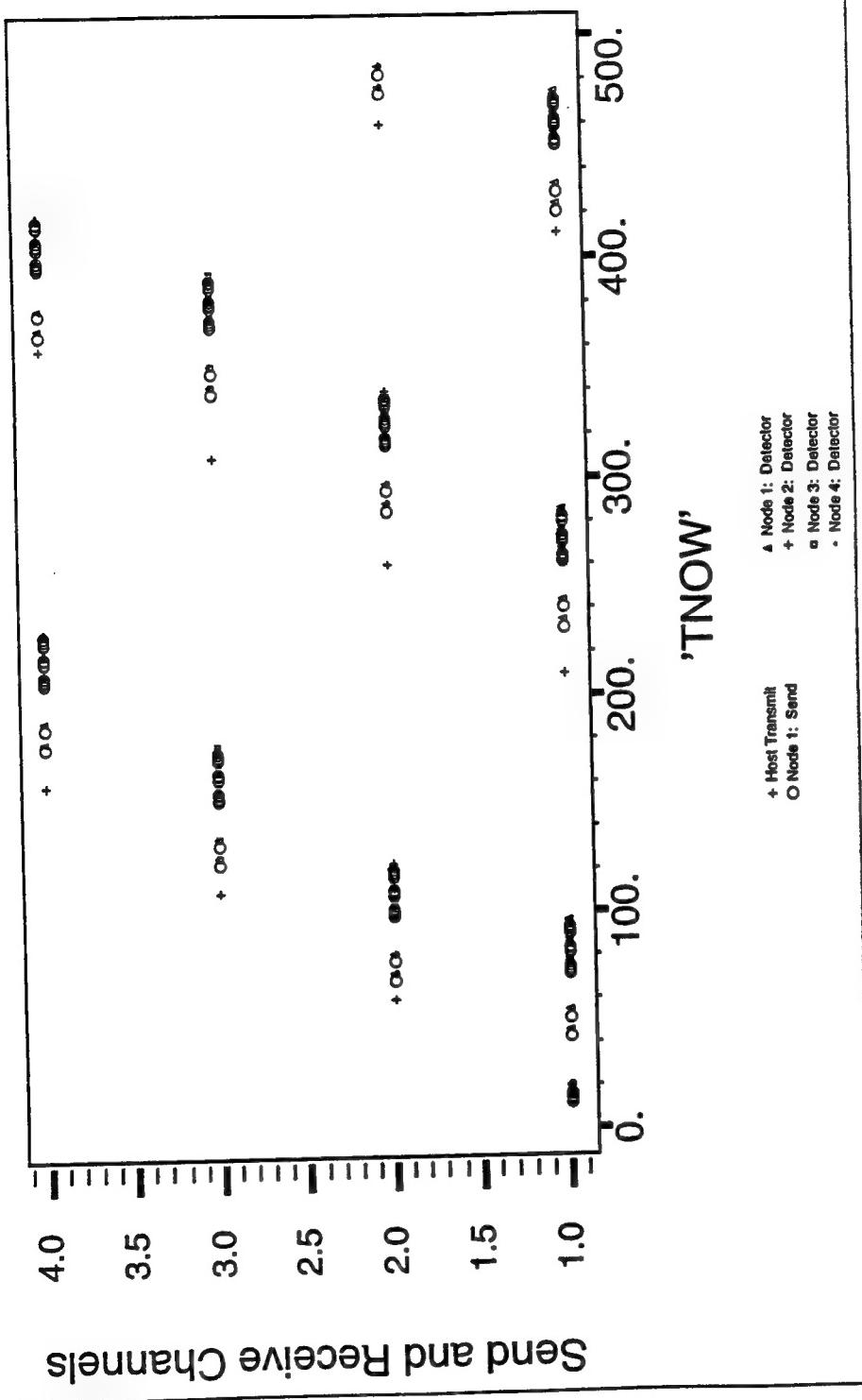
Send & Receive     [ 21-Dec-1998 11:39:47 ]

## Send & Receive

'Destination Channel'

4.0  3.5  3.0  2.5  2.0  1.5  1.0

0.     50.     100.     150.     200.

'TNOW'

+ Node 1: Host Output      □ Node 1: Detector
O Node 1: Send             ● Node 2: Detector
                           ● Node 3: Detector
                           ● Node 4: Detector

114
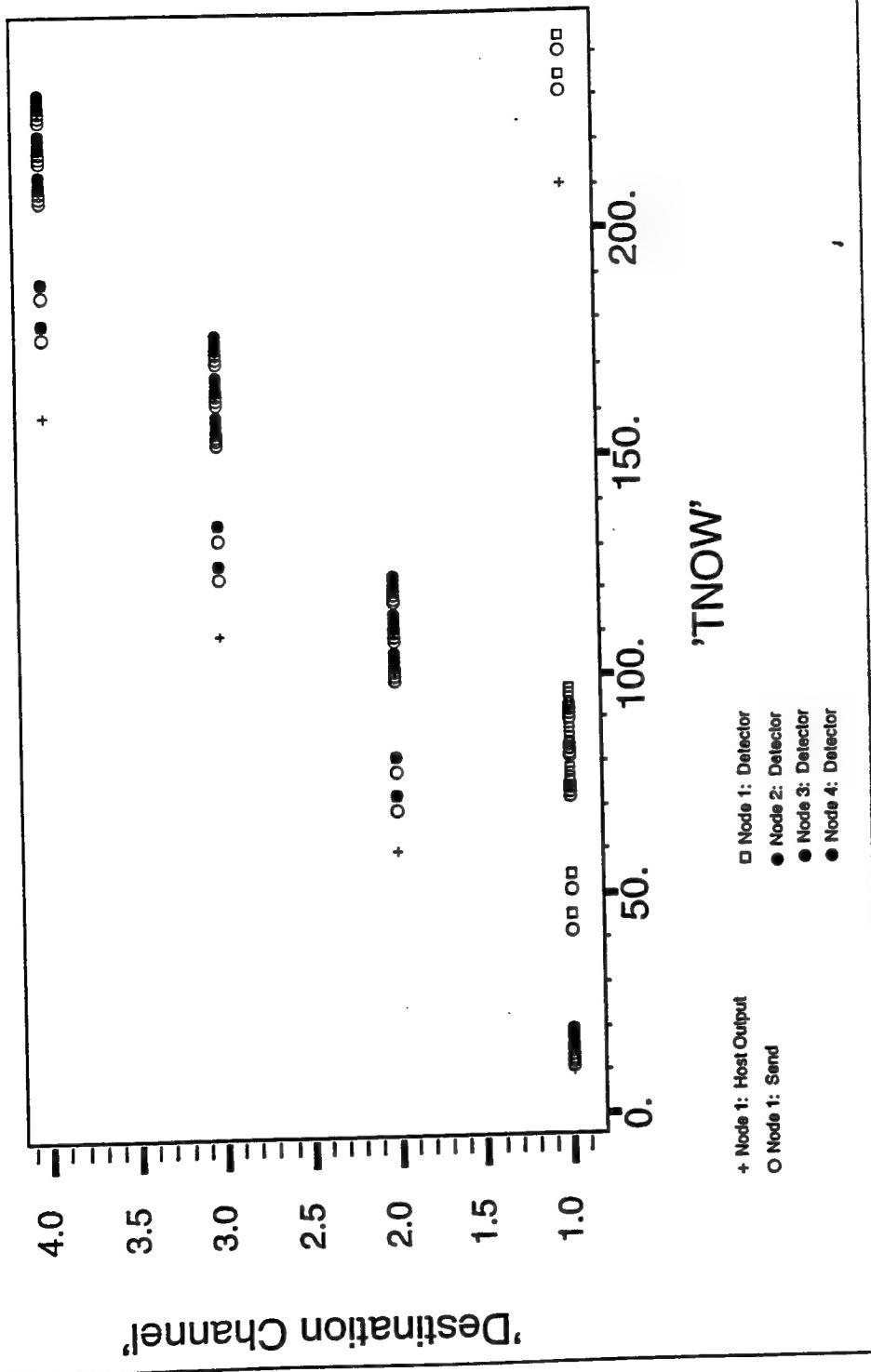
16 Node Network: I/O    [ 21-Dec-1998 11:56:20 ]

16 Node Network I/O

'Select Channel'

'TNOW'

+ n1_host_out
● n1_ONIC_out

□ n1_detector
□ n2_detector
□ n3_detector
□ n4_detector

□ n5_detector
□ n6_detector
□ n7_detector
□ n8_detector

□ n9_detector
□ n10_detector
□ n11_detector
□ n12_detector

□ n13_detector
□ n14_detector
□ n15_detector
□ n16_detector

115
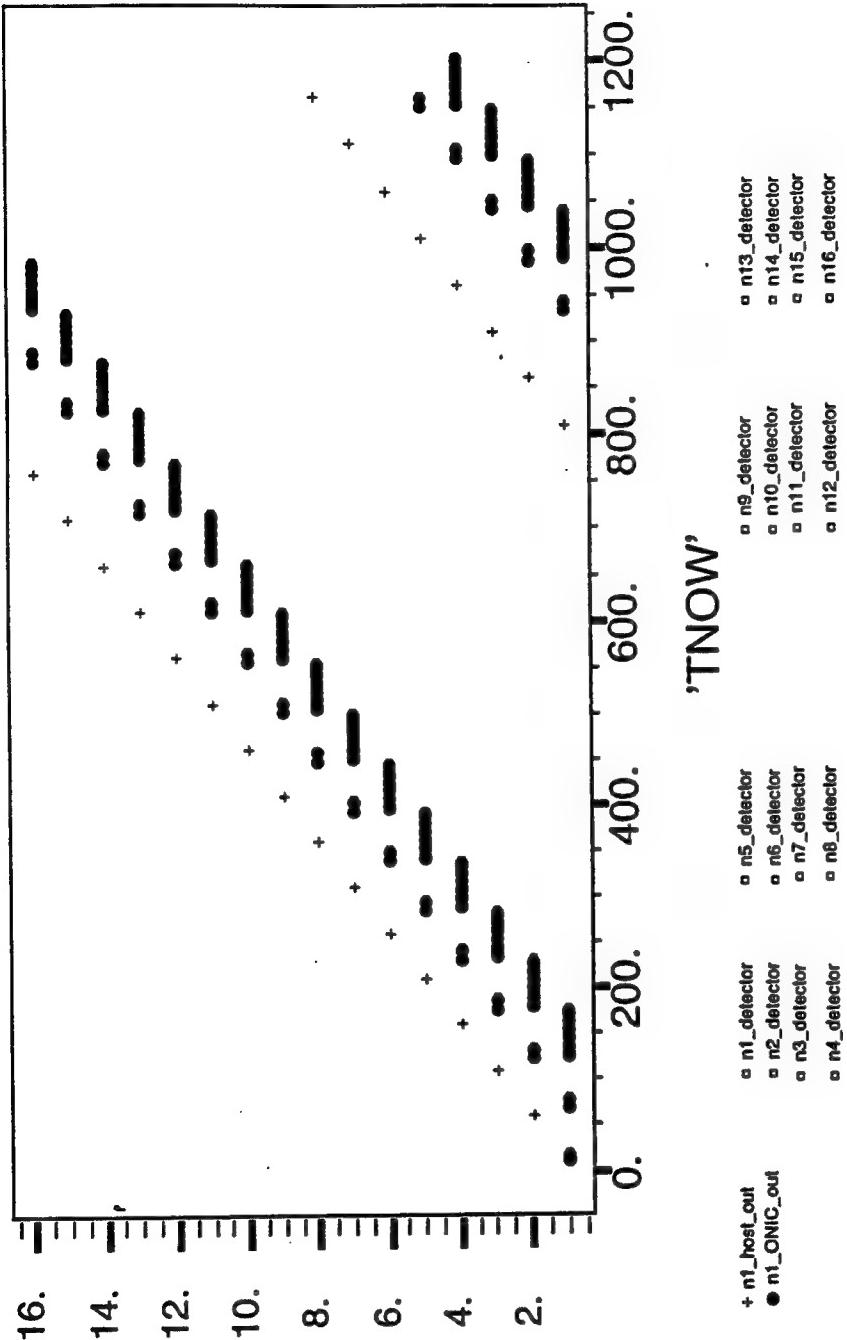
# Node 1: Host to ONIC Packet Transmissions



o n1_host_out
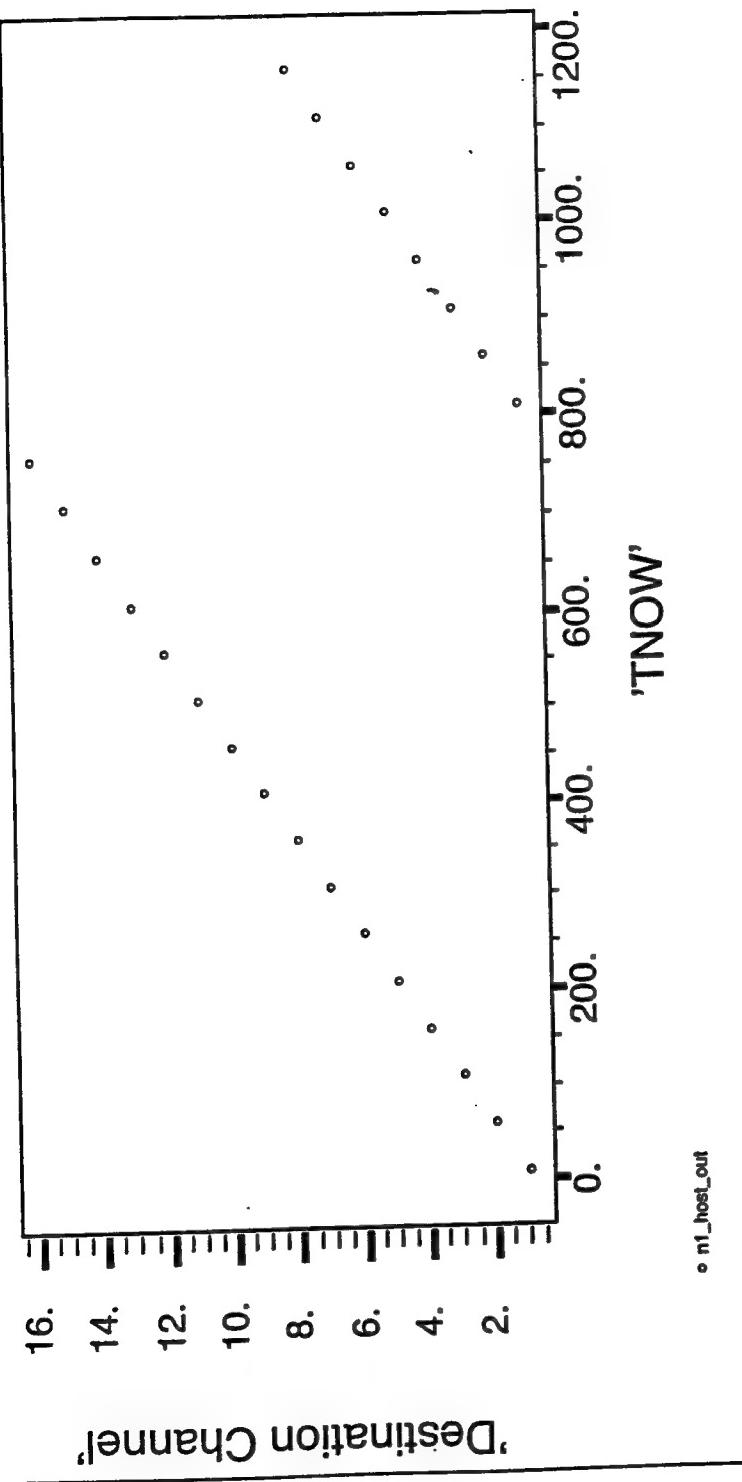
**Name: Basic Bit Message [Optical-Net]**
**Date: Wednesday, 3/31/99 11:02:18 am EST**

| Name | Type | Subrange | Default Value |
|------|------|----------|---------------|
| Message Type | INTEGER | [0, +Infinity) | 1 |
| Sequence Number | INTEGER | [0, +Infinity) | ... |
| Time Created | REAL | [0, +Infinity) | 0.0 |

117

**Name: cm-npe-msg [Optical-Net]**
**Date: Wednesday, 3/31/99 11:02:19 am EST**

| Name | Type | Subrange | Default Value |
|------|------|----------|---------------|
| Message Type | INTEGER | [0, +Infinity) | 1 |
| Sequence Number | INTEGER | [0, +Infinity) | ... |
| Time Created | REAL | [0, +Infinity) | 0.0 |

**Name: mll-pps-msg [Optical-Net]**

**Date: Wednesday, 3/31/99 11:02:19 am EST**

| Name | Type | Subrange | Default Value |
|------|------|----------|---------------|
| *Message Type* | *INTEGER* | *[0, +Infinity)* | *1* |
| *Sequence Number* | *INTEGER* | *[0, +Infinity)* | *...* |
| *Time Created* | *REAL* | *[0, +Infinity)* | *0.0* |
| Pulse Magnitude | *REAL* | *[0, +Infinity)* | *1.0* |
| Pulse Width | *REAL* | *[0, +Infinity)* | *0.1* |

**Name: fdr-mod-msg [Optical-Net]**

**Date: Wednesday, 3/31/99 11:02:19 am EST**

| Name | Type | Subrange | Default Value |
|------|------|----------|---------------|
| Message Type | INTEGER | [0, +Infinity) | 1 |
| Sequence Number | INTEGER | [0, +Infinity) | ... |
| Time Created | REAL | [0, +Infinity) | 0.0 |
| Pulse Magnitude | REAL | [0, +Infinity) | 1.0 |
| Pulse Width | REAL | [0, +Infinity) | 0.1 |
| Time Sent | REAL | [0, +Infinity) | 1.0 |

**Name: fdr-toad-msg [Optical-Net]**
**Date: Wednesday, 3/31/99 11:02:19 am EST**

| Name | Type | Subrange | Default Value |
|------|------|----------|---------------|
| Message Type | INTEGER | [0, +Infinity) | 1 |
| Sequence Number | INTEGER | [0, +Infinity) | ... |
| Time Created | REAL | [0, +Infinity) | 0.0 |
| Pulse Magnitude | REAL | [0, +Infinity) | 1.0 |
| Pulse Width | REAL | [0, +Infinity) | 0.1 |
| Time Sent | REAL | [0, +Infinity) | 1.0 |

**Name: pps-fiber-msg [Optical-Net]**

**Date: Wednesday, 3/31/99 11:02:19 am EST**

| Name | Type | Subrange | Default Value |
|------|------|----------|---------------|
| Message Type | INTEGER | [0, +Infinity) | 1 |
| Sequence Number | INTEGER | [0, +Infinity) | ... |
| Time Created | REAL | [0, +Infinity) | 0.0 |
| Pulse Magnitude | REAL | [0, +Infinity) | 1.0 |
| Pulse Width | REAL | [0, +Infinity) | 0.1 |
| Select Channel | INTEGER | [0, +Infinity) | 1 |

**Name: fiber-fdr-msg [Optical-Net]**

**Date: Wednesday, 3/31/99 11:02:19 am EST**

| Name | Type | Subrange | Default Value |
|------|------|----------|---------------|
| Message Type | INTEGER | [0, +Infinity) | 1 |
| Sequence Number | INTEGER | [0, +Infinity) | ... |
| Time Created | REAL | [0, +Infinity) | 0.0 |
| Pulse Magnitude | REAL | [0, +Infinity) | 1.0 |
| Pulse Width | REAL | [0, +Infinity) | 0.1 |
| Select Channel | INTEGER | [0, +Infinity) | 1 |
| Time Sent | REAL | [0, +Infinity) | 1.0 |

123

**Name: fdr-rvd-msg [Optical-Net]**
**Date: Wednesday, 3/31/99 11:02:20 am EST**

| Name | Type | Subrange | Default Value |
|------|------|----------|---------------|
| Message Type | INTEGER | [0, +Infinity) | 1 |
| Sequence Number | INTEGER | [0, +Infinity) | ... |
| Time Created | REAL , | [0, +Infinity) | 0.0 |
| Pulse Magnitude | REAL | [0, +Infinity) | 1.0 |
| Pulse Width | REAL | [0, +Infinity) | 0.1 |
| Select Channel | INTEGER | [0, +Infinity) | 1 |
| Time Sent | REAL | [0, +Infinity) | 1.0 |

**Name: cm-rvd-cmd [Optical-Net]**

**Date: Wednesday, 3/31/99 11:02:20 am EST**

| Name | Type | Subrange | Default Value |
|------|------|----------|---------------|
| Message Type | INTEGER | [0, +Infinity) | 1 |
| Sequence Number | INTEGER | [0, +Infinity) | ... |
| Time Created | REAL | [0, +Infinity) | 0.0 |
| Pulse Magnitude | REAL | [0, +Infinity) | 1.0 |
| Pulse Width | REAL | [0, +Infinity) | 0.1 |
| Select Channel | INTEGER | [0, +Infinity) | 1 |
| Time Sent | REAL | [0, +Infinity) | 1.0 |

**Name: rvd-toad-msg [Optical-Net]**

**Date: Wednesday, 3/31/99 11:02:20 am EST**

| Name | Type | Subrange | Default Value |
|---|---|---|---|
| Message Type | INTEGER | [0, +Infinity) | 1 |
| Sequence Number | INTEGER | [0, +Infinity) | ... |
| Time Created | REAL | [0, +Infinity) | 0.0 |
| Pulse Magnitude | REAL | [0, +Infinity) | 1.0 |
| Pulse Width | REAL | [0, +Infinity) | 0.1 |
| Select Channel | INTEGER | [0, +Infinity) | 1 |
| Time Sent | REAL | [0, +Infinity) | 1.0 |

126

**Name: toad-det-msg [Optical-Net]**

**Date: Wednesday, 3/31/99 11:02:20 am EST**

| Name | Type | Subrange | Default Value |
|------|------|----------|---------------|
| Message Type | INTEGER | [0, +Infinity) | 1 |
| Sequence Number | INTEGER | [0, +Infinity) | ... |
| Time Created | REAL | [0, +Infinity) | 0.0 |
| Pulse Magnitude | REAL | [0, +Infinity) | 1.0 |
| Pulse Width | REAL | [0, +Infinity) | 0.1 |
| Select Channel | INTEGER | [0, +Infinity) | 1 |
| Time Sent | REAL | [0, +Infinity) | 1.0 |

**Name: det-cm-msg [Optical-Net]**

**Date: Wednesday, 3/31/99 11:02:21 am EST**

| Name | Type | Subrange | Default Value |
|---|---|---|---|
| Message Type | INTEGER | [0, +Infinity) | 1 |
| Sequence Number | INTEGER | [0, +Infinity) | ... |
| Time Created | REAL | [0, +Infinity) | 0.0 |
| Pulse Magnitude | REAL | [0, +Infinity) | 1.0 |
| Pulse Width | REAL | [0, +Infinity) | 0.1 |
| Select Channel | INTEGER | [0, +Infinity) | 1 |
| Time Sent | REAL | [0, +Infinity) | 1.0 |
| Bit Value | INTEGER | [0, +Infinity) | 1 |
| Packet Bit Number | INTEGER | [0, +Infinity) | 1 |

128

**Name: npe-cm-pkt-hdr [Optical-Net]**

**Date: Wednesday, 3/31/99 11:02:21 am EST**

| Name | Type | Subrange | Default Value |
|------|------|----------|---------------|
| Message Type | INTEGER | [0, +Infinity) | 1 |
| Sequence Number | INTEGER | [0, +Infinity) | ... |
| Time Created | REAL | [0, +Infinity) | 0.0 |
| Destination Channel | INTEGER | [0, +Infinity) | 1 |
| Packet Number | INTEGER | [0, +Infinity) | 1 |

**Name: cm-tvd-cmd [Optical-Net]**
**Date: Wednesday, 3/31/99 11:02:21 am EST**

| Name | Type | Subrange | Default Value |
|------|------|----------|---------------|
| Message Type | INTEGER | [0, +Infinity) | 1 |
| Sequence Number | INTEGER | [0, +Infinity) | ... |
| Time Created | REAL | [0, +Infinity) | 0.0 |
| Destination Channel | INTEGER | [0, +Infinity) | 1 |
| Packet Number | INTEGER | [0, +Infinity) | 1 |

**Name: npe-cm-msg [Optical-Net]**

**Date: Wednesday, 3/31/99 11:02:21 am EST**

| Name | Type | Subrange | Default Value |
|------|------|----------|---------------|
| *Message Type* | *INTEGER* | *[0, +Infinity)* | *1* |
| *Sequence Number* | *INTEGER* | *[0, +Infinity)* | ... |
| *Time Created* | *REAL* | *[0, +Infinity)* | *0.0* |
| *Destination Channel* | *INTEGER* | *[0, +Infinity)* | *1* |
| *Packet Number* | *INTEGER* | *[0, +Infinity)* | *1* |
| Packet Bit Number | INTEGER | [0, +Infinity) | 1 |
| Bit Value | INTEGER | [0, +Infinity) | 0 |
| Bit Type | INTEGER | [0, 1] | 0 |

131

**Name: cm-mod-cmd [Optical-Net]**

**Date: Wednesday, 3/31/99 11:02:21 am EST**

| Name | Type | Subrange | Default Value |
|------|------|----------|---------------|
| Message Type | INTEGER | [0, +Infinity) | 1 |
| Sequence Number | INTEGER | [0, +Infinity) | ... |
| Time Created | REAL | [0, +Infinity) | 0.0 |
| Destination Channel | INTEGER | [0, +Infinity) | 1 |
| Packet Number | INTEGER | [0, +Infinity) | 1 |
| Packet Bit Number | INTEGER | [0, +Infinity) | 1 |
| Bit Value | INTEGER | [0, +Infinity) | 0 |
| Bit Type | INTEGER | [0, 1] | 0 |
| Time Sent | REAL | [0, +Infinity) | 0.0 |

**Name: mod-tvd-msg [Optical-Net]**

**Date: Wednesday, 3/31/99 11:02:22 am EST**

| Name | Type | Subrange | Default Value |
|---|---|---|---|
| Message Type | INTEGER | [0, +Infinity) | 1 |
| Sequence Number | INTEGER | [0, +Infinity) | ... |
| Time Created | REAL | [0, +Infinity) | 0.0 |
| Destination Channel | INTEGER | [0, +Infinity) | 1 |
| Packet Number | INTEGER | [0, +Infinity) | 1 |
| Packet Bit Number | INTEGER | [0, +Infinity) | 1 |
| Bit Value | INTEGER | [0, +Infinity) | 0 |
| Bit Type | INTEGER | [0, 1] | 0 |
| Time Sent | REAL | [0, +Infinity) | 0.0 |

**Name: fiber-pps-msg [Optical-Net]**
**Date: Wednesday, 3/31/99 11:02:22 am EST**

| Name | Type | Subrange | Default Value |
|------|------|----------|---------------|
| Message Type | INTEGER | [0, +Infinity) | 1 |
| Sequence Number | INTEGER | [0, +Infinity) | ... |
| Time Created | REAL | [0, +Infinity) | 0.0 |
| Destination Channel | INTEGER | [0, +Infinity) | 1 |
| Packet Number | INTEGER | [0, +Infinity) | 1 |
| Packet Bit Number | INTEGER | [0, +Infinity) | 1 |
| Bit Value | INTEGER | [0, +Infinity) | 0 |
| Bit Type | INTEGER | [0, 1] | 0 |
| Time Sent | REAL | [0, +Infinity) | 0.0 |

134

**Name: tvd-fiber-msg [Optical-Net]**
**Date: Wednesday, 3/31/99 11:02:22 am EST**

| Name | Type | Subrange | Default Value |
|---|---|---|---|
| Message Type | INTEGER | [0, +Infinity) | 1 |
| Sequence Number | INTEGER | [0, +Infinity) | ... |
| Time Created | REAL | [0, +Infinity) | 0.0 |
| Destination Channel | INTEGER | [0, +Infinity) | 1 |
| Packet Number | INTEGER | [0, +Infinity) | 1 |
| Packet Bit Number | INTEGER | [0, +Infinity) | 1 |
| Bit Value | INTEGER | [0, +Infinity) | 0 |
| Bit Type | INTEGER | [0, 1] | 0 |
| Time Sent | REAL | [0, +Infinity) | 0.0 |

135

# DISTRIBUTION LIST

| addresses | number of copies |
|---|---|
| AIR FORCE RESEARCH LABORATORY/SNDP<br>JOHN MALOWICKI<br>25 ELECTRONIC PKY<br>ROME NY  13441-4515 | 5 |
| LOCKHEED MARTIN COMPANY<br>65 SPIT BROOK RD<br>NASHUA NH  03061-0868 | 5 |
| AFRL/IFOIL<br>TECHNICAL LIBRARY<br>26 ELECTRONIC PKY<br>ROME NY 13441-4514 | 1 |
| ATTENTION:  DTIC-OCC<br>DEFENSE TECHNICAL INFO CENTER<br>8725 JOHN J. KINGMAN ROAD, STE 0944<br>FT. BELVOIR, VA 22060-6218 | 2 |
| DEFENSE ADVANCED RESEARCH<br>PROJECTS AGENCY<br>3701 NORTH FAIRFAX DRIVE<br>ARLINGTON VA 22203-1714 | 1 |
| ATTN: NAN PFRIMMER<br>IIT RESEARCH INSTITUTE<br>201 MILL ST.<br>ROME,  NY  13440 | 1 |
| AFIT ACADEMIC LIBRARY<br>AFIT/LDR, 2950 P.STREET<br>AREA B, BLDG 642<br>WRIGHT-PATTERSON AFB OH 45433-7765 | 1 |
| AFRL/MLME<br>2977 P STREET, STE 6<br>WRIGHT-PATTERSON AFB OH 45433-7739 | 1 |

```
ATTN:   SMDC IM PL                            1
US ARMY SPACE & MISSILE DEF CMD
P.O. BOX 1500
HUNTSVILLE AL 35807-3801


COMMANDER, CODE 4TL000D                       1
TECHNICAL LIBRARY, NAWC-WD
1 ADMINISTRATION CIRCLE
CHINA LAKE   CA  93555-6100


CDR, US ARMY AVIATION & MISSILE CMD           2
REDSTONE SCIENTIFIC INFORMATION CTR
ATTN: AMSAM-RD-OB-R, (DOCUMENTS)
REDSTONE ARSENAL AL 35898-5000


REPORT LIBRARY                                1
MS P364
LOS ALAMOS NATIONAL LABORATORY
LOS ALAMOS NM 87545


AFIWC/MSY                                     1
102 HALL BLVD, STE 315
SAN ANTONIO TX 78243-7016


USAF/AIR FORCE RESEARCH LABORATORY            1
AFRL/VSOSA(LIBRARY-BLDG 1103)
5 WRIGHT DRIVE
HANSCOM AFB  MA  01731-3004


ATTN:   EILEEN LADUKE/D460                     1
MITRE CORPORATION
202 BURLINGTON RD
BEDFORD MA 01730


DUSD(P)/DTSA/DUTD                             1
ATTN:  PATRICK G. SULLIVAN, JR.
400 ARMY NAVY DRIVE
SUITE 300
ARLINGTON VA 22202

RICHARD PAYNE                                 1
AIR FORCE RESEARCH LAB/SNH
HANSCOM AFB, MA  01731-5000
```

JOSEPH P. LORENZO, JR.                          1
AIR FORCE RESEARCH LAB/SNHC
HANSCOM AFB, MA   01731-5000


JOSEPH L. HORNER                                1
AIR FORCE RESEARCH LAB/SNHC
HANSCOM AFB, MA   01731-5000


RICHARD A. SOREF                                1
AIR FORCE RESEARCH LAB/SNHC
HANSCOM AFB, MA   01731-5000


ALBERT A. JAMBERDINO                            1
AIR FORCE RESEARCH LAB/IFED
32 HANGAR RD
ROME NY   13441-4114


AIR FORCE RESEARCH LAB/SND                      1
25 ELECTRONIC PKY
ROME NY   13441-4515


JOANNE L. ROSSI                                 1
AIR FORCE RESEARCH LAB/SNW
25 ELECTRONIC PKY
ROME NY   13441-4515


NY PHOTONIC DEVELOPMENT CORP                    1
MVCC ROME CAMPUS
UPPER FLOYD AVE
ROME, NY   13440


ROBERT T. KEMERLEY                              1
AIR FORCE RESEARCH LABORATORY/SND
2241 AVIONICS CIRCLE, RM C2G69
WRIGHT-PATTERSON AFB OH 45433-7322